R-1070-PR
March 1973

High-Performance Composite Materials for Vehicle Construction: An Elastoplastic Analysis of Crack Propagation in a Unidirectional Composite

Donald F. Adams

A Report prepared for

UNITED STATES AIR FORCE PROJECT RAND

DISCLAIMER NOTICE

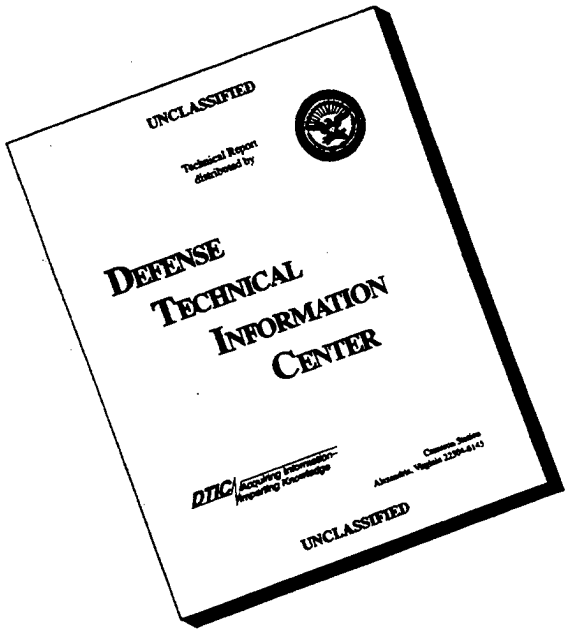

THIS DOCUMENT IS BEST QUALITY AVAILABLE. THE COPY FURNISHED TO DTIC CONTAINED A SIGNIFICANT NUMBER OF PAGES WHICH DO NOT REPRODUCE LEGIBLY.

The research described in this Report was sponsored by the United States Air Force under Contract No. F44620-73-C-0011 — Monitored by the Directorate of Operational Requirements and Development Plans, Deputy Chief of Staff, Research and Development, Hq USAF. Reports of The Rand Corporation do not necessarily reflect the opinions or policies of the sponsors of Rand research.

R-1070-PR
March 1973

High-Performance Composite Materials for Vehicle Construction: An Elastoplastic Analysis of Crack Propagation in a Unidirectional Composite

Donald F. Adams

A Report prepared for

UNITED STATES AIR FORCE PROJECT RAND

Published by The Rand Corporation

PREFACE

This report is one of a series of studies on the behavior of materials under stress conducted under Air Force Project RAND. The investigation was initiated at a time when composite materials had begun to make substantial impact on new airframe design under Air Force sponsorship.

An important aspect of studies of the application of composite materials is knowledge of their failure mechanisms. Theories to date treat only part of the problem--elastoplastic behavior of the composite material--and have not been able to treat the actual failure mode of the composite. The actual failures that have been observed seem to occur with the initiation of microscopic cracks at the boundary of the filament and the matrix and their subsequent propagation throughout the composite. The methodology presented in this report is a first attempt to realistically model this failure. The report complements other ongoing research and development now being sponsored by the Air Force, and should also be useful to the composite design community.

Dr. Adams, an Associate Professor of Mechanical Engineering at the University of Wyoming, is a consultant to The Rand Corporation.

SUMMARY

The behavior of materials under mechanical stress can be divided into three distinct regimes: (1) linear elastic response up to the elastic limit, (2) inelastic behavior beyond the elastic limit and up to that loading at which first failure occurs locally, and (3) subsequent crack propagation and total composite failure. The crack initiation and its subsequent propagation, described above as the third regime, is the subject of the present study.

A method has been developed for predicting the strength of a unidirectional composite material in terms of its micromechanical response to an applied stress. It includes elastoplastic material behavior, local failure that initiates a crack, and propagation of the crack to cause total failure of the composite.

Although the basic methodology is applicable to the general problem, a specific loading condition--transverse normal loading--has been selected for detailed analysis. It is often the transverse properties that limit the performance of the composite system. Therefore, this loading condition is of particular interest to composite materials technology because of the inherently low transverse strength of most high-performance composites.

The basic principles of the theory of plasticity have been combined with a finite element numerical analysis technique. The result is a rigorous analysis procedure capable of accurately modeling the complex boundary-value problem being considered, an initial step toward the ultimate goal of accurately predicting the strength of a material. A complete digital computer program has been developed as part of the investigation, permitting the ready application of the analysis to practical engineering problems. Because the primary goal of the study was to develop a method of analysis and to write an associated computer program, only limited numerical results have been obtained to date. These are discussed in detail, and examples demonstrating the type of information which can be obtained are given.

Finally, suggestions for a number of possible refinements and extensions of the present analysis are outlined, to encourage the

reader to use and to further develop the very promising analysis method discussed in this report. Problem areas for research range from improving the accuracy of the basic finite element solution technique to developing a more representative model of the propagating crack.

CONTENTS

SYMBOLS

$A = 6\tau_o^2 M_T$

A_n = area of nth triangular finite element

a, b = dimensions of the finite element grid

$B = 3\tau_o^2 + (1 + \nu)\frac{A}{E}$

$D = A + E s_{33}^2$

E = Young's modulus

f_{ij} = element node point forces

$[H]$ = plane strain elastoplastic stiffness matrix

$K = \Delta\bar{\sigma}_y / \Delta\bar{\sigma}_x$

$[K]$ = element stiffness matrix

$[\underline{K}]$ = array stiffness matrix

$2M_T$ = tangent modulus of the $\tau_o - \varepsilon_o^{(p)}$ curve

n = total number of node points in array

s_{ij} = deviatoric stress components

ΔT = incremental temperature change

$t_{\alpha\beta} = s_{\alpha\beta} + \nu s_{33}\delta_{\alpha\beta}$

u_i = displacement components

$\Delta u, \Delta v$ = boundary displacement increments

X_i = sum of forces acting at a node point

x_i = spatial coordinates

$x_{ij} = x_i - x_j$

$y_{ij} = y_i - y_j$

α = coefficient of thermal expansion

$\gamma_{xy}, \gamma_{zx}, \gamma_{zy}$ = engineering shear strain components

δ_{ij} = Kronecker delta

ε_x, ε_y, ε_z = normal strain components

ε_{12}, ε_{31}, ε_{32} = tensoral shear strain components

ε_{ij} = total strain components

$\varepsilon_{ij}^{(e)}$ = elastic strain components

$\varepsilon_{ij}^{(p)}$ = plastic strain components

$\varepsilon_o^{(p)}$ = octahedral plastic shear strain

$\dot{\lambda}$ = positive scalar function

ν = Poisson's ratio

σ_x, σ_y, σ_z = normal stress components

$\bar{\sigma}_x$, $\bar{\sigma}_y$, $\bar{\sigma}_z$ = components of average applied stress

$\Delta\bar{\sigma}_x$, $\Delta\bar{\sigma}_y$, $\Delta\bar{\sigma}_z$ = increments of applied stress

σ_{ij} = total stress components

τ_o = octahedral shear stress

τ_{xy}, τ_{zx}, τ_{zy} = shear stress components

Superscripts

(e) = elastic component

f = filament

i = boundary-value problem number

ℓ = elastic limit value

m = matrix

(p) = plastic component

T = transpose of a matrix

u = ultimate value

Subscripts

n = normal

t = tangential

I. INTRODUCTION

The behavior of materials can be divided into three distinct regimes: (1) linear elastic response up to the elastic limit, (2) inelastic behavior beyond the elastic limit and up to that loading at which first failure occurs locally, and (3) subsequent crack propagation and total composite failure. Behavior within the third regime is the subject of this report.

This investigation is a direct extension of work previously reported in Ref. 1, which had as its main topic behavior within the second of the regimes given above. Included in Ref. 1 is a brief review of the historical development of micromechanical analyses as applied to the important problem of understanding the transverse normal loading behavior of a unidirectional composite.

Transverse normal loading is of special interest in relation to unidirectional composites because of the very low transverse stiffness and strength characteristics of such materials relative to their stiffness and strength in the direction of reinforcement orientation. Since complex laminated composite systems are constructed of individual unidirectionally reinforced laminae bonded together, this highly anisotropic behavior exists within the individual lamina even when the laminated system is constructed to be nearly isotropic with respect to its gross properties. It is often the transverse properties that limit the performance of the composite system. But, since these properties are very low, there is a high potential for improvement.

For example, the transverse tensile strength of a unidirectionally reinforced, epoxy matrix composite is typically only 6000 to 8000 $lb/in.^2$, whereas the longitudinal tensile strength is often 150,000 to 200,000 $lb/in.^2$ or more. The tensile strength of the epoxy matrix itself is typically 12,000 to 15,000 $lb/in.^2$. Thus, with respect to transverse tensile strength, the presence of the filaments actually degrades the matrix material.

A detailed theoretical analysis is not needed to establish these characteristics of existing materials; they are regularly demonstrated

experimentally in the process of setting material property design allowables. Rather, the purpose of this micromechanical analysis, as well as those previously developed, is to provide a better understanding of the complex interactions between reinforcing filaments and the surrounding matrix material. With such an analysis, it is possible to perform a systematic study of the many variables that influence material behavior. Such variables include filament shape, filament packing geometry and spacings, filament and matrix mechanical properties, interface characteristics, the addition of filament coatings, and the presence of voids. Each of these can be accurately modeled using an analysis, and their influence on the gross behavior of the material system can be isolated. These same variables are usually difficult, if not impossible, to control accurately in an experiment.

This analysis of crack initiation and the subsequent propagation that leads to total failure is particularly directed toward the goal of predicting the ultimate strength of a composite material. There is currently no satisfactory method of prediction. However, since the strength of a material is governed by local effects (as opposed to composite stiffness, which is a gross response averaged over the entire material), it is reasonable to expect that a local or micromechanical analysis will be required. This investigation represents an initial step toward the ultimate goal of accurately predicting the strength of a material. The analysis is based firmly on the principles of solid mechanics. However, the specific methodology for modeling a crack and its propagation is relatively crude. In subsequent work, methods of applying the principles of fracture mechanics, which are rapidly being developed and improved upon, should be introduced. The finite element methodology that is used to obtain the numerical results given in Sec. IV also is being developed very rapidly at the present time. Improved element representations and larger, more economical digital computer facilities will have a very favorable influence on the subsequent progress of micromechanical analyses of this type.

A brief discussion of the major computational aspects of the finite element computer program and the data-plotting computer program that were developed as part of this investigation appears in Sec. III.

To the author's knowledge, this investigation represents the first attempt to predict crack initiation and propagation in a composite material.

II. METHOD OF ANALYSIS

PREVIOUS INVESTIGATIONS

Reference 1 gives details of the author's elastoplastic analysis of material behavior beyond the elastic limit and up to that transverse normal loading at which first failure occurs locally. The tangent modulus method of treating nonlinear material behavior and the Prandtl-Reuss flow rule are employed. A plane strain condition is assumed, and constant strain triangular finite elements are used. The stress-strain relationships representing each of the constituent materials are input point by point so that any monotonically increasing stress-strain curve can be considered; actual experimental data are typically used. Normal displacements at the boundaries must be specified in order to satisfy symmetry conditions for the boundary-value problem to be solved. It is usually of greater practical interest, however, to be able to specify instead the average normal stresses on each boundary (or more precisely, the ratio of these average normal stresses). To maintain this desired ratio exactly for each solution increment requires solving two separate boundary-value problems and superimposing the results in the proper ratio. This has been a standard procedure in prior works.[2] To reduce the required computer solution time by approximately one-half, a procedure was developed in Ref. 1 to estimate the boundary normal displacements required to produce the desired increments of average boundary normal stresses. Any deviation from the desired stress ratio was then corrected for in the succeeding increment. Quite satisfactory results were obtained using this predictor-corrector approach. A separate computer program was also written to prepare the output data for machine plotting of contours.

All of these features, with the exception of the predictor-corrector method, are retained in the analysis of crack initiation and propagation reported here. The predictor-corrector method was found to be insufficiently sensitive for the current application, as will be discussed in more detail in a subsequent subsection.

FILAMENT PACKING GEOMETRY

The physical problem to be considered is that of transverse normal loading of a unidirectionally reinforced composite, as illustrated in Fig. 1a. Assuming that the reinforcing filaments are oriented in the direction of the z-axis, as indicated, the x-y plane then represents the transverse loading plane. A normal loading component in the x-direction is illustrated in Fig. 1a.

In most composite materials, the filament packing is either completely random or exhibits only a very slight amount of preferred orientation, e.g., the nesting of filaments as the filament volume is increased. One exception is the relatively large diameter filaments such as those of boron (which, at approximately 0.004 in. in diameter, are an order of magnitude larger than most glass and graphite filaments in common use). These large diameter filaments are processed as monolayer tapes and tend to retain this layering characteristic in the finished part. This is particularly true when a woven-glass scrim-cloth backing layer is used to improve the manageability of the tape in fabrication.

A rigorous continuum mechanics analysis requires the establishment of a specific filament packing array, be it a periodic regular array or a random one. The problem of random filament packing, and a method of analyzing its influence on material properties, was discussed in Refs. 3 and 4. The necessity (in terms of computer storage capacity and running time) of selecting a representative material region sufficiently small to permit a detailed finite element representation and yet be physically meaningful makes the accurate modeling of a random array somewhat more difficult. Thus, in the current investigation, where the primary emphasis is on developing the concept of crack initiation and propagation, only regular packing geometries will be considered. The influence of randomness can be incorporated in subsequent investigations, as desired.

Two commonly assumed periodic regular arrays of filaments (cross sections in the x-y plane) are indicated in Figs. 1b and 1c. The rectangular array in Fig. 1b includes the square array as a special case (when $b = a$). The diamond array (sometimes called a staggered array) in Fig. 1c includes the hexagonal array as a special case (when $b = \sqrt{3}\, a$).

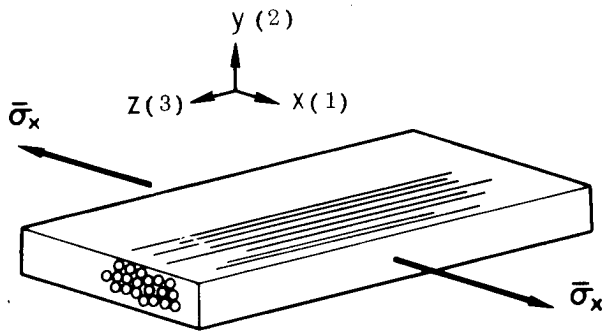

(a) Transverse normal loading of a unidirectionally reinforced composite

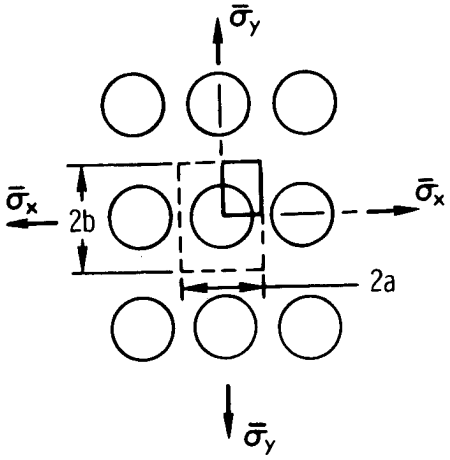

(b) Rectangular array

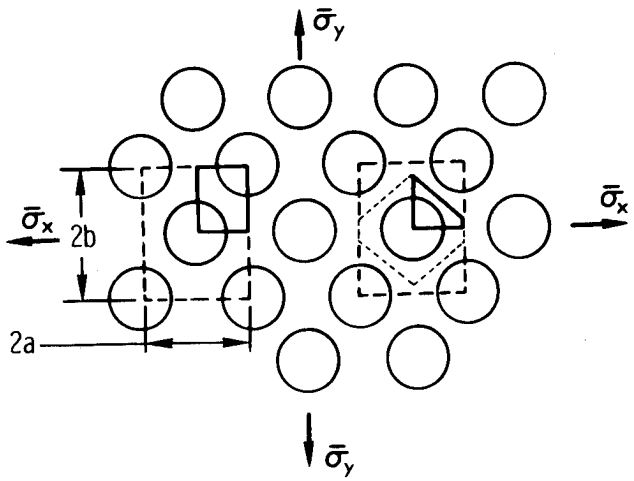

(c) Diamond array

Fig. 1 — Filament packing geometries

Because of the assumed periodicity, a typical repeating unit can be isolated in each case, as indicated in Figs. 1b and 1c. Only one quadrant of this repeating unit must be analyzed (two options are shown in the case of the diamond array), because of the assumed symmetry of the filament packing and the geometry of the individual filaments about both the x and y axes. The boundary conditions on the sides of the quadrant in Fig. 1b and the quadrant on the left side of Fig. 1c are identical. The sloping boundary of the element shown on the right side of Fig. 1c (solid lines) is defined as passing through the center of that quadrant of the repeating unit, i.e., it divides the quadrant in half. Either of the elements of Fig. 1c can be used, yielding identical results. The element on the left involves simpler boundary conditions; however, that on the right contains only one-half as much area and only one segment of filament-matrix interface. Thus, only one-half as many finite elements are required to define the area with the same resolution. This makes the use of the element on the right of Fig. 1c almost mandatory, based on economics alone. But the boundary conditions on the sloping boundary are more complicated, particularly for an elastoplastic analysis. This will be discussed in greater detail in Sec. VI. Only rectangular arrays will be analyzed in detail here since, to repeat, the main emphasis is on developing the concept of crack initiation and propagation.

The first quadrant of a typical repeating element, as indicated in Fig. 1b, is shown in Fig. 2. The cross-sectional geometry of the filament is arbitrary within the restriction that it must be symmetrical about both the x and y axes. Thus, a filament region of any arbitrary shape drawn in the first quadrant (Fig. 2) is allowable.

At one time there was considerable interest in using (glass) filaments of special shapes to enhance specific composite properties. For example, rectangular or hexagonal cross sections permit very high packing densities (theoretically, filament volumes as close to 100 percent as desired). Circular filaments in square and hexagonal arrays are limited to maximum filament volumes of 78.5 and 90.7 percent, respectively (when filaments are touching each other). Thus, the composite axial strength and stiffness will be higher for the specially shaped filaments. However,

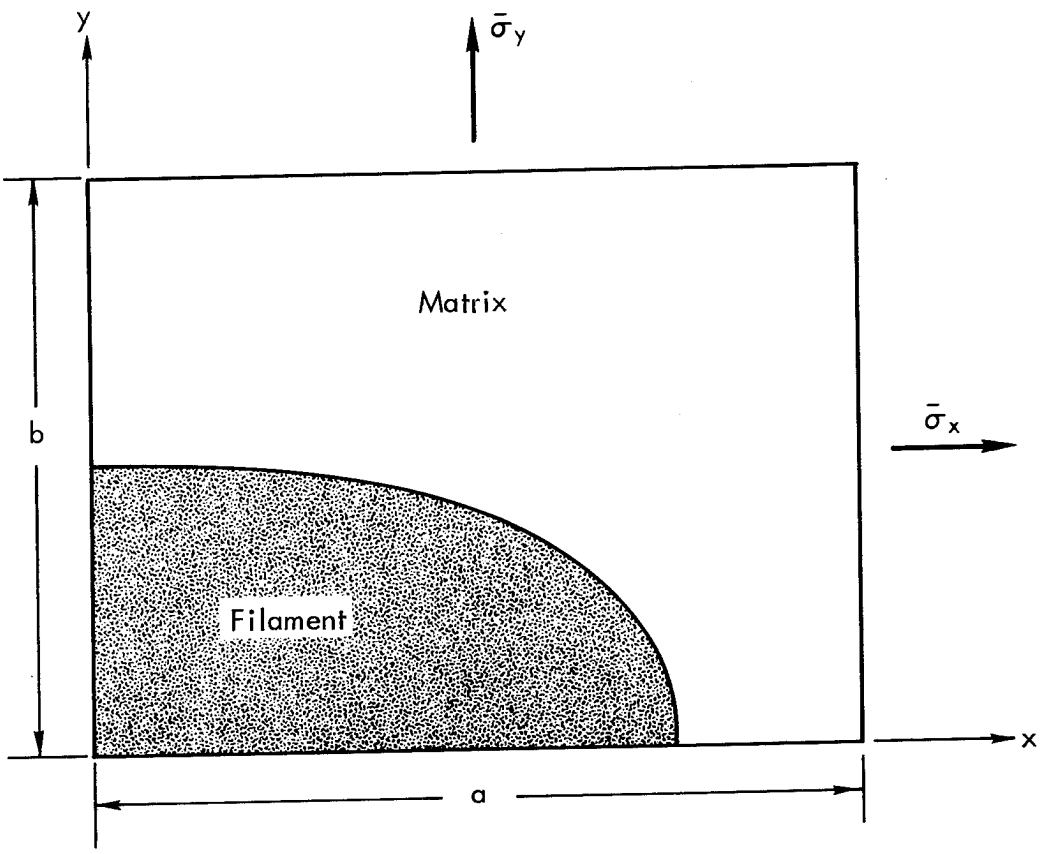

Fig. 2—First quadrant of a typical repeating unit

the difficulty of accurately placing the individual small filaments during fabrication to achieve the high packing densities, the fact that other important composite properties such as transverse normal and longitudinal shear strength are typically degraded, and perhaps most importantly, the introduction of high modulus filaments such as boron and graphite that are not produced by drawing from the melt (their shapes being relatively fixed) have resulted in a general loss of interest in shaped filaments as a method of controlling composite properties.

Boron filaments (boron deposited on a tungsten substrate) are circular in cross section. Graphite filaments produced from a PAN (polyacrylonitrile) precursor, which is circular, are approximately circular also. On the other hand, graphite filaments produced from a rayon precursor retain the irregular (crenulated) cross-sectional shape of this precursor material. Thus, there may be a renewed interest in the future in analyzing the influence of noncircular filament cross sections. The composite longitudinal shear strengths resulting from the use of rayon precursor graphite filaments, however, are typically low relative to PAN precursor graphite filament-reinforced composites. Whether this is due to the irregular shape of the rayon precursor filaments (creating unfavorable local shear stress concentrations) or to some other effect has not been established. This is a potential future application for an analysis similar to the one reported here. In the meantime, since this problem of low shear strength has not been resolved, more and more emphasis is being placed on PAN (and other) precursors, all of which result in a graphite filament of approximately circular cross section.

An interesting new organic filament developed by the DuPont Co.,[5] designated PRD-49-I, has very attractive dielectric as well as mechanical properties and a low density. It is also circular in cross section.

Thus, current interest in analyzing the influence of noncircular filaments is not very great. In this investigation, only examples of circular filaments have been used, but it should be emphasized that the analysis procedure is no more difficult for filaments of noncircular cross section. The necessary triangular element grid can be constructed just as readily, and the stress and displacement continuity requirements across the interface are automatically satisfied by the finite element formulation, independent of interface shape.

BOUNDARY CONDITIONS

Specific boundary conditions must be established along the sides of the material region to be analyzed--the first quadrant of the typical repeating element indicated in Fig. 2. Since a two-dimensional (plane strain) analysis is being used, two conditions must be prescribed at each point on the boundaries. When the entire composite body is subjected to any combination of average transverse normal stresses $\bar{\sigma}_x$ and $\bar{\sigma}_y$, as indicated in Fig. 1, a complex state of stress is induced locally within the material. This is the result of the dissimilar material properties of the filaments and surrounding matrix and also a result of interactions between filaments. Thus, the stress distributions along the boundaries of the first quadrant are unknown even though the average of the normal stresses acting along each side must equal the corresponding applied stress $\bar{\sigma}_x$ or $\bar{\sigma}_y$, from equilibrium considerations; and it is not possible to establish normal stress boundary conditions. Because of the assumed symmetry, however, the rectangular repeating element and its first quadrant (bounded by lines of symmetry) remain rectangular when transverse normal loads are applied; the normal component of displacement of each point on a given boundary of the first quadrant is identical. Thus, an arbitrary normal displacement of each boundary can be specified, and, because of the assumed symmetry, no shear stresses exist along the boundaries of the first quadrant.

These then are the two conditions to be specified at each boundary point: a uniform normal displacement and a zero shear stress.

Two boundary conditions must also be specified at each point on the interface between dissimilar materials, e.g., at the filament-matrix interface. Normally, it is desired to completely bond the filaments to the surrounding matrix during the fabrication process. In the analytical model, this corresponds to the specification of interface continuity conditions for both displacements and stresses, i.e.,

$$u_n^f = u_n^m, \qquad u_t^f = u_t^m$$

and

$$\sigma_n^f = \sigma_n^m, \qquad \tau_{nt}^f = \tau_{nt}^m$$

where the superscripts f and m represent filament and matrix, the subscripts n and t represent directions normal and tangent to the interface, and σ and τ represent the normal stress and shear stress. This is usually termed a perfect bond. When using the finite element method, these interface continuity conditions are automatically satisfied during the process of assembling elements at an interface node point.

In certain applications, interface boundary conditions other than the above continuity conditions may be desired. For example, it may be desired to model the effect of a lack of interface bond in a local region (perhaps due to a poor fabrication technique) or some similar initial defect. The interface boundary conditions can be modified accordingly.

CONSTITUTIVE RELATIONS

The material region of interest, as introduced in the preceding subsections, is to be incrementally loaded along its boundaries. As will be discussed quantitatively in Sec. IV, a suitable matrix material for use in a composite is typically selected for its ability to deform extensively without failing. This permits the large strain concentrations induced in the matrix region between adjacent filaments to be accommodated more readily. In real materials, most of this strain-to-failure occurs beyond the linearly elastic range of behavior. Thus, for loading beyond the elastic limit, the elastoplastic response of the material must be considered and a suitable constitutive relation derived.

The present analysis is not restricted to monotonic loading. Thus, material unloading from the elastoplastic region may occur, requiring that an unloading criterion be established also. It will be assumed that the material unloads linearly elastically, with a modulus equal to the initial Young's modulus. If reloading subsequently occurs, it is assumed that the material follows this same linear stress-strain response until it attains the state from which it began to unload. For additional loading beyond this point, the response is assumed to continue along the original elastoplastic curve.

The general constitutive relations that govern the elastoplastic response can be derived as follows. For each loading increment beyond the elastic limit, the corresponding increment of strain at any point in

the material region can be separated into an elastic (recoverable) and a plastic (irrecoverable) portion, i.e.,

$$\dot{\varepsilon}_{ij} = \dot{\varepsilon}_{ij}^{(e)} + \dot{\varepsilon}_{ij}^{(p)} \tag{1}$$

The elastic portion follows the generalized Hooke's law,

$$\dot{\varepsilon}_{ij}^{(e)} = \frac{1-2\nu}{3E} \dot{\sigma}_{kk}\delta_{ij} + \frac{1+\nu}{E} \dot{s}_{ij} \tag{2}$$

where

$$\dot{s}_{ij} = \dot{\sigma}_{ij} - \frac{1}{3} \dot{\sigma}_{kk}\delta_{ij} \tag{3}$$

is the deviatoric component of the rate of stress tensor $\dot{\sigma}_{ij}$, δ_{ij} is the Kronecker delta, and E and ν are the material Young's modulus and Poisson's ratio, respectively. The usual conventions of indicial notation apply. Latin indices have the range 1, 2, 3 and Greek 1, 2.

The plastic portion is assumed to obey the Prandtl-Reuss flow rule:

$$\dot{\varepsilon}_{ij}^{(p)} = \dot{\lambda} s_{ij} \tag{4}$$

where $\dot{\lambda}$ is a positive scalar function, in general a function of both time and the spatial coordinates, and s_{ij} bears the same relationship to σ_{ij} as $\dot{s}_{ij}$ to $\dot{\sigma}_{ij}$, indicated in Eq. (3). The key assumption is that the rate of change of the plastic strain is at any instant proportional to the deviatoric stress. It is also assumed, as in most plasticity theories, that there is no permanent change of volume. In other words, the plastic component of the mean normal strain is zero; the deviatoric components of the plastic strain are identical to the plastic strain components. The Prandtl-Reuss flow rule is particularly applicable to the case of contained plastic flow, which is typical of the condition existing in the composite material geometries being considered here.

In such a case, the region of elastoplastic material behavior is typically surrounded or contained by elastic material. Thus, the magnitudes of the elastic and plastic components of strain are comparable.

The Prandtl-Reuss flow rule does not model viscosity, i.e., time-dependent, effects. However, most of the composite materials in common use, e.g., the metal matrix composites and those incorporating a high polymer matrix such as an epoxy, do not exhibit a significant time-dependent response at ambient temperatures. Thus, this is not usually an important limitation.

The Prandtl-Reuss flow rule is the one most frequently used today primarily because of its more general applicability and ease of implementation. Other flow rules that incorporate specific restrictive assumptions also are occasionally used. For example, the assumption of complete incompressibility may greatly simplify an analysis, and provide adequate accuracy in some problems. Also, if the plastic flow is unrestricted rather than contained, so that the plastic strains are much larger than the elastic strains, the latter can often be neglected, resulting in a simpler rigid-plastic analysis.

In the applications considered in this report, however, these various simplifying assumptions are not adequate and will not be used. Rather, the Prandtl-Reuss flow rule as represented by Eq. (4) will be incorporated into the analysis directly.

To put $\dot{\lambda}$ into a usable form for present purposes, Eq. (4) can be multiplied by itself and solved for $\dot{\lambda}$ to give

$$\dot{\lambda} = \frac{(\dot{\varepsilon}_{ij}^{(p)} \dot{\varepsilon}_{ij}^{(p)})^{\frac{1}{2}}}{(s_{kl} s_{kl})^{\frac{1}{2}}} \tag{5}$$

Defining the octahedral plastic shear strain rate as

$$\dot{\varepsilon}_o^{(p)} = (\frac{1}{3} \dot{\varepsilon}_{ij}^{(p)} \dot{\varepsilon}_{ij}^{(p)})^{\frac{1}{2}} \tag{6}$$

and the octahedral shear stress as

$$\tau_o = (\frac{1}{3} s_{ij} s_{ij})^{\frac{1}{2}} \tag{7}$$

Eq. (5) can be rewritten as

$$\dot{\lambda} = \frac{\dot{\varepsilon}_o^{(p)}}{\tau_o} \tag{8}$$

thus defining the positive scalar function $\dot{\lambda}$ in Eq. (4), which becomes

$$\dot{\varepsilon}_{ij}^{(p)} = \frac{\dot{\varepsilon}_o^{(p)}}{\tau_o} s_{ij} \tag{9}$$

Now a relationship must be established between $\dot{\varepsilon}_o^{(p)}$ and τ_o. This can be done by applying Eq. (9) to a problem for which both $\dot{\varepsilon}_o^{(p)}$ and τ_o are known. For example, since we will be interested in using actual constituent material experimental data in generating numerical results, we can employ the results of a simple uniaxial test, for which

$$\sigma_{11} \neq 0, \quad \sigma_{22} = \sigma_{33} = \sigma_{12} = \sigma_{13} = \sigma_{23} = 0 \tag{10a}$$

and

$$\begin{aligned} &\dot{\varepsilon}_{11}^{(p)} \neq 0, \quad \dot{\varepsilon}_{22}^{(p)} = \dot{\varepsilon}_{33}^{(p)} = -\frac{1}{2}\dot{\varepsilon}_{11}^{(p)}, \\ &\dot{\varepsilon}_{12}^{(p)} = \dot{\varepsilon}_{13}^{(p)} = \dot{\varepsilon}_{23}^{(p)} = 0 \end{aligned} \tag{10b}$$

Substituting Eqs. (10b) into Eq. (6) and solving for $\dot{\varepsilon}_{11}^{(p)}$ gives

$$\dot{\varepsilon}_{11}^{(p)} = \sqrt{2}\,\dot{\varepsilon}_o^{(p)} \tag{11}$$

Since σ_{11} and $\dot{\varepsilon}_{11}^{(p)}$ are uniform throughout the test specimen, they are functions of t only, and Eq. (11) can be rewritten as

$$\dot{\varepsilon}_{11}^{(p)} = \sqrt{2}\frac{d\varepsilon_o^{(p)}}{dt} = \sqrt{2}\frac{d\varepsilon_o^{(p)}}{d\tau_o}\frac{d\tau_o}{dt} = \frac{\sqrt{2}\,\dot{\tau}_o}{2M_T} \tag{12}$$

where, by definition, $2M_T = d\tau_o/d\varepsilon_o^{(p)}$ is the tangent modulus of the octahedral shear stress-octahedral plastic shear strain curve for the elastoplastic material, and

$$\dot{\tau}_o = \frac{s_{ij}\dot{s}_{ij}}{3\tau_o} \tag{13}$$

is obtained by differentiating Eq. (7). Substituting the rate of plastic strain values defined by Eqs. (10b) and (12) into Eq. (6), we obtain

$$\dot{\varepsilon}_o^{(p)} = \frac{\dot{\tau}_o}{2M_T} \tag{14}$$

Substituting Eq. (14) into Eq. (9) gives

$$\dot{\varepsilon}_{ij}^{(p)} = \frac{\dot{\tau}_o s_{ij}}{2\tau_o M_T} \tag{15}$$

This is the form of the Prandtl-Reuss flow rule desired.

Substituting Eqs. (2) and (15) into Eq. (1), the constitutive relations can be expressed as

$$\dot{\varepsilon}_{ij} = \frac{1-2\nu}{3E}\dot{\sigma}_{kk}\delta_{ij} + \frac{1+\nu}{E}\dot{s}_{ij} + \frac{\dot{\tau}_o s_{ij}}{2\tau_o M_T} \tag{16}$$

Substituting Eqs. (3) and (13) into Eq. (16) and rearranging terms gives

$$\dot{\varepsilon}_{ij} = \frac{1+\nu}{E}\dot{\sigma}_{ij} - \frac{\nu}{E}\dot{\sigma}_{kk}\delta_{ij} + \frac{s_{ij}s_{kl}\dot{\sigma}_{kl}}{6\tau_o^2 M_T} \tag{17}$$

In obtaining the last term, use has been made of the fact that no plastic work is done by the hydrostatic component of the applied stress,[6] i.e.,

$$s_{kl}\dot{s}_{kl} = s_{kl}(\dot{\sigma}_{kl} - \frac{1}{3}\dot{\sigma}_{mm}\delta_{kl}) = s_{kl}\dot{\sigma}_{kl}$$

since

$$s_{kl}\dot{\sigma}_{mm} = 0$$

Equation (17) is the general flow rule relating the total strain and stress increments.

Ideally, a full three-dimensional analysis of the boundary-value problem outlined in the previous subsection would be preferred. This would permit the consideration of stress and strain gradients in the direction of filament reinforcement (the 3-direction indicated in Fig. 1a) as well as in the transverse (1-2) plane. For example, it would be possible to analyze the behavior of discontinuous reinforcements such as whiskers and chopped fibers (as in the transfer of stresses at the fiber ends into adjacent fibers) and particulate-reinforced composites. It would also facilitate the modeling of voids, local debonding, and similar manufacturing defects. The analytical formulation of a truly three-dimensional model is straightforward, and the above derivation is directly applicable. However, even for a two-dimensional analysis, the complexity of the boundary-value problem makes a numerical solution technique mandatory. Large amounts of digital computer storage are required and the computer running times are relatively long. The present generation of digital computers, e.g., the IBM Model 360 and its counterparts, do not have sufficient storage capacity and computational speed to make practical three-dimensional analyses feasible. The same type of comments applied to the analysis being presented here just a few years ago, when computers such as the IBM Model 7094 and its counterparts were typically being used--it would have been difficult to overcome storage limitations, and computer running times required would have been prohibitive in most cases. In the future, solutions of truly three-dimensional practical problems will undoubtedly be routinely performed. Now, however, certain idealizations must be made in order to make the problem amenable to practical solution.

One way of achieving this is to reduce the problem to a two-dimensional formulation. Since we are interested in composite material response in the transverse plane, it is logical to assume that stress

and strain gradients in the axial direction (the 3-direction in Fig. 1a) are negligible relative to those in the transverse plane. This is the classical plane stress or plane strain condition. A plane stress condition assumes that the stress in the direction normal to the plane of interest (the σ_{33} component of stress, normal to the 1-2 plane in Fig. 1a) is zero, and is usually associated with the analysis of thin plates (thin in the 3-direction) subjected to in-plane loadings. But for a continuous-filament-reinforced lamina, as indicated in Fig. 1a, the dimension in the direction of reinforcement (the 3-direction) is typically very large. This corresponds more closely to the plane strain condition, i.e., zero displacement in the 3-direction. Since there are assumed to be no gradients in the 3-direction, the strains ε_{i3} and correspondingly the increments of strain $\dot{\varepsilon}_{i3}$ are equal to zero, i.e.,

$$\begin{aligned} \dot{\varepsilon}_{13} &= \frac{\partial \dot{u}_1}{\partial x_3} + \frac{\partial \dot{u}_3}{\partial x_1} = 0 \\ \dot{\varepsilon}_{23} &= \frac{\partial \dot{u}_2}{\partial x_3} + \frac{\partial \dot{u}_3}{\partial x_2} = 0 \\ \dot{\varepsilon}_{33} &= \frac{\partial \dot{u}_3}{\partial x_3} = 0 \end{aligned} \tag{18}$$

where $\dot{u}_i$ and $\dot{x}_i$ represent the displacement increment components and spatial coordinates, respectively.

For plane strain,

$$\dot{\sigma}_{13} = \dot{\sigma}_{23} = 0 \tag{19}$$

as can be verified by substitution into Eq. (17), using Eqs. (18).

Although, by definition, the axial strain increment $\dot{\varepsilon}_{33}$ is zero everywhere, the axial stress increment $\dot{\sigma}_{33}$ is not. It is not an independent quantity, however, and can be expressed in terms of the other nonzero stress increment components as follows. Setting $i = j = 3$ in Eq. (17), we obtain

$$(1 + \nu)\ \dot{\sigma}_{33} - \nu\dot{\sigma}_{kk} + \frac{E}{A}\, s_{33}s_{k1}\dot{\sigma}_{k1} = 0 \tag{20}$$

where $A = 6\tau_o^2 M_T$. Solving Eq. (20) for $\dot{\sigma}_{33}$,

$$\dot{\sigma}_{33} - \nu\dot{\sigma}_{\gamma\gamma} + \frac{E}{A}\, s_{33}s_{33}\dot{\sigma}_{33} + \frac{E}{A}\, s_{33}s_{\gamma\delta}\dot{\sigma}_{\gamma\delta} = 0$$

or

$$\dot{\sigma}_{33}\left(\frac{A + Es_{33}s_{33}}{A}\right) = \nu\dot{\sigma}_{\gamma\gamma} - \frac{E}{A}\, s_{33}s_{\gamma\delta}\dot{\sigma}_{\gamma\delta}$$

or

$$\dot{\sigma}_{33} = \frac{1}{D}\,(A\nu\dot{\sigma}_{\gamma\gamma} - Es_{33}s_{\gamma\delta}\dot{\sigma}_{\gamma\delta}) \tag{21}$$

where

$$D = A + Es_{33}^2$$

and where, as previously noted, the Greek indices have the range 1, 2.

Utilizing Eqs. (19), Eq. (21) can be substituted into Eq. (17) to give

$$\dot{\varepsilon}_{\alpha\beta} = \frac{1+\nu}{E}\,\dot{\sigma}_{\alpha\beta} - \frac{\nu}{E}\,\delta_{\alpha\beta}\left(\dot{\sigma}_{\gamma\gamma} + \frac{A\nu\dot{\sigma}_{\gamma\gamma} - Es_{33}s_{\gamma\delta}\dot{\sigma}_{\gamma\delta}}{D}\right)$$

$$+ \frac{s_{\alpha\beta}s_{\gamma\delta}\dot{\sigma}_{\gamma\delta}}{A} + \frac{s_{\alpha\beta}s_{33}}{A}\left(\frac{A\nu\dot{\sigma}_{\gamma\gamma} - Es_{33}s_{\gamma\delta}\dot{\sigma}_{\gamma\delta}}{D}\right)$$

Collecting terms in $\dot{\sigma}_{\gamma\gamma}$ and $\dot{\sigma}_{\gamma\delta}$ gives

$$\dot{\varepsilon}_{\alpha\beta} = \frac{1+\nu}{E}\,\dot{\sigma}_{\alpha\beta} - \left[\frac{\nu}{E}\,\delta_{\alpha\beta}\left(\frac{D + A\nu}{D}\right) - \frac{\nu s_{\alpha\beta}s_{33}}{D}\right]\dot{\sigma}_{\gamma\gamma}$$

$$+ \left[\frac{\nu}{D}\,\delta_{\alpha\beta}s_{33}s_{\gamma\delta} + \frac{s_{\alpha\beta}s_{\gamma\delta}}{A} - \frac{E}{AD}\,s_{\alpha\beta}s_{33}^2 s_{\gamma\delta}\right]\dot{\sigma}_{\gamma\delta}$$

or, making use of the relation $D = A + Es_{33}^2$,

$$\dot{\varepsilon}_{\alpha\beta} = \frac{1+\nu}{E}\dot{\sigma}_{\alpha\beta} - \left[\frac{\nu}{E}\delta_{\alpha\beta}\frac{A(1+\nu)}{D} + \frac{\nu\delta_{\alpha\beta}s_{33}^2}{D} - \frac{\nu s_{\alpha\beta}s_{33}}{D}\right]\dot{\sigma}_{\gamma\gamma}$$

$$+\left[\frac{\nu}{D}\delta_{\alpha\beta}s_{33}s_{\gamma\delta} + \frac{s_{\alpha\beta}s_{\gamma\delta}}{\cancel{A}}\left(\frac{\cancel{A} + \cancel{Es_{33}^2} - \cancel{Es_{33}^2}}{D}\right)\right]\dot{\sigma}_{\gamma\delta}$$

Removing the common denominator D and rearranging terms gives

$$\dot{\varepsilon}_{\alpha\beta} = \frac{1+\nu}{E}\dot{\sigma}_{\alpha\beta} + \frac{1}{D}\Big[-\nu(1+\nu)\frac{A}{E}\delta_{\alpha\beta}\dot{\sigma}_{\gamma\gamma}$$

$$+ \nu s_{33}(s_{\alpha\beta} - s_{33}\delta_{\alpha\beta})\dot{\sigma}_{\gamma\gamma} \qquad (22)$$

$$+ (\nu s_{33}\delta_{\alpha\beta} + s_{\alpha\beta})s_{\gamma\delta}\dot{\sigma}_{\gamma\delta}\Big]$$

Equation (22) is equivalent to Eq. (9) of Ref. 4, as demonstrated by Swedlow as follows. Let

$$s_{\alpha\beta} = t_{\alpha\beta} - \nu s_{33}\delta_{\alpha\beta} \qquad (23)$$

Equation (22) becomes

$$\dot{\varepsilon}_{\alpha\beta} = \frac{1+\nu}{E}\dot{\sigma}_{\alpha\beta} + \frac{1}{D}\Big\{-\nu(1+\nu)\frac{A}{E}\delta_{\alpha\beta}\dot{\sigma}_{\gamma\gamma}$$

$$+ \nu s_{33}\left[t_{\alpha\beta} - (1+\nu)s_{33}\delta_{\alpha\beta}\right]\dot{\sigma}_{\gamma\gamma} + t_{\alpha\beta}s_{\gamma\delta}\dot{\sigma}_{\gamma\delta}\Big\}$$

Collecting terms on $\nu(1+\nu)$ and $t_{\alpha\beta}$ gives

$$\dot{\varepsilon}_{\alpha\beta} = \frac{1+\nu}{E}\dot{\sigma}_{\alpha\beta} + \frac{1}{D}\Big[-\nu(1+\nu)\left(\frac{A}{E} + s_{33}^2\right)\delta_{\alpha\beta}\dot{\sigma}_{\gamma\gamma}$$

$$+ t_{\alpha\beta}(\nu s_{33}\dot{\sigma}_{\gamma\gamma} + s_{\gamma\delta}\dot{\sigma}_{\gamma\delta})\Big] \qquad (24)$$

Noting that $(\frac{A}{E} + s_{33}^2) = \frac{D}{E}$, $\dot{\sigma}_{\gamma\gamma} = \dot{\sigma}_{\gamma\delta}\delta_{\gamma\delta}$, and, as previously defined, $(\nu s_{33}\delta_{\gamma\delta} + s_{\gamma\delta}) = t_{\gamma\delta}$, the above equation reduces to

$$\dot{\varepsilon}_{\alpha\beta} = \frac{1+\nu}{E}\dot{\sigma}_{\alpha\beta} + \frac{1}{D}\left[-\nu(1+\nu)\frac{D}{E}\delta_{\alpha\beta}\dot{\sigma}_{\gamma\gamma} + t_{\alpha\beta}t_{\gamma\delta}\dot{\sigma}_{\gamma\delta}\right]$$

or

$$\dot{\varepsilon}_{\alpha\beta} = \frac{1+\nu}{E}(\dot{\sigma}_{\alpha\beta} - \nu\dot{\sigma}_{\gamma\gamma}\delta_{\alpha\beta}) + \frac{1}{D}t_{\alpha\beta}t_{\gamma\delta}\dot{\sigma}_{\gamma\delta} \tag{25}$$

which is Eq. (5) of Ref. 7.

The finite element numerical analysis will be formulated and solved in terms of displacement components. Thus, the inverse of Eq. (25) is needed so that stresses, and thus node point forces, can be readily expressed in terms of strain components, which in turn are simple functions of the displacements.

The inverse of Eq. (25) is

$$\dot{\sigma}_{\alpha\beta} = \frac{E}{1+\nu}\left[\dot{\varepsilon}_{\alpha\beta} + \frac{\nu}{1-2\nu}\dot{\varepsilon}_{\gamma\gamma}\delta_{\alpha\beta} - \frac{s_{\alpha\beta}s_{\gamma\delta}\dot{\varepsilon}_{\gamma\delta}}{3\tau_o^2 + (1+\nu)A/E}\right] \tag{26}$$

Methods of obtaining this inverse are given in Appendix A. (It should be noted that there is a minor typographical error in the inverse given as Eq. (6) in Ref. 7; M_T should be $2M_T$--the factor 2 is missing.)

Equation (26) will be used extensively in the subsequent development of the finite element representation. For this purpose it is convenient to expand Eq. (26) into the three equations it represents, i.e., $\dot{\sigma}_{11}$, $\dot{\sigma}_{22}$, and $\dot{\sigma}_{12}$. The index notation will also be changed at this point to conventional engineering notation. Thus, $\dot{\sigma}_{11}$, $\dot{\sigma}_{22}$, $\dot{\sigma}_{12}$, $\dot{\varepsilon}_{11}$, $\dot{\varepsilon}_{22}$, $\dot{\varepsilon}_{12}$ will be replaced by $\dot{\sigma}_x$, $\dot{\sigma}_y$, $\dot{\tau}_{xy}$, $\dot{\varepsilon}_x$, $\dot{\varepsilon}_y$, $\frac{1}{2}\dot{\gamma}_{xy}$, respectively. This notation is more consistent with that used in previously published micromechanics and finite element analyses.

Note in particular that $\dot{\varepsilon}_{12}$ has been replaced by $\frac{1}{2}\dot{\gamma}_{xy}$, to convert from tensoral shear strain to engineering shear strain. Engineering shear strain will be used throughout the remainder of this analysis.

Expanding Eq. (26):

$$\dot{\sigma}_x = \frac{E}{1+\nu}\left[\left(1 + \frac{\nu}{1-2\nu} - \frac{s_{11}^2}{B}\right)\dot{\varepsilon}_x + \left(\frac{\nu}{1-2\nu} - \frac{s_{11}s_{22}}{B}\right)\dot{\varepsilon}_y - \left(\frac{2s_{11}s_{12}}{B}\right)\frac{1}{2}\dot{\gamma}_{xy}\right]$$

or

$$\dot{\sigma}_x = \frac{E}{1+\nu}\left[\left(\frac{1-\nu}{1-2\nu} - \frac{s_{11}^2}{B}\right)\dot{\varepsilon}_x + \left(\frac{\nu}{1-2\nu} - \frac{s_{11}s_{22}}{B}\right)\dot{\varepsilon}_y - \left(\frac{s_{11}s_{12}}{B}\right)\dot{\gamma}_{xy}\right] \tag{27}$$

where

$$B = 3\tau_o^2 + (1 + \nu)\frac{A}{E}$$

Correspondingly, for $\dot{\sigma}_y$ and $\dot{\tau}_{xy}$,

$$\dot{\sigma}_y = \frac{E}{1+\nu}\left[\left(\frac{\nu}{1-2\nu} - \frac{s_{11}s_{22}}{B}\right)\dot{\varepsilon}_x + \left(\frac{1-\nu}{1-2\nu} - \frac{s_{22}^2}{B}\right)\dot{\varepsilon}_y - \left(\frac{s_{22}s_{12}}{B}\right)\dot{\gamma}_{xy}\right] \tag{28}$$

$$\dot{\tau}_{xy} = \frac{E}{1+\nu}\left[-\left(\frac{s_{11}s_{12}}{B}\right)\dot{\varepsilon}_x - \left(\frac{s_{22}s_{12}}{B}\right)\dot{\varepsilon}_y + \left(\frac{1}{2} - \frac{s_{12}^2}{B}\right)\dot{\gamma}_{xy}\right] \tag{29}$$

Equations (27), (28), and (29) can be expressed in matrix notation as

$$[\dot{\sigma}] = [H][\dot{\varepsilon}] \tag{30}$$

where

$$[\dot{\sigma}] = \begin{bmatrix} \dot{\sigma}_x \\ \dot{\sigma}_y \\ \dot{\tau}_{xy} \end{bmatrix}, \qquad [\dot{\varepsilon}] = \begin{bmatrix} \dot{\varepsilon}_x \\ \dot{\varepsilon}_y \\ \dot{\gamma}_{xy} \end{bmatrix}$$

$$[H] = \frac{E}{1+\nu} \begin{bmatrix} \left(\frac{1-\nu}{1-2\nu} - \frac{s_{11}^2}{B}\right) & \left(\frac{\nu}{1-2\nu} - \frac{s_{11}s_{22}}{B}\right) & \left(-\frac{s_{11}s_{12}}{B}\right) \\ \left(\frac{\nu}{1-2\nu} - \frac{s_{11}s_{22}}{B}\right) & \left(\frac{1-\nu}{1-2\nu} - \frac{s_{22}^2}{B}\right) & \left(-\frac{s_{22}s_{12}}{B}\right) \\ \left(-\frac{s_{11}s_{12}}{B}\right) & \left(-\frac{s_{22}s_{12}}{B}\right) & \left(\frac{1}{2} - \frac{s_{12}^2}{B}\right) \end{bmatrix}$$

Note that [H] is a symmetric matrix.

FINITE ELEMENT REPRESENTATION

Even when the filament packing has been idealized to a periodic regular array and the stress distribution reduced to a two-dimensional plane strain condition, the resulting elastoplastic boundary-value problem is not amenable to a closed-form analytical solution. This also was true in prior elastic micromechanics studies, which led to the application of several different numerical analyses, including stress function, finite difference, and finite element formulations. An historical review of these developments may be found in Ref. 3. Primarily because of the greater ease of representing the irregular material regions and boundaries (such as those indicated in Figs. 1 and 2), the finite element analysis has clearly emerged as the preferred method.

The basic finite element analysis methodology has become well-developed in recent years, and has been used extensively in structural analysis applications. A number of texts are now available, e.g., that by Zienkiewicz,[8] which describe the method in detail. Particular emphasis today is on the development of improved element representations, including three-dimensional elements.

Constant strain triangular elements have been used in this investigation. That is, the displacement field in each triangular element is assumed to be linear. The first step is to divide the material region of interest into triangular elements, as is indicated in Fig. 3. As a general rule, the individual elements should be compact, i.e., shaped as close to equilateral triangles as is practical to best represent the assumed constant strain condition within each element.

The amount of computer solution time required is a direct function of the number of element node points. The strain field can thus be most accurately determined, for a given number of node points, by using small elements in regions where gradients are expected to be high (for example, in regions between directly adjacent filaments such as along the x and y axes of Fig. 3), and larger elements elsewhere. However, this procedure is not completely satisfactory for the present crack propagation analysis. As the numerical results will indicate, it is not always readily apparent beforehand where the crack will initiate, or where it will propagate to. Also, once the crack propagation process begins, there will be a significant redistribution of strains, particularly near the crack tip. To achieve total failure, the crack must eventually propagate across the entire material region. Thus, it is better to keep the grid array relatively uniform in size.

Of course, one constituent material may be much stronger than the other (or others, if more than two constituents are represented), so that crack propagation is certain to occur only in the weaker constituent. In this case, a coarser grid can be used in the region of strong material in order to conserve node points. Such a grid is indicated in Fig. 3, where the circular filament region is represented by a coarser grid than the surrounding matrix region. The displacement of a given node point is, however, a function of the displacements of all of the immediately surrounding node points (and the material properties of the elements they bound). Thus, for the local strain gradients to be reasonably represented from element to element, it is desirable to use a transition from small to large elements, as is indicated in Fig. 3, rather than an abrupt change. Each node point and each element must be numbered for

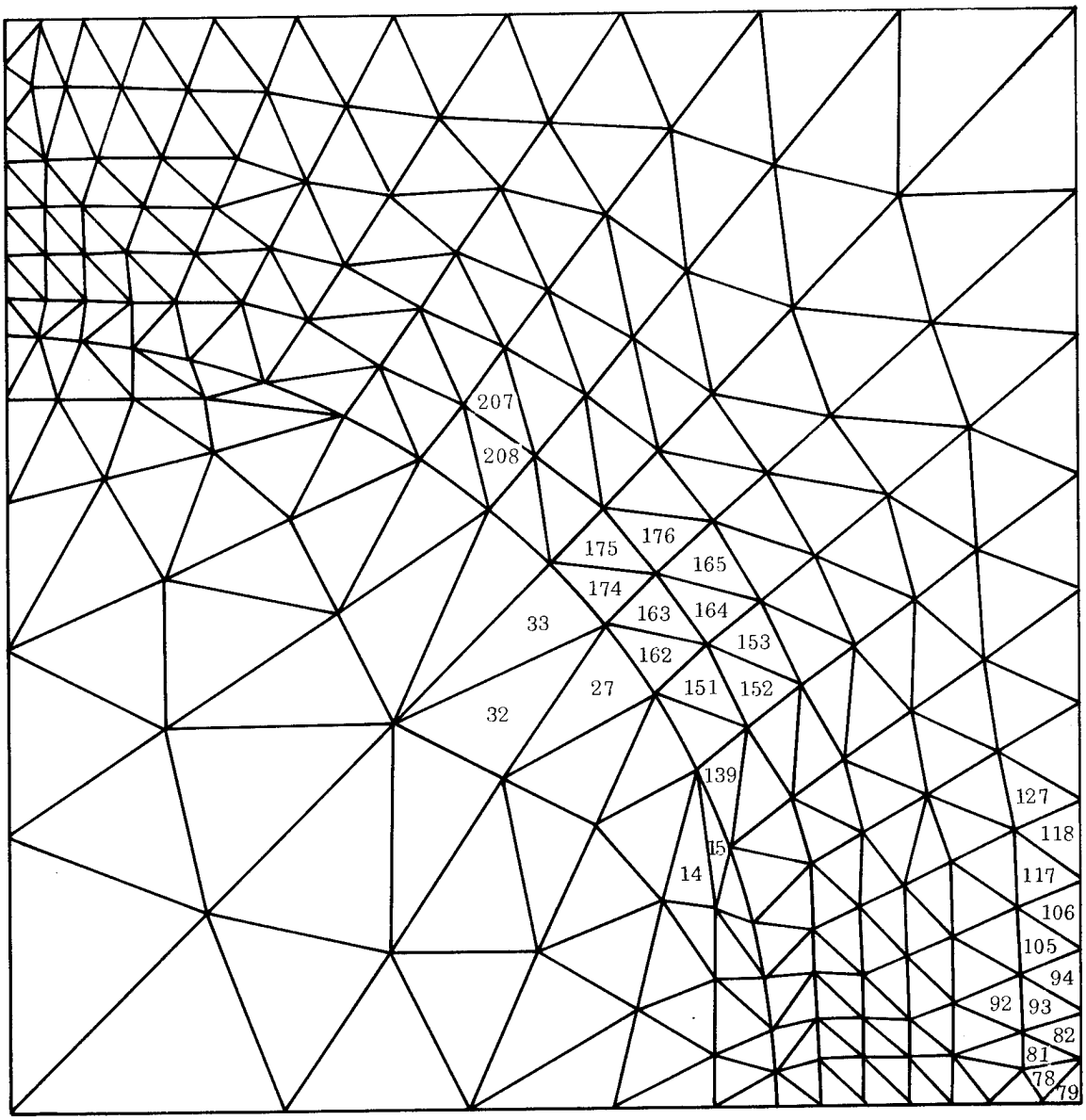

Fig. 3 — Typical finite element grid: square array, 40-percent filament volume, 176 nodes, 304 elements

identification. For clarity, in Fig. 3 only the numbers of those elements that are specifically referred to in Sec. IV or Appendix B are shown.

Having constructed a suitable finite element grid, each triangular element is defined by the x, y coordinates of its three node points, i, j, k, as indicated in Fig. 4--i.e., x_i, y_i, x_j, y_j, x_k, y_k. Because of the nonlinear (elastoplastic) material behavior, the loading is to be applied in small increments beyond the elastic limit, as will be described in the next subsection. For each load increment, the increment of displacement of any point within an element can be represented as

$$\begin{aligned} \dot{u} &= \alpha_1 x + \alpha_2 y + \alpha_3 \\ \dot{v} &= \beta_1 x + \beta_2 y + \beta_3 \end{aligned} \tag{31}$$

where $\dot{u}$ and $\dot{v}$ are the x and y components, respectively, of the increment of displacement of any point in the element. The six constants represented by the α and β coefficients can be evaluated by substituting the values of $\dot{u}$, $\dot{v}$, x, and y for each of the three node points of the element into Eqs. (31). The resulting three equations containing the three unknown α constants can then be solved simultaneously to evaluate α_1, α_2, α_3. The remaining three equations correspondingly yield β_1, β_2, β_3. Substituting these values of α and β into Eqs. (31) gives

$$\begin{aligned} \dot{u} = \frac{1}{2A_n} \Big\{ & \Big[(x_j y_k - x_k y_j) + y_{jk} x + x_{kj} y \Big] \dot{u}_i \\ & + \Big[(x_k y_i - x_i y_k) + y_{ki} x + x_{ik} y \Big] \dot{u}_j \\ & + \Big[(x_i y_j - x_j y_i) + y_{ij} x + x_{ji} y \Big] \dot{u}_k \Big\} \end{aligned} \tag{32}$$

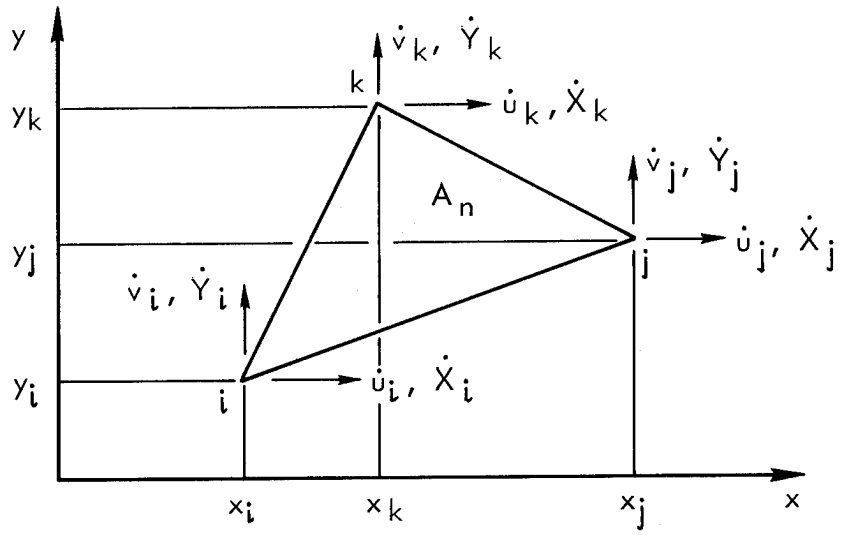

Fig. 4 — nth triangular element

$$\dot{v} = \frac{1}{2A_n}\left\{\left[(x_j y_k - x_k y_j) + y_{jk}x + x_{kj}y\right]\dot{v}_i + \left[(x_k y_i - x_i y_k) + y_{ki}x + x_{ik}y\right]\dot{v}_j + \left[(x_i y_j + x_j y_i) + y_{ij}x + x_{ji}y\right]\dot{v}_k\right\} \tag{33}$$

where

$$A_n = \frac{1}{2}(x_{ij}y_{jk} - x_{jk}y_{ij})$$

represents the area of the triangular element n and the notations

$$x_{ij} = x_i - x_j, \qquad y_{ij} = y_i - y_j$$

have been used. These displacement increment functions, Eqs. (32) and (33), assure continuity of displacements between adjacent elements, because displacements are necessarily equal at common node points at each end of the common side and vary linearly along the side.

The strain increment-displacement increment relations

$$\begin{aligned} \dot{\varepsilon}_x &= \frac{\partial \dot{u}}{\partial x} \\ \dot{\varepsilon}_y &= \frac{\partial \dot{v}}{\partial y} \\ \dot{\gamma}_{xy} &= \frac{\partial \dot{u}}{\partial y} + \frac{\partial \dot{v}}{\partial x} \end{aligned} \tag{34}$$

can be expressed in terms of the node point displacement increments by taking the partial derivatives of Eqs. (32) and (33). (Note that, as previously discussed, $\dot{\gamma}_{xy}$ in Eqs. (34) represents the increment of engineering shear strain, and not the tensoral value.) Equations (34) become

$$[\dot{\varepsilon}] = [\theta]\,[\dot{\delta}] \tag{35}$$

where

$$[\dot{\varepsilon}] = \begin{bmatrix} \dot{\varepsilon}_x \\ \dot{\varepsilon}_y \\ \dot{\gamma}_{xy} \end{bmatrix}, \qquad [\dot{\delta}] = \begin{bmatrix} \dot{u}_i \\ \dot{v}_i \\ \dot{u}_j \\ \dot{v}_j \\ \dot{u}_k \\ \dot{v}_k \end{bmatrix}$$

$$[\theta] = \frac{1}{2A_n} \begin{bmatrix} y_{jk} & 0 & y_{ki} & 0 & y_{ij} & 0 \\ 0 & x_{kj} & 0 & x_{ik} & 0 & x_{ji} \\ x_{kj} & y_{jk} & x_{ik} & y_{ki} & x_{ji} & y_{ij} \end{bmatrix}$$

Element stress increments can be expressed in terms of node point displacement increments by substituting Eq. (35) into Eq. (30):

$$[\dot{\sigma}] = [H]\ [\theta]\ [\dot{\delta}] \tag{36}$$

These stress increments, uniformly distributed in the element and thus along its boundaries, can be replaced by statically equivalent force increments acting at each node point of the element. These equivalent force increments will be defined in terms of their x and y coordinates as

$$[\dot{F}] = \begin{bmatrix} \dot{X}_i \\ \dot{Y}_i \\ \dot{X}_j \\ \dot{Y}_j \\ \dot{X}_k \\ \dot{Y}_k \end{bmatrix} \tag{37}$$

The finite element analysis is based on the establishment of equilibrium of the forces contributed by each surrounding element at each node point in the element array. Thus, it is necessary to express the node point force increments for each element in terms of the node point displacement increments. One simple procedure is to impose arbitrary (virtual) node point displacements and to equate the external and internal work by the various force and stress increments acting on the element.

In general, such forces may include body force components distributed over the element, stress distributions due to temperature changes, processing residual stresses, and so forth. These effects can be introduced in a straightforward manner, if desired (see, for example, Ref. 8 for a detailed discussion); they are not included here.

The work done by the node point force increments (external work) is equal to the sum of the dot products of the individual force components and the corresponding displacement increment components, i.e.,

$$W_E = [\dot{\delta}^*]^T \cdot [\dot{F}] \tag{38}$$

where

$$[\dot{\delta}^*] = \begin{bmatrix} \dot{u}_i^* \\ \dot{v}_i^* \\ \dot{u}_j^* \\ \dot{v}_j^* \\ \dot{u}_k^* \\ \dot{v}_k^* \end{bmatrix}$$

represents the virtual displacements at the element node points, $[\dot{F}]$ is defined in Eq. (37), and the superscript T denotes the transpose of the matrix.

The internal work per unit volume done by the stress increments is

$$W_i = [\dot{\varepsilon}^*]^T [\dot{\sigma}] \tag{39}$$

where

$$[\dot{\varepsilon}^*] = [\theta] [\dot{\delta}^*]$$

as indicated in Eq. (35); $[\dot{\delta}^*]$ is defined in Eq. (38). The transpose of $[\dot{\varepsilon}^*]$ is

$$[\dot{\varepsilon}^*]^T = ([\theta]\ [\dot{\delta}^*])^T = [\dot{\delta}^*]^T\ [\theta]^T \tag{40}$$

Substituting Eqs. (36) and (40) into Eq. (39) gives

$$W_i = [\dot{\delta}^*]^T\ [\theta]^T\ [H]\ [\theta]\ [\dot{\delta}]$$

The total internal work is then obtained by integrating this work per unit volume over the volume of the finite element

$$W_I = [\dot{\delta}^*]^T \int [\theta]^T\ [H]\ [\theta]\ [\dot{\delta}]\ d(vol) \tag{41}$$

Equating the external and internal work done, i.e., Eqs. (38) and (41),

$$[\dot{F}] = [K]\ [\dot{\delta}] \tag{42}$$

where

$$[K] = \int [\theta]^T\ [H]\ [\theta]\ d(vol)$$

is the element stiffness matrix. For the case considered here, where the stresses and strains are constant throughout the element, both $[\theta]$ and $[H]$ are constant and the integration is trivial, i.e.,

$$[K] = A_n[\theta]^T\ [H]\ [\theta] \tag{43}$$

The above procedure for obtaining the required relationship between node point force increments and node point displacement increments, Eq. (42), is applicable for any assumed strain distribution in the element. However, for the case where the strains (and hence stresses) are assumed to be constant within each element, an even simpler and perhaps more physically intuitive procedure can be followed, as was done, for

example, by Foye.[9] The triangular element of Fig. 4 is assumed to be inscribed in a rectangular region of material, the sides of which are parallel to the x-y coordinate axes. The stresses throughout this rectangular region, including along its sides, are assumed to be constant, as they are in the triangular element. This rectangular region can then be divided into four free bodies, as indicated in Fig. 5; the equivalent force increments (per unit thickness in the z-direction) acting on the sides are as shown in the figure. Since the stresses $\dot{\sigma}_x$, $\dot{\sigma}_y$, $\dot{\tau}_{xy}$ are constant along each side, the equivalent force increments, $\dot{\sigma}_x y_{ji}$, $\dot{f}^x_{ij}$, etc., can be assumed to be acting at the midpoints of the sides, as indicated. Summing forces in the x and y directions for each of the three free bodies surrounding the actual finite element gives

$$
\begin{aligned}
\dot{f}^x_{ij} &= \dot{\sigma}_x y_{ji} + \dot{\tau}_{xy} x_{ij} \\
\dot{f}^y_{ij} &= \dot{\sigma}_y x_{ij} + \dot{\tau}_{xy} y_{ji} \\
\dot{f}^x_{jk} &= \dot{\sigma}_x y_{kj} + \dot{\tau}_{xy} x_{jk} \\
\dot{f}^y_{jk} &= \dot{\sigma}_y x_{jk} + \dot{\tau}_{xy} y_{kj} \\
\dot{f}^x_{ik} &= \dot{\sigma}_x y_{ik} + \dot{\tau}_{xy} x_{ki} \\
\dot{f}^y_{ik} &= \dot{\sigma}_y x_{ki} + \dot{\tau}_{xy} y_{ik}
\end{aligned}
\qquad (44)
$$

These are the statically equivalent force increment components acting on the midpoints of the sides of the nth triangular element of area A_n, as indicated in Fig. 5. These force increments can then be divided equally between the two end points of the side on which each acts. For example, the sum of the x-components of these divided forces at the node point i of the nth element is, using the notation of Eq. (37),

$$\dot{X}_i = \frac{1}{2}\left(\dot{f}^x_{ij} + \dot{f}^x_{ik}\right)$$

$$= \frac{1}{2}\left[\dot{\sigma}_x(y_{ji} + y_{ik}) + \dot{\tau}_{xy}(x_{ij} + x_{ki})\right]$$

Expanding the terms in parentheses, cancelling terms, and then reintroducing the contracted notation gives

$$\dot{X}_i = \frac{1}{2}\left(\dot{\sigma}_x y_{jk} + \dot{\tau}_{xy} x_{kj}\right) \tag{45}$$

The remaining force increments of Eq. (37) are obtained in the same manner.

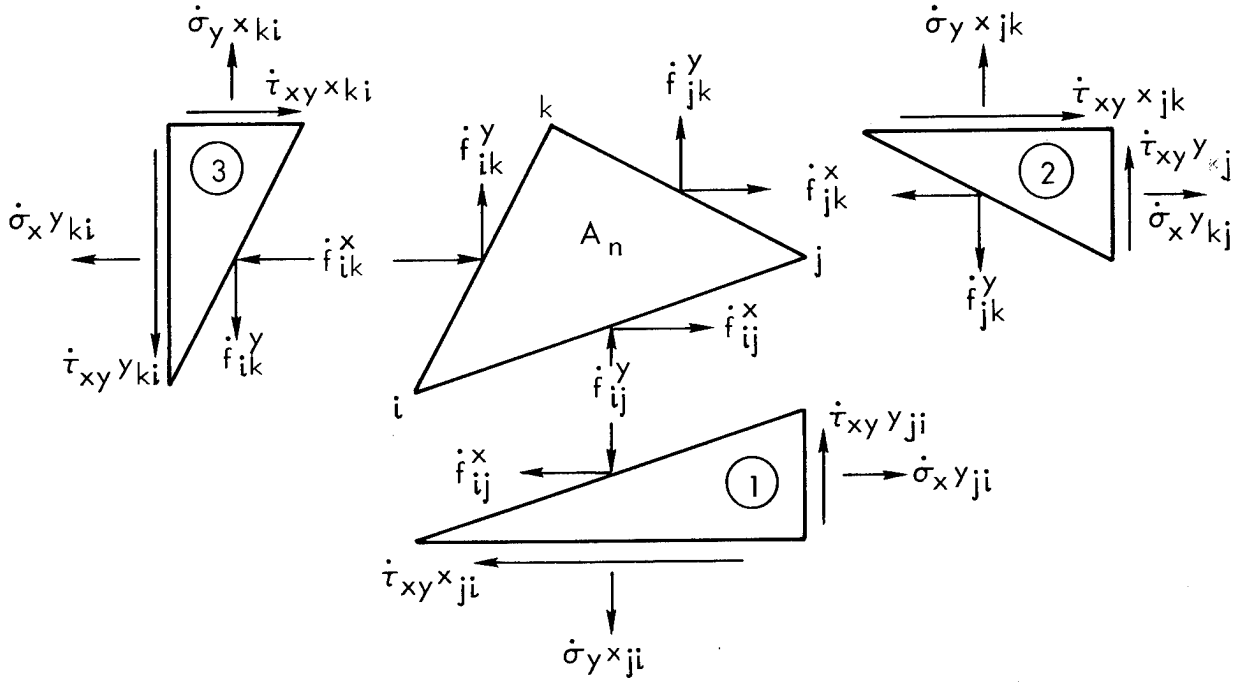

Fig. 5— Force-stress relations

It can be readily shown that these equations are equivalent to Eq. (42). Integrating Eq. (39) over the volume of the nth triangular element gives

$$W_I = \int [\dot{\varepsilon}^*]^T [\dot{\sigma}] \, d(\text{vol})$$
$$= A_n [\dot{\varepsilon}^*]^T [\dot{\sigma}] \tag{46}$$

since $[\dot{\varepsilon}^*]^T$ and $[\dot{\sigma}]$ are constant throughout the element. Substituting Eq. (40) for $[\dot{\varepsilon}^*]^T$ into Eq. (46) and equating the result to Eq. (38) gives

$$[\dot{F}] = A_n [\theta]^T [\dot{\sigma}] \tag{47}$$

where $[\dot{F}]$, $[\theta]$, and $[\dot{\sigma}]$ are defined in Eqs. (37), (35), and (30), respectively. Equation (45) is the first of the set of equations represented by Eq. (47). The remaining equations are similarly equivalent. Equation (36) can be substituted into the set of equations represented by Eq. (45) to obtain Eq. (42).

Equation (47) will be used later when the problem of accounting for failed elements is discussed.

Equation (42) relates the node point force increment equivalents of the stress increments in each element to the node point displacement increments. If body forces are present (a situation not included in this investigation), an additional set of node point force increment equivalents would exist. Also, if the boundaries of the material region represented by the finite element array are subjected to distributed external loadings, the equivalent force increment components acting on the individual boundary nodes must be included. This will result in an additional set of node point force increments $[\dot{R}]$.

Having defined all of the equivalent node point forces acting on each element, the next step is to reassemble the individual elements in the array. The net force at each node point in the array is then obtained by summing up the force increment components contributed by the surrounding elements:

$$[\underline{\dot{F}}] = [\underline{K}]\ [\underline{\dot{\delta}}] \tag{48}$$

where the bars represent summations in each coordinate direction at every node point in the array. Thus, $[\underline{\dot{F}}]$ and $[\underline{\dot{\delta}}]$ will be column vectors, each with 2N entries, where N is the total number of node points in the array. The entries in $[\underline{\dot{F}}]$ are the sum of the components of force at each node point in the array contributed by the stresses in the elements surrounding that node point, i.e., the sum of the equivalent force components represented by Eq. (42) for each surrounding element. Because each node point must remain in equilibrium, this sum must equal the externally applied force component at that node point, or the corresponding entry in $[\dot{R}]$. Thus, for interior node points (where no boundary force components are acting, and the entry in $[\dot{R}]$ is therefore zero), the sum of these equivalent force components must be zero, resulting in a zero entry in $[\underline{\dot{F}}]$. For node points on the boundary, the sum of the equivalent force components from Eq. (42) must equal the component of the equivalent boundary force acting there, the corresponding entry in $[\dot{R}]$. At boundary node points where an equivalent boundary force increment component of known magnitude is applied, the sum of the equivalent force increment components due to element stresses must equal this magnitude in order to maintain equilibrium, i.e., the corresponding entry in $[\underline{\dot{F}}]$ must equal this known value. At boundary node points where a displacement increment component of known magnitude is applied, the associated boundary force component increment is an unknown quantity, to be evaluated as part of the solution process. The corresponding entry in $[\underline{\dot{F}}]$ is, then, an unknown. Thus, the 2N entries in the column vector $[\underline{\dot{F}}]$ represent the sum of the x and y components of the equivalent force increments at the N nodes of the array contributed by each of the surrounding elements. Since most of the nodes in a typical array are interior nodes, most of the entries in $[\underline{\dot{F}}]$ will be zero.

The $[\underline{K}]$ in Eq. (48) is a $2N \times 2N$ symmetric positive definite matrix. Each entry in $[\underline{K}]$ is the sum of terms arising from the application of Eq. (42) for each element surrounding a given node. Since the total number of nodes N is typically large relative to the number of elements (and therefore the number of nodes) surrounding a given node, $[\underline{K}]$ will be a

sparse matrix, i.e., most of its entries will be zero. Advantage will be taken of this sparseness later when discussing details of the procedure for solving Eq. (48) for the unknown displacement increments.

As will be discussed in the next subsection, the boundary-value problems to be solved here are of the mixed-mixed type; at most of the boundary node points, a force increment in one coordinate direction and a displacement increment in the other is prescribed. (Note that corresponding components of force and displacement cannot both be prescribed.) Equation (48) can be rearranged* so that it may be partitioned in the form

$$\begin{bmatrix} \dot{\underline{F}}^k \\ \hdashline \dot{\underline{F}}^u \end{bmatrix} = \left[\begin{array}{c:c} \underline{K}_{11} & \underline{K}_{12} \\ \hdashline \underline{K}_{21} & \underline{K}_{22} \end{array}\right] \begin{bmatrix} \dot{\underline{\delta}}^u \\ \hdashline \dot{\underline{\delta}}^k \end{bmatrix} \tag{49}$$

where $[\dot{\underline{F}}^k]$ and $[\dot{\underline{F}}^u]$ are the known and unknown node point force increments, respectively, and $[\dot{\underline{\delta}}^u]$ and $[\dot{\underline{\delta}}^k]$ are the corresponding unknown and known node point displacement increments. The unknown force increments $[\dot{\underline{F}}^u]$ can be evaluated directly from Eq. (49) once the unknown displacement increments $[\dot{\underline{\delta}}^u]$ are solved for:

$$[\dot{\underline{F}}^u] = [\underline{K}_{21}]\ [\dot{\underline{\delta}}^u] + [\underline{K}_{22}]\ [\dot{\underline{\delta}}^k] \tag{50}$$

$[\dot{\underline{\delta}}^u]$ remains to be solved. From Eq. (49),

$$[\dot{\underline{F}}^k] = [\underline{K}_{11}]\ [\dot{\underline{\delta}}^u] + [\underline{K}_{12}]\ [\dot{\underline{\delta}}^k]$$

which can be rewritten as

$$[\dot{\underline{\delta}}^u] = [\underline{K}_{11}]^{-1} \left([\dot{\underline{F}}^k] - [\underline{K}_{12}]\ [\dot{\underline{\delta}}^k] \right) \tag{51}$$

---

*Note that if two rows of $[\underline{K}]$ are interchanged, the corresponding columns are also interchanged. Thus, the symmetry of the matrix is preserved.

where $[\underline{K}_{11}]^{-1}$ is the inverse of $[\underline{K}_{11}]$. In practice, the challenging problem is to develop an efficient computational procedure for obtaining this inverse, since the order of $[\underline{K}_{11}]$ is typically large.

The solution of Eq. (51) for the unknown node point displacement increment components is the key step in the solution procedure. The unknown force increment components (at node points where the corresponding displacement increment components are known initially) can then be computed, if required, from Eq. (50). Strain increment components within each finite element are computed by substituting the node point displacement increments into Eq. (35). The corresponding element stress increment components can be computed either by substituting the node point displacement increment components into Eq. (36) or by substituting the computed strain increment components into Eq. (30). Thus, the complete solution is obtained for the given applied stress increment at the boundary.

The detailed computational procedure for assembling these incremental solutions into a complete analysis can now be introduced.

INCREMENTAL ANALYSIS METHODOLOGY

The constitutive relations for elastoplastic material behavior (which were derived in a previous subsection) are piecewise linear if the slope of the octahedral shear stress-octahedral plastic shear strain curve (the tangent modulus $2M_T$ in Eq. (12)) can be approximated to be constant during each (small) increment of loading. Thus, the full loading of a material well into the nonlinear (elastoplastic) region can be treated as a sequence of linear loading increments.

Two general approaches have been developed for treating this incremental loading problem: the method of initial strains and the tangent modulus method. Each has advantages and disadvantages as applied to the composite materials problem.

The method of initial strains is based on the fact that plastic strain components do not cause a change in stress. At the beginning of each load increment, an initial guess of the increments of plastic strain that will occur in each element is made. (For simplicity, zero values

may be assumed.) Treating these values as initial strains, a linear elastic analysis is performed for the prescribed increment of boundary loading. After obtaining the resulting stress increments for each element, a revised estimate of the plastic strain increments in each element can be computed using these stress increments, the material constitutive relations (Eq. (15)), and the value of $2M_T$ appropriate to the current level of accumulated stress in each element. These revised estimates of the plastic strain increments are then used as initial strains and the iterative procedure is repeated as many times as is necessary to achieve adequate convergence. A common criterion of adequacy is that the current estimates differ by not more than a prescribed amount from those obtained in the previous iteration.

The principal advantage of the method of initial strains is associated with the fact that only linear elastic boundary-value problems need to be solved. The elastic stiffness matrix, analogous to the elastoplastic stiffness matrix $[\underline{K}]$ in Eq. (48), involves only the elastic material constants E and ν, which are known constants. Thus, the stiffness matrix does not change throughout the loading process, which means that its inverse need only be computed once. The displacement increments for each iteration are computed directly from a set of equations analogous to those of Eq. (51). Terms similar to those in parentheses in Eq. (51) change from iteration to iteration and increment to increment, but the stiffness matrix does not.

A potential disadvantage of the method of initial strains is the possible slow convergence of the iteration process. In practical applications this is particularly likely to occur for loadings well beyond the elastic limit, where the slope of the material stress-strain curve (the tangent modulus $2M_T$) usually becomes small. In such cases, a small increase in stress in the element corresponds to a large increment of plastic strain, causing the iteration process to converge very slowly, or possibly not at all. Since in the current investigation we are interested in accurately representing the material response within each finite element to full failure (crack initiation and propagation), this can become a very serious problem.

The tangent modulus method of analysis of elastoplastic material behavior uses the same general solution techniques that were developed previously for linear elastic analyses. The elastoplastic constitutive relations, Eq. (17), replace the simpler linear elastic relations (and reduce to them as a special case when the plastic strain is zero, i.e., when the last term in Eq. (17) is zero, corresponding to $2M_T = \infty$). This slope of the governing octahedral shear stress-octahedral plastic shear strain curve ($2M_T$ in Eq. (17)), is assumed to remain constant during each load increment. A new value is determined for each element at the beginning of each load increment. Thus, the strain increments given by Eq. (17) are a linear function of the stress increments during each load increment.

The principal advantage of the tangent modulus method is that the solution for each load increment is obtained directly rather than by iteration. However, the stiffness matrix $[\underline{K}]$ in Eq. (48) contains a nonzero value of $2M_T$ for each element that has exceeded its material elastic limit, and these values usually change from one load increment to the next. Thus, it is necessary to construct a new $[\underline{K}]$ at the beginning of each load increment, and invert the corresponding submatrix $[\underline{K}_{11}]$ for use in Eq. (51). It is particularly the inversion of $[\underline{K}_{11}]$ that consumes computer time.

In actual practice, the determination of which method will require less computation time will depend upon the rate of convergence of the method of initial strains solution. For example, Marcal[10] has cited a typical problem for which the computing time required to achieve equal accuracy using the method of initial strains was twice as long as for the tangent modulus method. A similar trend can be expected for the composite material problem, discussed here, since large strains (to failure) are of principal interest.

As is generally true when employing iterative schemes, it is very difficult to estimate beforehand the amount of computation time required when using the method of initial strains. Conversely, the time required per load increment when using the tangent modulus method can be accurately estimated in advance, because it is directly proportional to the number of unknown node point displacements to be solved for (and the bandwidth

of the diagonalized stiffness matrix to be inverted, as will be discussed later).

Considering the various advantages and disadvantages of the two approaches discussed in this subsection, the tangent modulus method, as developed for use in the previously reported inelastic analysis,[1] has been retained for this investigation of crack initiation and propagation. An example of the application of the method of initial strains to inelastic composite material behavior has been given by Foye and Baker.[11]

INCREMENTAL LOADING TO FIRST FAILURE

Elastoplastic material behavior beyond the elastic limit and up to that transverse normal loading at which the stress in any element reaches its ultimate strength value is the subject of a previous report.[1] Because the problem is not formulated there in detail and because a number of refinements have been made during the present investigation, a fuller discussion will be included here.

The general boundary conditions on the sides of the rectangular first quadrant (the region over which the solution is to be obtained; see Fig. 2) and the continuity conditions at the filament-matrix interface were defined in a previous subsection. A perfect interface bond will be assumed, this being the condition of predominant interest. These interface continuity conditions are automatically satisfied under a standard finite element formulation and need not be considered explicitly.

In the usual transverse normal loading problem (and loading problems in general), it is desirable to be able to specify the magnitude of the applied normal loading (applied stress) increments, i.e., increments of $\bar{\sigma}_x$ and $\bar{\sigma}_y$ (see Fig. 1 or 2). But the boundary conditions to be satisfied at each boundary node point for the problem under study must be expressed in terms of normal displacements rather than normal stresses, as previously explained. This is significant because it complicates the solution process and increases the amount of computation required.

One method of achieving specified applied stress increments at the boundaries while satisfying the normal displacement conditions is to solve more than one boundary-value problem for each applied stress increment. Since the material response is approximated to be linear within

each increment, these individual solutions then can be superposed to obtain the desired result. The procedure is basically the same as that used in previous linear elastic analyses.[2] To permit the specification of arbitrary applied stress increments $\Delta\bar{\sigma}_x$ and $\Delta\bar{\sigma}_y$, two separate boundary-value problems must be solved for each increment. They are (referring to Fig. 2):

Problem 1

$\Delta\tau_{xy} = 0$ along all four rectangular boundaries

$\Delta u = 0$ along $x = 0$ (boundary node points remain on the coordinate axis because of symmetry)

$\Delta u = 1$ along $x = a$ (arbitrarily specified uniform displacement increment)

$\Delta v = 0$ along $y = 0$ (boundary node points remain on the coordinate axis because of symmetry)

$\Delta v = 0$ along $y = b$ (any uniform displacement increment is admissible)

Problem 2

Same as problem 1 except:

$\Delta u = 0$ along $x = a$

$\Delta v = 1$ along $y = b$

For each problem, having solved for the displacement increment fields Δu^i and Δv^i (Eq. (51)), where $i = 1, 2$ represent the results of Problems 1 and 2, respectively, the unknown normal force increment components at each node point along the boundaries $x = a$ and $y = b$ can be computed from Eq. (50). The sums of these force increment components along each boundary, divided by the corresponding boundary length b or a, represent the average applied stress increments $\Delta\bar{\sigma}_x^{\,i}$ and $\Delta\bar{\sigma}_y^{\,i}$ associated with each problem.

Problems 1 and 2 then can be combined as follows to obtain the solution for arbitrarily specified applied stress increments $\Delta\bar{\sigma}_x$ and $\Delta\bar{\sigma}_y$. Multiply the results of Problem 2 by a constant α such that the

ratio K of the desired stress increments is obtained. (K is permitted to vary from increment to increment in this analysis.)

$$K = \frac{\Delta\bar{\sigma}_y}{\Delta\bar{\sigma}_x} = \frac{\Delta\bar{\sigma}_y^{\,1} + \alpha\Delta\bar{\sigma}_y^{\,2}}{\Delta\bar{\sigma}_x^{\,1} + \alpha\Delta\bar{\sigma}_x^{\,2}} \tag{52}$$

Solving for α:

$$\alpha = \frac{K\Delta\bar{\sigma}_x^{\,1} - \Delta\bar{\sigma}_y^{\,1}}{\Delta\bar{\sigma}_y^{\,2} - K\Delta\bar{\sigma}_x^{\,2}} \tag{53}$$

The sum of the Problem 1 results plus the Problem 2 results multiplied by α then can be multiplied by a constant γ to obtain the specific values of $\Delta\bar{\sigma}_x$ and $\Delta\bar{\sigma}_y$ desired, e.g.,

$$\Delta\bar{\sigma}_x = \gamma(\Delta\bar{\sigma}_x^{\,1} + \alpha\Delta\bar{\sigma}_x^{\,2}) \tag{54}$$

which defines γ,

$$\gamma = \frac{\Delta\bar{\sigma}_x}{\Delta\bar{\sigma}_x^{\,1} + \alpha\bar{\sigma}_x^{\,2}} \tag{55}$$

Specifically, it is the node point displacement fields of Problems 1 and 2 that are to be combined in the above ratio, i.e.,

$$\begin{aligned} \Delta u &= \gamma(\Delta u^1 + \alpha\Delta u^2) \\ \Delta v &= \gamma(\Delta v^1 + \alpha\Delta v^2) \end{aligned} \tag{56}$$

All other quantities of interest are then computed using these node point displacement increments. For example, the strain increment components in each finite element can be obtained from Eq. (35). The corresponding stress increment components can be obtained by substituting the node point

displacement increment components into Eq. (36), or, if the strain increment components have already been computed, by substituting these strain increment components into Eq. (30).

In this analysis, the components $\Delta\bar{\sigma}_x$ and $\Delta\bar{\sigma}_y$ for each applied stress increment can be specified arbitrarily, rather than only in a fixed ratio as in Ref. 1. Because of this nonproportional loading, local unloading may occur even if the applied stresses are increased monotonically; and, of course, widespread element unloading will occur if the applied stress increments are reversed in sign from previous increments. Thus, it is necessary to provide for unloading response.

The plastic component of the total strain is assumed to be nonrecoverable and hence material unloading will be linearly elastic. Computationally, the procedure is as follows. At the end of each load increment, the computed octahedral shear stress τ_o in each element is compared with the corresponding value from the previous load increment. If τ_o has decreased in magnitude, the element is unloading. The element material properties are set equal to the elastic values for the next and subsequent load increments, and held constant until the computed value of τ_o at the end of any load increment again equals or exceeds the value computed for the increment in which unloading was detected. If this occurs, the element is again assigned an appropriate value of the elastoplastic material parameter $2M_T$ (as defined in Eq. (12)) for the next load increment. Since the load increments are assumed to be small and the element stress-strain response is constrained to follow closely the specified piecewise linear curve, errors due to overshoot and similar response lags are negligible.

The above procedure for combining Problems 1 and 2 is used for all applied stress increments except the first, up to first failure. Since the initial material response is linearly elastic, an applied stress increment of arbitrary magnitude is permissible within this region. Thus, rather than solve for a number of small stress increments within the elastic region, one increment just large enough to stress the material of any one of the elements to its elastic limit value is computed as part of the solution for the first increment. The procedure is as follows. Problems 1 and 2 are solved as outlined above, and a value of α is computed

(Eq. (53)) for the specified ratio K (Eq. (52)) for the first (elastic limit) load increment. The displacement fields of Problems 1 and 2 are combined using Eq. (56) with γ deleted (i.e., as if $\gamma = 1$). The corresponding element stresses are then computed as outlined previously. The octahedral shear stress τ_o in each element can now be computed from Eq. (7). The material of each element has an elastic limit value of octahedral shear stress τ_o^{ℓ} defined by its stress-strain curve. Thus, the ratio τ_o/τ_o^{ℓ} can be computed for each element and that element having the highest ratio identified. Note that, in general, this highest ratio may be greater or less than unity depending upon the magnitude of the assumed boundary displacement increments used in Problems 1 and 2 (indicated as unity here). The displacement increment fields from Eq. (56) (with $\gamma = 1$) are divided by this ratio to give the displacement increments corresponding to the elastic limit loading of the composite. The applied stress increments $\Delta\bar{\sigma}_x$ and $\Delta\bar{\sigma}_y$ are then computed from these displacement increments as previously outlined, as are the other quantities of interest.

Thus, to summarize, for the first applied stress increment, only the desired ratio K of the applied stress components is specified; the specific values of $\Delta\bar{\sigma}_x$ and $\Delta\bar{\sigma}_y$ corresponding to the elastic limit are computed as part of the solution process. For subsequent applied stress increments up to first failure, values of $\Delta\bar{\sigma}_x$ and $\Delta\bar{\sigma}_y$ are specified and solved for.

A slightly different procedure was used in the earlier investigation described in Ref. 1. The intent there was to avoid the need for solving two boundary-value problems for each loading increment beyond the first. The solution of these individual boundary-value problems constitutes the dominant part of the total computational time required (whether it be the two matrix inversions with the tangent modulus method, or the two iteration processes with the method of initial strains). Thus, the total computational time required can be cut almost in half if only one boundary-value problem per increment is necessary.

The first (elastic limit) increment was obtained as outlined here, solving for a specified ratio of the applied stress components; $K = \Delta\bar{\sigma}_y/\Delta\bar{\sigma}_x$. However, unlike this analysis, in which $\Delta\bar{\sigma}_x$ and $\Delta\bar{\sigma}_y$ can

be arbitrarily specified positive or negative values for each loading increment, the ratio K was held constant for all loading increments, i.e., proportional loading was assumed. Thus, only a value of $\Delta\bar{\sigma}_x$ needed to be specified for each loading increment. This proportional loading and an additional assumption of monotonically increasing applied stresses (positive values of $\Delta\bar{\sigma}_x$ only) insured that no local material unloading occurred. On these bases, a predictor-corrector technique was developed in which the boundary displacement increment Δv was estimated in terms of the assumed value of Δu and the results of the previous load increment (thus providing the reason for solving for the first load increment in the usual manner). The ratio of the corresponding average boundary stress increments $\Delta\bar{\sigma}_y/\Delta\bar{\sigma}_x$ will differ, in general, from the desired ratio K, indicating the error in the approximation of Δv. By making a suitable correction in the estimated Δv of the next increment, however, this error was kept negligibly small. Full details of the procedure and the equations used are presented in Ref. 1.

This procedure worked well, being adequately stable in loading the composite to first failure. However, several subsequent attempts to adopt a similar procedure for post-first-failure applied stress increments and the related adjustment increments (which will be described in the next subsection) were unsuccessful. Attempts to correct for even small errors in Δv resulted in serious instabilities. The amount of computation time required and the possible errors introduced in attempting to switch from a predictor-corrector method before first failure to a two-problem solution after first failure led to the abandonment of this approach. The slight savings in computation time were more than offset by the errors and uncertainties introduced. Thus, a two-problem incremental solution has been adopted in the current investigation, for all applied stress (and adjustment) increments.

At some point as the incremental loading procedure is continued, the octahedral shear stress and/or the octahedral plastic shear strain in one or more elements will exceed the ultimate values τ_o^u and $\varepsilon_o^{(p)u}$ for that element as defined by the material stress-strain curve. Note that in theory the material response should follow the stress-strain curve exactly, and thus τ_o^u and $\varepsilon_o^{(p)u}$ would be reached simultaneously. When

approximating the curve by linear segments as is done here, however, it is possible that one limiting value may be exceeded without exceeding the other. The criterion for element failure used here will be that both τ_o^u and $\varepsilon_o^{(p)u}$ must be reached.

If both τ_o^u and $\varepsilon_o^{(p)u}$ are exceeded in at least one element for a given applied stress increment, the specified values of $\Delta\bar{\sigma}_x$ and $\Delta\bar{\sigma}_y$ for that increment are then reduced to values just sufficient to cause failure of only one element. If τ_o^u or $\varepsilon_o^{(p)u}$ (but not both) is exceeded in at least one element, the specified values of $\Delta\bar{\sigma}_x$ and $\Delta\bar{\sigma}_y$ for that increment are then reduced to values just sufficient to cause either τ_o^u or $\varepsilon_o^{(p)u}$ to be reached in just one element. In this latter case, an element failure has not occurred, however, and the next load increment is applied and the process repeated.

This reduction of the applied stress increments $\Delta\bar{\sigma}_x$ and $\Delta\bar{\sigma}_y$ for load increments beyond the first (linearly elastic) increment cannot be achieved by a simple linear adjustment such as was used in obtaining the elastic limit values in the first load increment. For an applied stress increment, both τ_o and $\varepsilon_o^{(p)}$ (Eqs. (7) and (6), respectively) are functions of terms of the form $(\sigma_x + \Delta\sigma_x)^2$, where σ_x is a stress component in an element at the beginning of the increment and $\Delta\sigma_x$ represents the incremental increase. Thus, terms of the form $\sigma_x^2 + 2\sigma_x\Delta\sigma_x + \Delta\sigma_x^2$ must be scaled down to achieve the desired value of τ_o^u or $\varepsilon_o{}^{(p)u}$. That is, a quadratic equation must be solved in determining the scale factor in each case.

These quadratic equations reduce to a single linear relation for the first load increment since the stress components at the beginning of the increment (those represented by σ_x in the above expression) are zero, making the previously discussed linear scaling procedure (Eqs. (54) and (55)) valid.

Equaling or exceeding both τ_o^u and $\varepsilon_o^{(p)u}$ for one element defines first failure of the composite body. This local failure must then be accounted for, as will be discussed in the next subsection.

CRACK INITIATION AND PROPAGATION TO TOTAL FAILURE

When the material in a local region is stressed to its ultimate value, as defined by the stress-strain response for that constituent material, it will fail. If this occurs in a region of high stress gradients such as typically exist in a composite material, the surrounding material may be able to absorb the redistribution of stresses caused by the local failure without additional failure occurring at that level of applied stress. If this is the case, the initial failure becomes a local discontinuity--a crack--within the material. As additional loading is applied, this crack may grow in size (propagate), or additional cracks may be initiated in other regions of high stress within the material. Eventually, the remaining material will be unable to carry the applied loads and total failure--a crack completely across the material cross section--will result.

Thus, it is first necessary to model the crack. Since the material region is represented by elements of finite size, in each of which the stresses and strains are assumed constant, the imminence of a local failure is identified with a particular finite element. An obvious method, and that used here, is to subsequently set the material properties of that element equal to zero, i.e., the stresses and the stiffness properties within the element are reduced to zero. Thus, the crack is assumed to have the dimensions of the failed element. In an actual material, the width of the crack will typically be considerably smaller.

This "failed element" approximation of a crack has two implications. A finite amount of material is assumed to be removed from the system, which is not actually the case, and the crack is not likely to completely close up under subsequent loadings because of its exaggerated width. Should an actual crack subsequently close up, it could support compressive normal forces and shear forces across its surfaces. Of course, as the finite elements are made smaller and smaller, the model representation of an actual crack improves.

There are alternative methods of modeling the crack that do not involve the undesirable features noted above; one of them is outlined in Appendix B. However, practical difficulties in implementing such methods have thus far prevented their use. In this investigation, we

use the "failed element" concept of setting the element material properties equal to zero and defining the resulting void as the crack. As will be demonstrated in Secs. IV and V, this method has proven to be quite satisfactory.

The finite element method involves the maintenance of force equilibrium at each node point in the array. Each element surrounding a given node point exerts a force on that node, and the magnitude of these forces is proportional to the stresses in the elements, as given by Eq. (47). Thus, to represent the unloading due to failure of an element, equal and opposite force components are applied at the corresponding three node points. This reduces the node point force contribution of that element to zero; since the material stiffness properties of the element are simultaneously set equal to zero, no stresses will be developed within the element during subsequent applied stress increments.

These negating node point forces will cause a complete redistribution of displacements, strains, and stresses through the composite material. Thus, after each applied stress increment in which an element failure is indicated, an "adjustment" increment must be performed to apply these negating force components. The effect of an element failure during an applied stress increment is hence accounted for in the subsequent adjustment increment.

As in the case of the applied stress increments, certain boundary conditions must be satisfied during the adjustment increment. These conditions are zero shear stresses and uniform displacements along the rectangular boundaries of the first quadrant (see Fig. 2).

A choice can be made at this point between maintaining constant average boundary stresses ($\Delta\bar{\sigma}_x = \Delta\bar{\sigma}_y = 0$) during the adjustment increment, constant boundary displacements ($\Delta\bar{u} = \Delta\bar{v} = 0$), or a combination of these conditions. In this study, a combination has been used that simulates the conditions of a typical uniaxial test using a constant deformation testing machine. The test specimen is held fixed in the loading direction (along the x-axis) during the adjustment process, with its lateral dimension (along the y-direction) free to expand or contract while maintaining a constant average stress (which, by definition, is zero for the special case of uniaxial loading). This

combination requires the solution of two separate boundary-value problems, as does the applied stress increments. The required boundary conditions are different, but the method of combining them is basically the same. The previously defined Problem 2 is unchanged. However, Problem 1 is replaced by Problem 3, defined as follows:

Problem 3

$\Delta\tau_{xy} = 0$ along all four rectangular boundaries
$\Delta u = 0$ along $x = 0$ and $x = a$
$\Delta v = 0$ along $y = 0$ and $y = b$

Force components of equal magnitude but opposite sign from those given by Eq. (47) are applied at the node points of the failed element.

Problems 2 and 3 are then combined to obtain the following adjustment increment results:

$\Delta u = 0$ along $x = a$ (obtained automatically since $\Delta\bar{u} = 0$ for both Problems 2 and 3)
$\Delta\bar{\sigma}_y = 0$ along $y = b$

The displacement, strain, and stress increment fields are then added to the previously accumulated sums in the usual manner.

The redistributions of stresses due to this adjustment increment may cause one or more additional elements to exceed their ultimate octahedral shear stress and octahedral plastic shear strain values, i.e., to fail. If this happens, an additional adjustment increment is solved for. This process is repeated until no additional elements fail during an adjustment increment. The next applied stress increment is then applied in the usual manner.

As previously noted, adjustment increment boundary conditions other than those selected for this analysis can also be used, the choice depending upon the physical problem to be simulated.

For example, to simulate a constant deformation (e.g., screw-driven) biaxial loading testing machine, the adjustment increment boundary

conditions $\Delta u = 0$ along $x = a$ and $\Delta v = 0$ along $y = b$ would be appropriate. Since this corresponds to Problem 3 outlined above, only one boundary-value problem would have to be solved per adjustment increment, and no combining of individual problems is necessary.

To simulate a constant load (e.g., hydraulic or dead load) biaxial loading testing machine, the adjustment increment boundary conditions $\Delta\bar{\sigma}_x = 0$ along $x = a$ and $\Delta\bar{\sigma}_y = 0$ along $y = b$ would be appropriate. This would require the combination of solutions for Problems 1, 2, and 3 for each adjustment increment. A procedure for combining three problems is discussed in detail in Ref. 12 (in considering the influence of a uniform temperature change) and is not repeated here.

These and similar other adjustment increment boundary conditions can be alternatively readily incorporated as desired.

Total failure of the composite occurs when a continuous band of failed elements extends completely across the first quadrant, either from the $x = 0$ boundary to the $x = a$ boundary, or from the $y = 0$ boundary to the $y = b$ boundary. This necessarily corresponds to either $\bar{\sigma}_y = 0$ or $\bar{\sigma}_x = 0$, with no further change in $\bar{\sigma}_y$ or $\bar{\sigma}_x$ possible. In summary, a crack has propagated completely across the composite material, causing total failure.

III. COMPUTATIONAL ASPECTS

This section is intended for those who are interested in the general characteristics of the numerical solution procedure.

Constant strain triangular elements, as defined in Sec. II, are used to depict the region of interest. The computer program is presently dimensioned to allow the use of up to 350 elements and 200 node points. The size of the element array, and specifically the number of node points, directly influences the computer time required per solution increment since the solution is obtained in terms of node point displacement components. Thus, a trade-off must always be made between improving the resolution by using a larger number of elements and node points, and keeping the required computation time within acceptable bounds. The limits on the array size have been more than adequate to date. Much can be done to improve the resolution, without increasing computation time, by carefully constructing the finite element grid.

The composite material configuration that can be portrayed within the region being analyzed (the first quadrant of the typical repeating unit indicated in Fig. 2) is completely arbitrary. Any filament shape that can be represented by a group of triangular elements is admissible, and more than one filament can be included in the first quadrant. A void can be expressed by setting the Young's modulus equal to zero for those elements that represent its shape. The program is dimensioned to handle as many as five different materials.

Since an elastoplastic analysis is being performed, the complete stress-strain response to total failure for each constituent material must be given. The analysis permits any monotonic response (i.e., single-valued relation between stress and strain) to be specified. The stress-strain curve for each material is input point by point, usually using actual experimental data. The applied stress components $\Delta\bar{\sigma}_x$ and $\Delta\bar{\sigma}_y$ can be arbitrarily specified for each solution increment. The program is dimensioned to handle as many as 50 pre-first-failure load increments and 50 post-first-failure load increments. A typical problem may require 10 to 12 pre-first-failure load increments and 12 to 15 post-first-failure load increments.

The finite element computer program provides a printout of results for each applied stress increment and each adjustment increment, namely, the increments of average composite stress actually solved for, the corresponding increments of composite strain, the accumulated sums of these quantities, and the accumulated node point displacement components. It also prints out for each element the accumulated values of the strains ε_x, ε_y, γ_{xy}, $\varepsilon_o^{(p)}$ and the following normalized quantities: the stress components $\sigma_x/\bar{\sigma}_x$, $\sigma_y/\bar{\sigma}_x$, $\sigma_z/\bar{\sigma}_x$, $\tau_{xy}/\bar{\sigma}_x$; the octahedral shear stress τ_o/τ_o^{ℓ}; the maximum principal stress $\sigma_1/\bar{\sigma}_x$; and the maximum principal strain $\varepsilon_1/\bar{\varepsilon}_x$. Furthermore, it prints out the numbers of the elements for which either τ_o^u or $\varepsilon_o^{(p)u}$ has been exceeded during the solution increment.

In addition to this printed output, the program prepares a tape containing those results that are required for input to the contour plotting computer program, used by a Stromberg-DatagraphiX S-D 4060 plotter.

The finite element grid, which is input node by node into the finite element computer program, can be plotted with and without element numbers being printed. This serves as a ready visual check for the correctness of the input data. Contour plots of any of the following element quantities can be specified (normalized as indicated): maximum principal stress $\sigma_1/\bar{\sigma}_x$, maximum principal strain $\varepsilon_1/\bar{\varepsilon}_x$, octahedral plastic shear strain $\varepsilon_o^{(p)}$, and octahedral shear stress τ_o/τ_o^{ℓ}. Values of the contours to be plotted are specified as input data.

Failed elements are also indicated on the contour plots. These elements are outlined and shaded, making it easy to follow visually the progress of a crack on plots of successive solution increments.

IV. NUMERICAL RESULTS

Because the primary goal of this investigation has been to develop a method of analysis and to write an associated computer program, most of the concentration has been on attempting to improve computational techniques and solution accuracy. Only very limited numerical results have been obtained to date.

However, in the process of refining the detailed aspects of the numerical solution procedure and correcting programming errors, a significant number of computer runs have been made. This development effort involved the study of effects of changing finite element grid patterns in local regions, modifying boundary conditions, reshaping the governing stress-strain curves of the constituent materials, varying the size of the applied stress increments, and so forth. Thus, the few examples presented here and the numerical analysis used to obtain their solutions constitute a summary of the knowledge gained to date.

There was no single computer run that was completely satisfactory in terms of modeling all aspects of the composite material response from the first (elastic limit) applied stress increment, to first failure, and then to complete crack propagation and total composite failure. Each of these separate phases, however, was successfully run at various times during the computer program development process. An inherent numerical inaccuracy of the constant strain triangular finite element technique, which remains to be resolved (as will be discussed in the next section), combined with a lack of available computer time has limited the number of numerical results obtained.

The examples presented here are intended to demonstrate the type of information which can be obtained, even though the results are too limited to provide conclusive predictions of actual crack propagation and composite failure. Many more computer runs will be required to achieve this.

A boron-aluminum composite was assumed in most of the numerical examples considered. The distinct change in slope of the stress-strain curve beyond the elastic limit for the annealed 6061 aluminum alloy

matrix material that was selected offered a good test of the elasto-plastic response representation of the analysis. Actual experimental data provided by TRW-Cleveland* were used; the stress-strain curve obtained from a uniaxial tensile test of this matrix material is shown in Fig. 6. The complete curve is input point by point into the computer program. The measured Young's modulus was 9.4×10^6 lb/in.^{2}, the elastic limit stress was 6280 lb/in.^{2}, and failure occurred at an ultimate stress of 18,900 lb/in.^{2} and a strain of 30 percent. The boron filaments were assumed to exhibit linearly elastic response to failure, based upon longitudinal tensile tests of individual filaments. Their measured Young's modulus was 55.0×10^6 lb/in.^{2}, and an ultimate strength of 500,000 lb/in.^{2} was assumed as being sufficiently high to insure that failure would occur in the matrix only. This was the observed failure mode in the actual composite material being modeled. The Poisson's ratios for the aluminum and boron were assumed to be 0.32 and 0.20, respectively.

Complete stress-strain curves to failure for a number of uniaxial, transverse normal tensile tests of composites using these constituent materials were provided by TRW-Cleveland, in the form of strip chart records.* Photomicrographs of the test specimens before and after failure were also available.[13] All specimens using the annealed aluminum matrix failed in the matrix. Other composite specimens, using the same 6061 aluminum alloy but in the heat-treated condition, also exhibited failures in the filaments. The alloy is much stronger in the heat-treated condition, as indicated by the experimental curve in Fig. 6. A complete discussion of the test procedures, specimen designs, material processing, and experimental program in general may be found in Ref. 13.

One specific test result, TRW Specimen $4F_o2/2$, that was selected to be modeled by the analysis is an annealed specimen containing 40 volume percent (v_f = 40 percent) of boron filaments. This specimen was selected because it exhibited a stress-strain curve that represented well the data available. The filament packing was very regular and in approximately a square array. Photomicrographs are included in Ref. 13.

---

*Private communication of unpublished experimental data from I. J. Toth, TRW, Inc., Cleveland, Ohio.

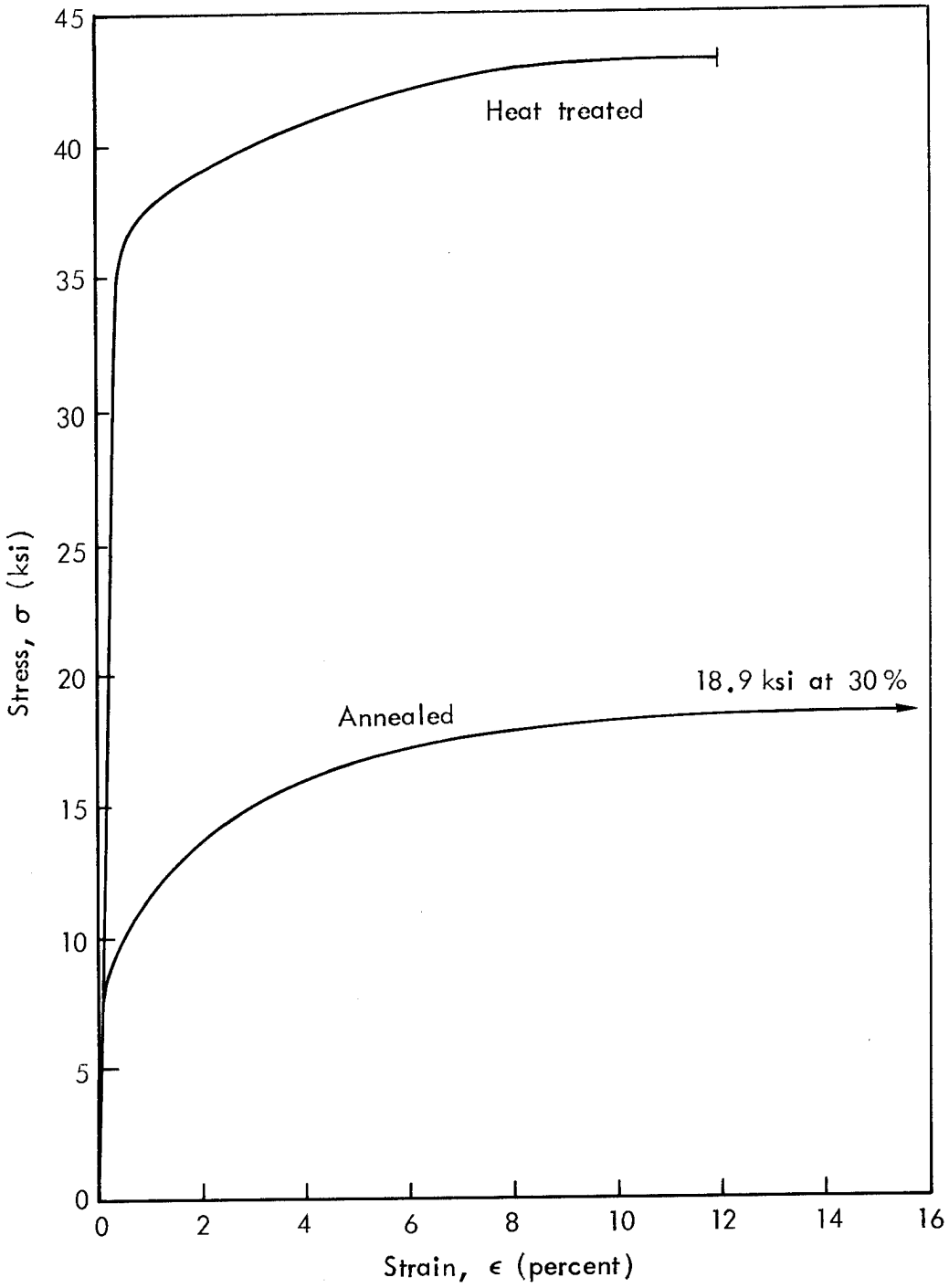

Fig. 6— Uniaxial tensile stress-strain curves, 6061 aluminum alloy matrix materials (data from Ref. 13)

The finite element grid shown in Fig. 3 was constructed to model this geometry, boron filaments being circular in cross section. This is a relatively large grid, containing 176 nodes and 304 elements, and it models the matrix region very well. A coarse element grid was used in the filament region since the boron filaments remain elastic and do not fail. This conserved node points and should not significantly affect solution accuracy.

The actual composite stress-strain response obtained experimentally by TRW is indicated by the solid curve in Fig. 7. This was a uniaxial, transverse normal tensile test, corresponding to a $\bar{\sigma}_x$ component of applied stress, as indicated in Fig. 1; $\bar{\sigma}_y$ is zero. One set of numerical results of the present analysis, computer run 8A-10-17, is illustrated by the dashed curve in Fig. 7.

First yielding was predicted to occur in the matrix along the x-axis midway between adjacent filaments--in element 79 in the lower right corner of the grid of Fig. 3. This is consistent with the results obtained in Ref. 1. As noted in Fig. 7, first yielding was predicted to occur at an applied stress of 5539 lb/in.^{2} and a composite strain of 0.0296 percent, resulting in a predicted composite elastic modulus of 18.7×10^6 lb/in.^{2}. The experimentally measured elastic modulus was 17.3×10^6 lb/in.^{2}. As indicated in Fig. 7, the initial portions of the two curves are in good agreement.

The composite was then loaded in 500 lb/in.^{2} increments up to first failure, which was predicted to occur in element 139, an element of matrix material located at the filament-matrix interface (see Fig. 3). This occurred during applied stress increment no. 29, at an applied stress of 19,519 lb/in.^{2}. This point is marked *first failure* in Fig. 7. The failed element is outlined in Fig. 8; the number inside the element indicates the applied stress increment during which failure occurred. Octahedral shear stress contours (which have been normalized by dividing by the value of the octahedral shear stress at which yielding of the matrix material occurs, i.e., τ_o^{ℓ} = 2960 lb/in.^{2}) are also indicated. Matrix failure occurs at an octahedral shear stress of 8910 lb/in.^{2}, corresponding to a normalized value of τ_o^u/τ_o^{ℓ} = 8910/2960 = 3.01. Thus, the contours having the value 1.0 indicate the initiation of yielding,

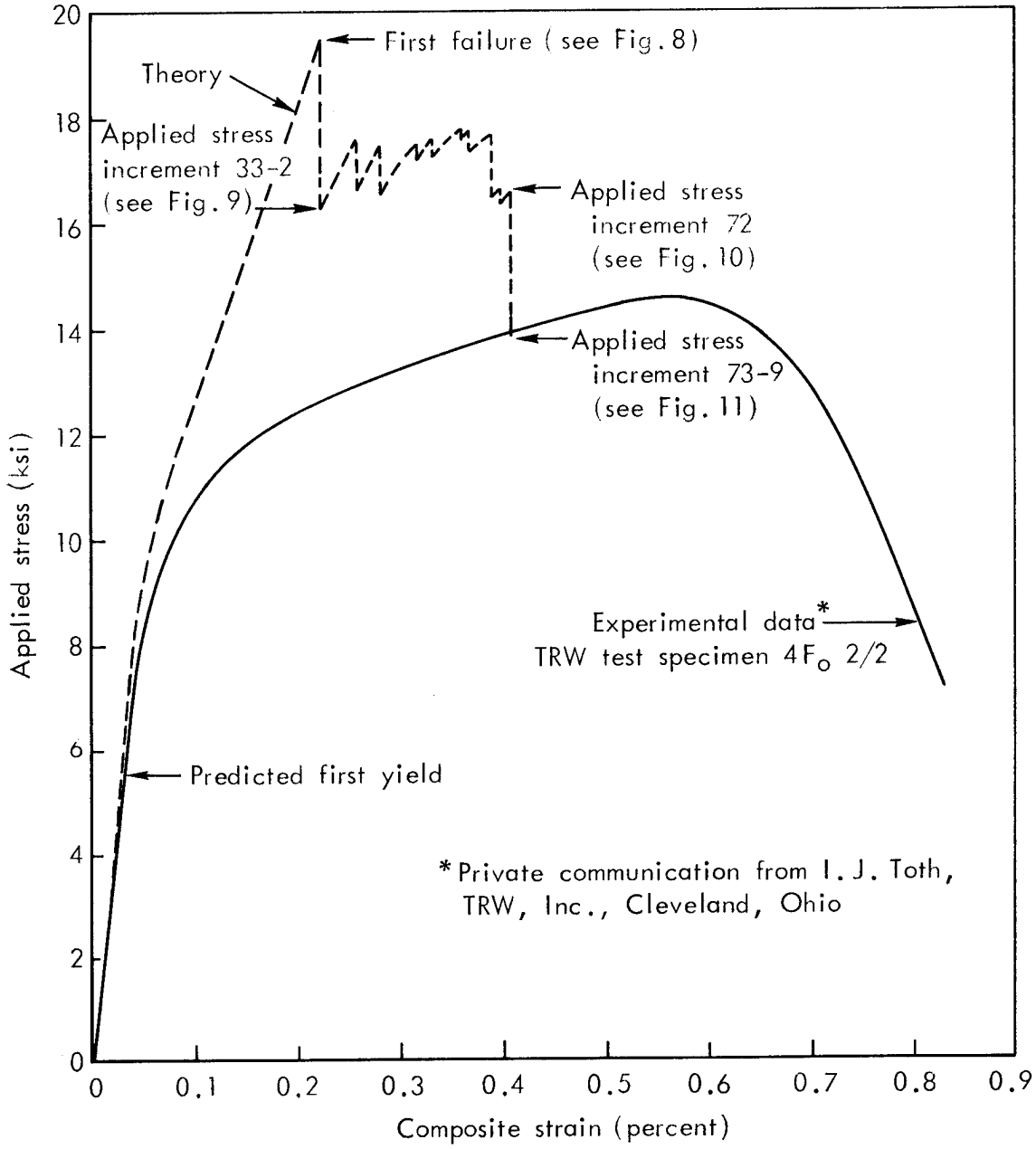

Fig. 7— Predicted and experimental stress-strain curves
Computer run 8A-10-17

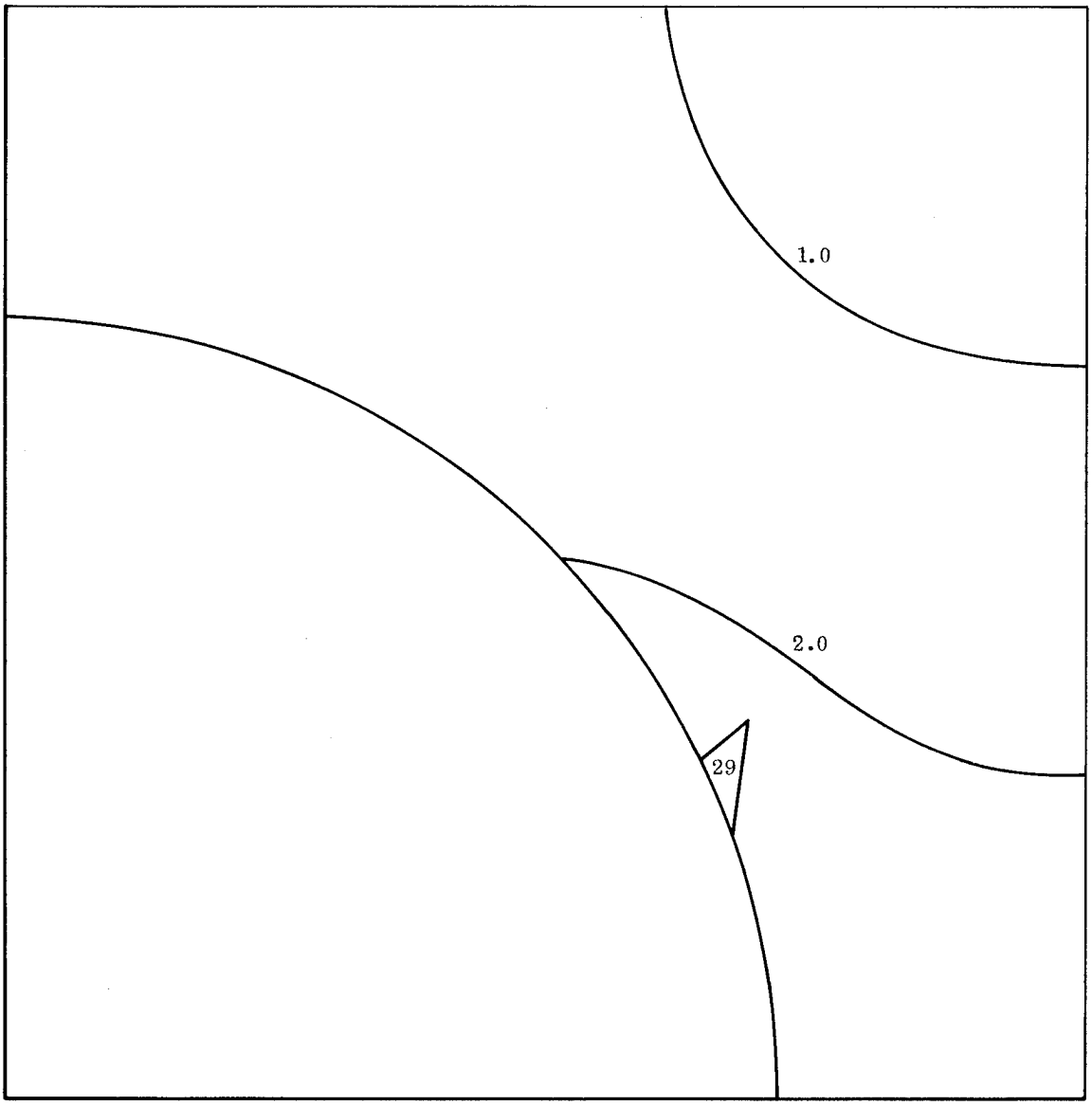

Fig. 8— First element failure and octahedral shear stress contours (normalized)
Computer run 8A-10-17, applied stress increment 29

and those having the value 2.0 indicate a stress level approximately midway between yielding and failure.

The first element failure, as indicated in Fig. 8, resulted in a decrease of 196 lb/in.^{2} in the applied stress during the immediately subsequent adjustment increment (which is always required when an element fails), and this adjustment did not cause additional elements to fail.

Beyond first failure, 200 lb/in.^{2} applied stress increments were used. During applied stress increment no. 30, the plastic octahedral shear strain ultimate $\varepsilon_o^{(p)u}$ (but not the octahedral shear stress ultimate τ_o^u) was exceeded in element 81 (see Fig. 3). This 200 lb/in.^{2} applied stress increment was thus automatically normalized to give the value $\varepsilon_o^{(p)u}$ for element 81, which corresponded to an actual applied stress increment of 87 lb/in.^{2}.

During the next applied stress increment, element 81 failed, at a stress increment of only 24 lb/in.^{2}. The subsequent adjustment increment caused a decrease in applied stress of 85 lb/in.^{2}, and τ_o^u (but not $\varepsilon_o^{(p)u}$) was exceeded in elements 78 and 79. These two elements failed during the next applied stress increment, increment no. 32. When this occurred, a total of four adjustment increments were required to again achieve equilibrium. During the first adjustment increment, element 93 failed. Thus, a second adjustment increment was required, during which element 82 failed. This required a third adjustment, during which elements 92, 94, and 105 failed. A stable condition was achieved during the fourth adjustment increment, although τ_o^u had been exceeded in element 117. At this point the applied stress had decreased to 17,282 lb/in.^{2}.

During the next applied stress increment, increment no. 33, element 117 failed after only 10 lb/in.^{2} of the allowable 200 lb/in.^{2} increment had been applied. This in turn caused element 106 to fail during the subsequent adjustment increment, requiring a second adjustment increment. This restored equilibrium, at an applied stress of 16,246 lb/in.^{2}, and completed the first major decrease in applied stress, as indicated in Fig. 7. The elements which had failed at this point are indicated in Fig. 9. When the number within an element is hyphenated, the first

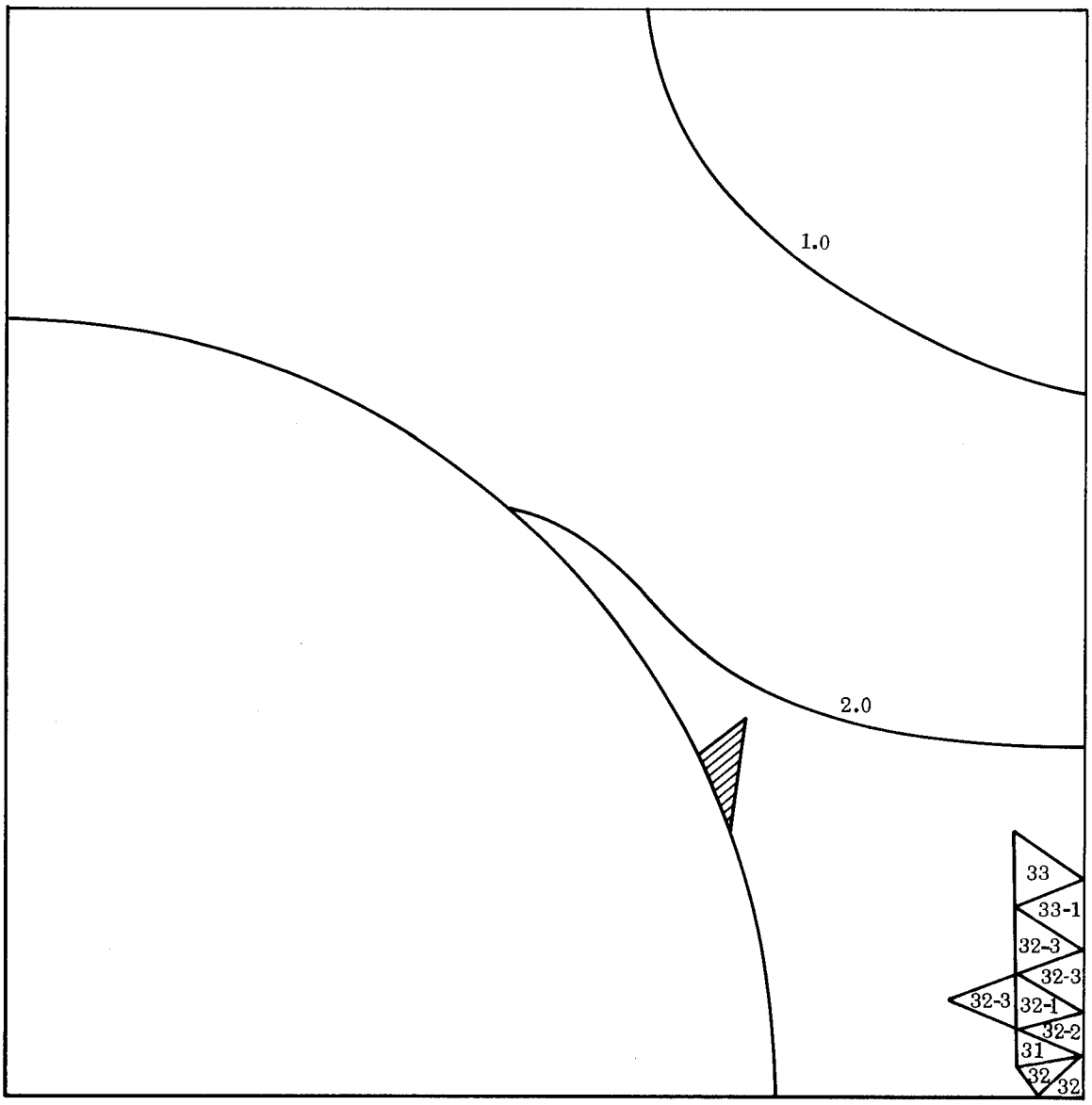

Fig. 9— Failed elements and octahedral shear stress contours (normalized)
Computer run 8A-10-17, applied stress increment 33-2

digits indicate the applied stress increment number, and those after the hyphen indicate the adjustment increment within that applied stress increment during which the element failed. When the number is not hyphenated, it indicates that that element failed during the applied stress increment itself. Shading identifies the element that failed in the previous figure.

Seven additional 200 lb/in.^{2} applied stress increments, nos. 34 through 40, were then employed; no additional elements failed. At 83 lb/in.^{2} of increment no. 41, element 127 failed. This in turn caused element 118 to fail, and equilibrium was restored at an applied stress of 16,707 lb/in.^{2}. This decrease is represented by the second sharp drop in applied stress in Fig. 7, at a composite strain of 0.258 percent.

The process of applying stress increments and causing additional elements to fail was continued as outlined above, resulting in the jagged stress-strain response indicated in Fig. 7. During this time, the crack initially continued to propagate upward along the right boundary of the first quadrant, and then a second crack began to propagate along the interface. At applied stress increment no. 72, when element 208 failed (see Fig. 3), the applied stress dropped suddenly. This point is noted in Fig. 7. Elements which had failed at this time are indicated in Fig. 10.

Element 207 failed immediately during the next applied stress increment, marking the point at which the crack turned away from the interface, propagating out into the matrix material region. During the first nine adjustment increments following this applied stress increment, the crack continued to propagate upward and at the same time it connected with the original crack, as indicated in Fig. 11. At this point a numerical instability interrupted the solution process.

In view of later results, it is fairly obvious that the crack extending out into the matrix from the interface would have continued to propagate upward to the top boundary of the material region if the solution process had been continued. This would have constituted total failure. Looking again at Fig. 7, it is anticipated that the predicted stress-strain curve would have continued downward with only minor fluctuations. For all practical purposes, failure had effectively occurred

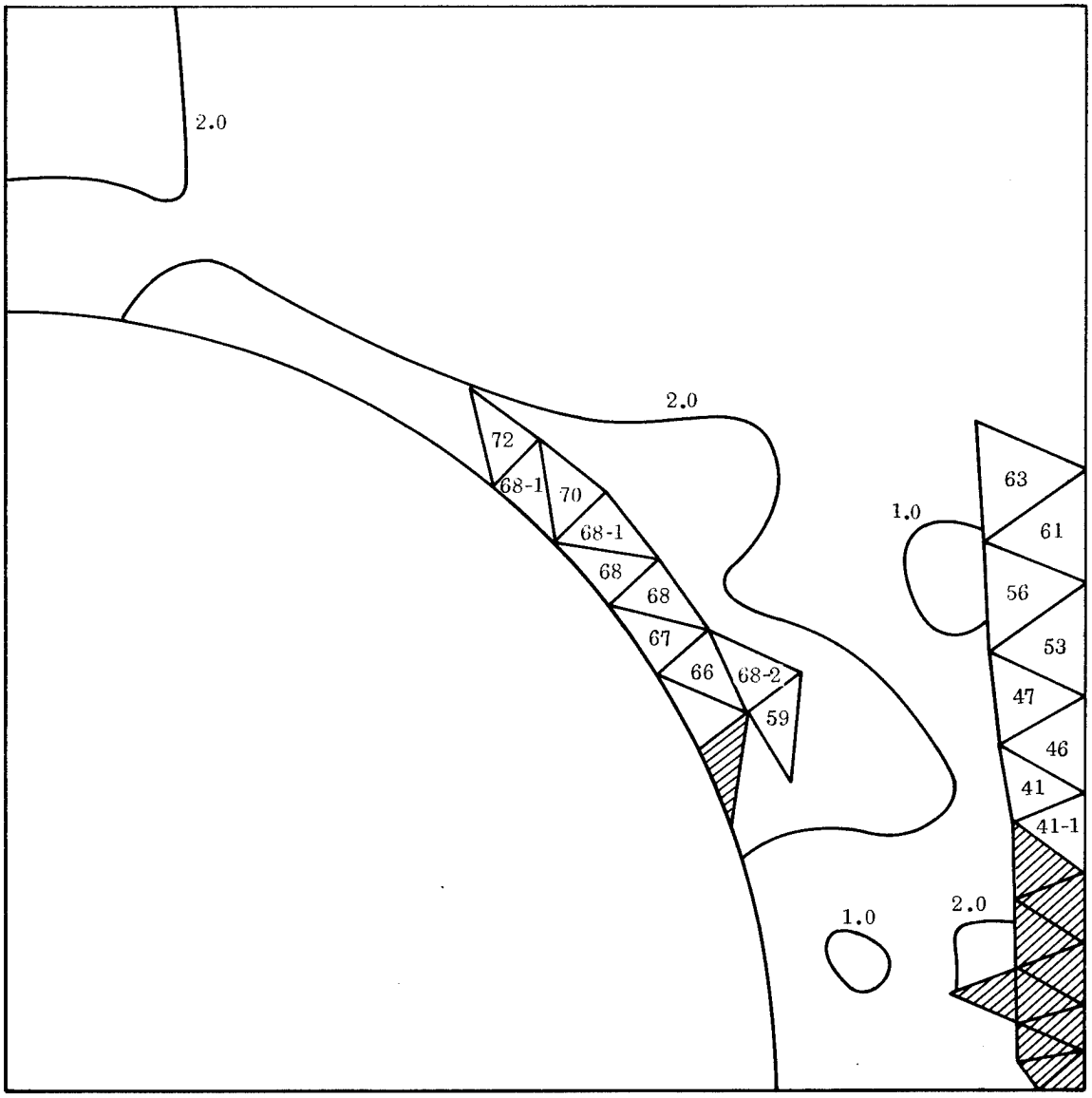

Fig. 10 — Failed elements and octahedral shear stress contours (normalized)
Computer run 8A-10-17, applied stress increment 72

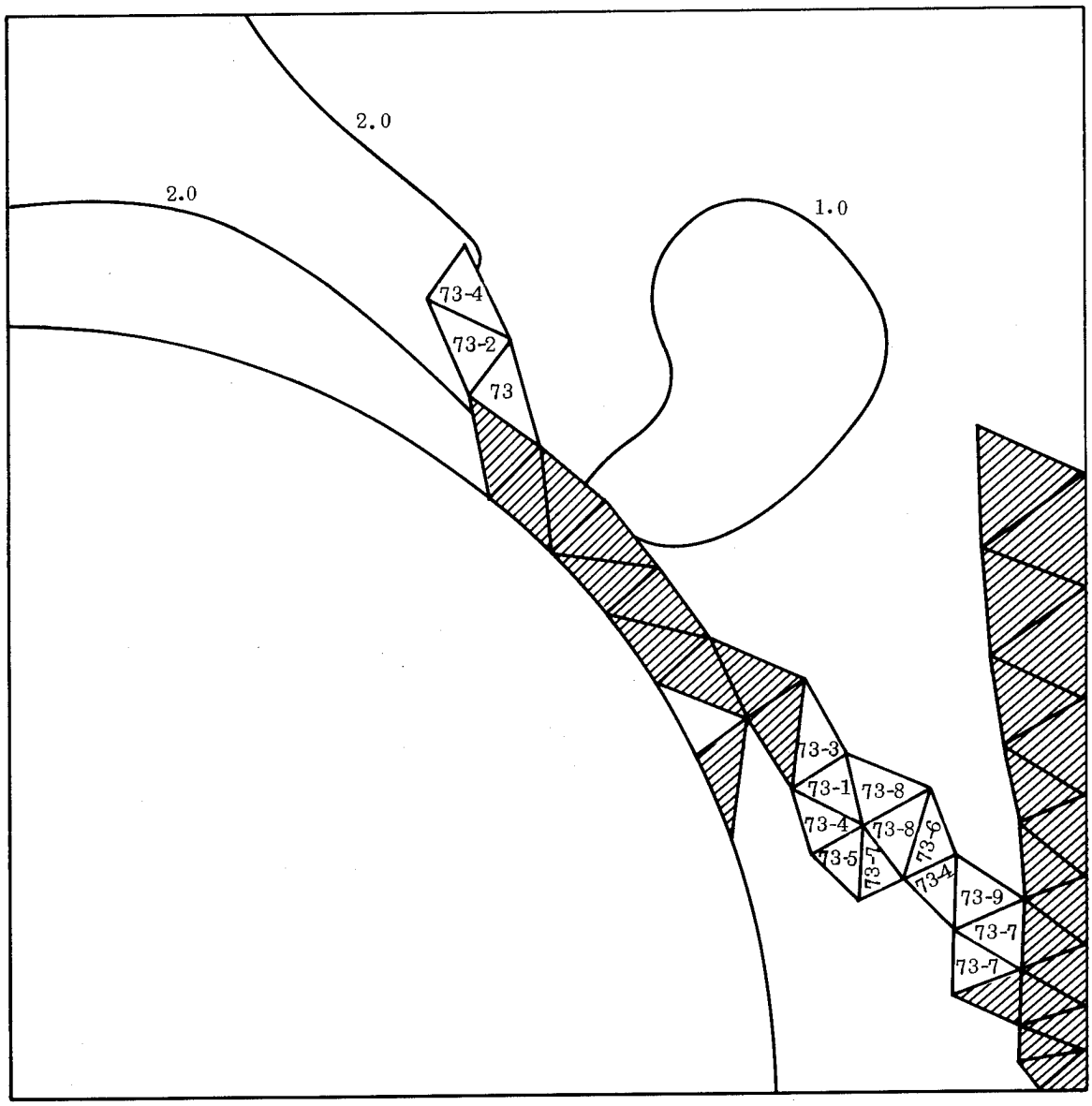

Fig. 11 — Failed elements and octahedral shear stress contours (normalized)
Computer run 8A-10-17, applied stress increment 73-9

during applied stress increment no. 66, when the crack began to propagate along the interface. Beyond this point the applied stress decreased rapidly, with only minor pauses.

Although the first crack began at the interface (during applied stress increment no. 29), the major crack propagation was initially along the right boundary (up the midline between adjacent filaments). Actually, the fact that first failure occurred in element 139 may have been an anomaly, caused by the distorted shape of element 15 in the filament directly across the interface (see Fig. 3). This distortion was introduced while minimizing the matrix bandwidth during construction of the grid array. Element 81 was also very near to failure when element 139 failed. At applied stress increment no. 66, during which the second element near the interface failed, the magnitude of the applied stress was 17,757 $lb/in.^2$, and the composite strain was 0.388 percent. The composite was already near total failure.

The composite stress-strain curve presented in Fig. 7 is exactly as obtained in computer run 8A-10-17. Later, however, several relatively minor errors in the computer program were discovered and corrected. The principal effects of these corrections were to approximately double the plastic component of the composite strain, and to decrease the applied stress at which first failure occurred. Because of a numerical instability problem that is yet to be resolved (as will be discussed in the next section) and to conserve available computer time, a complete rerun of this example problem was not attempted. However, a computer rerun (8C-1) up to first failure was made. The result is plotted in Fig. 12 along with the original post-first-failure results, which have been approximately corrected for the previous error by doubling the plastic component of the composite strain values. Thus it must be emphasized that Fig. 12 does not represent an actual result of a single computer run, but rather is an estimate of the type of behavior that can reasonably be expected in subsequent investigations.

The postulated stress-strain curve of Fig. 12 is clearly in good agreement with the experimental data. One fact that should be kept in mind, however, is that the experimental data represent the results of a test of a composite containing hundreds of individual filaments that were

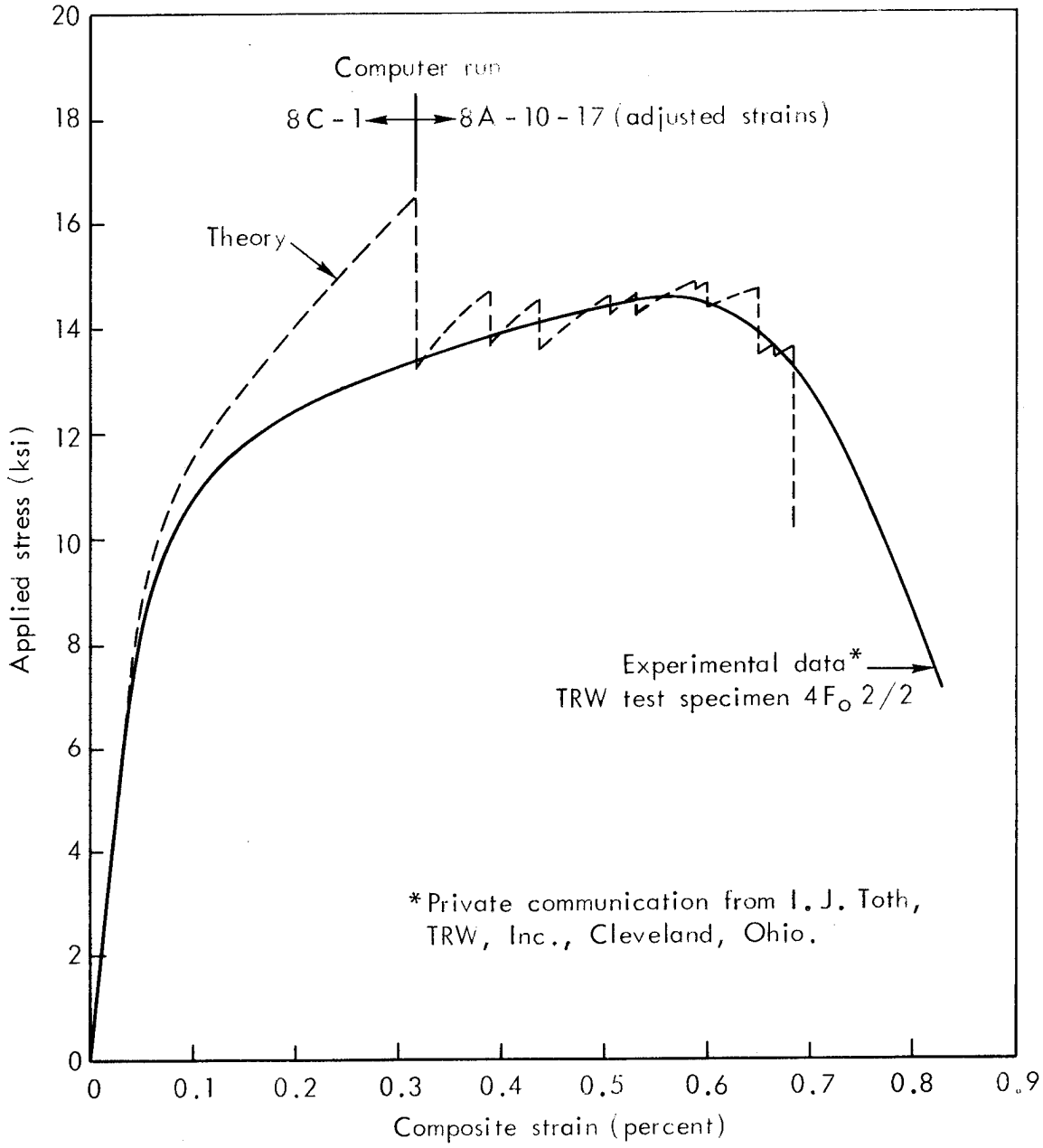

Fig. 12 — Predicted and experimental stress-strain curves
Combined computer runs 8C-1 and 8A-10-17
(adjusted strains)

not all perfectly spaced in a square array. It would be very informative to determine the influence of minor variations of filament spacing on both the predicted composite stress-strain response and the actual crack propagation pattern. The experimental curve represents a statistical average of such a variation.

The first example discussed, computer run 8A-10-17, was unique in that a very large number of applied stress increments were required, a total of 73. This was necessitated by the relatively small size of the applied stress increments specified--500 lb/in.^{2} prior to first failure, and 200 lb/in.^{2} after first failure. A study of the nearly 50 computer runs that were made during the investigation have somewhat quantified what is intuitively obvious: the numerical results are influenced by the size of the increments used.

For example, computer run 8C-1 used larger applied stress increments that did computer run 8A-10-17. The pre-first-failure applied stress increments were specified as 500 lb/in.^{2} for increment nos. 2 and 3, 1000 lb/in.^{2} for increment no. 4, and 1500 lb/in.^{2} for all additional pre-first-failure increments required. (The magnitude of the first (elastic limit) applied stress increment is solved for in the analysis directly, as previously discussed.) The computer program was then immediately rerun (8C-2) using all 500 lb/in.^{2} applied stress increments. Although it terminated prior to first failure because of a numerical instability, the predicted stress-strain curves as obtained from runs 8C-1 and 8C-2, up to the point where the instability occurred in run 8C-2, were somewhat different. The applied stress at a given composite strain was slightly lower when the larger increments were used. Also, it was indicated that the applied stress at which first failure would have occurred in computer run 8C-2 would have been somewhat higher than was actually obtained in computer run 8C-1 because local stress concentrations within the composite tended to be lower. (Probable reasons for this will be discussed in conjunction with the next example.) It would probably have been more accurate to use run 8C-2 as the first portion of the predicted curve in Fig. 12 (to first failure), if a numerical instability had not occurred just prior to that point, making the stress at first failure indeterminate.

The influence of applied stress increment size was also demonstrated in another computer run, 8A-19-25. It was run immediately after 8A-10-17, with only very minor changes in the computer program. The significant difference between these two runs was in the size of the applied stress increments specified. Computer run 8A-19-25 used larger increments. The pre-first-failure applied stress increments were 500 lb/in.^{2} for increment nos. 2 and 3, 1000 lb/in.^{2} for increment no. 4, and 1500 lb/in.^{2} for all subsequent pre-first-failure increments required. All post-first-failure applied stress increments were specified as 500 lb/in.^{2}.

Total failure was achieved in this example; the resulting composite stress-strain curve is shown in Fig. 13. As in computer run 8A-10-17 (see Fig. 7), the plastic component of the computed composite strain was in error by a factor of approximately two. This accounts for the small strains in Fig. 13, since the curve was plotted exactly as obtained from the computer printout.

As in 8A-10-17, first failure occurred at the interface, again in element 139 (see Fig. 3). However, the applied stress at first failure, 13,285 lb/in.^{2}, was considerably less than the 19,512 lb/in.^{2} previously achieved, as was the composite strain, 0.123 percent versus 0.221 percent. First failure occurred during applied stress increment no. 9.

Unlike computer run 8A-10-17, the crack that initiated at the interface immediately propagated along the interface, upward slightly at first, as illustrated in Fig. 14. However, when the third element failed during applied stress increment no. 11, a total of nine adjustment increments were required before equilibrium was again achieved. During this time the crack continued to propagate along the interface, primarily downward; the condition at adjustment increment no. 11-6 is shown in Fig. 15. Equilibrium was achieved during adjustment increment no. 11-9, when the crack reached the lower boundary, as indicated in Fig. 16. However, during the next two applied stress increments, the crack propagated upward along the interface an additional two elements, causing the applied stress to drop to 4563 lb/in.^{2}. This marked the end of the nearly vertical first major drop in applied stress beyond first failure.

The applied stress then increased during the next three applied stress increments, with no additional elements failing. At this point

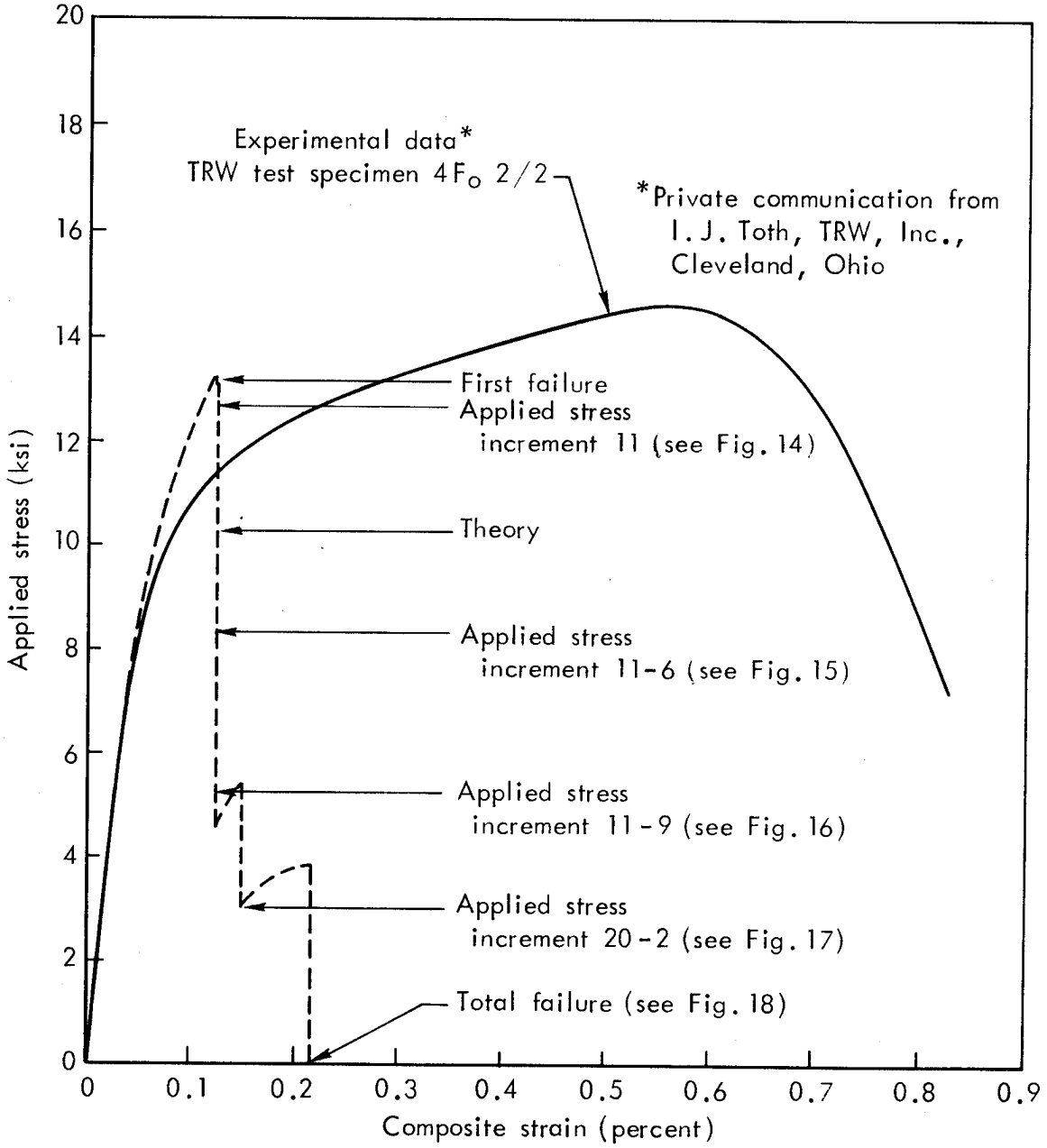

Fig. 13 — Predicted and experimental stress-strain curves
Computer run 8A-19-25

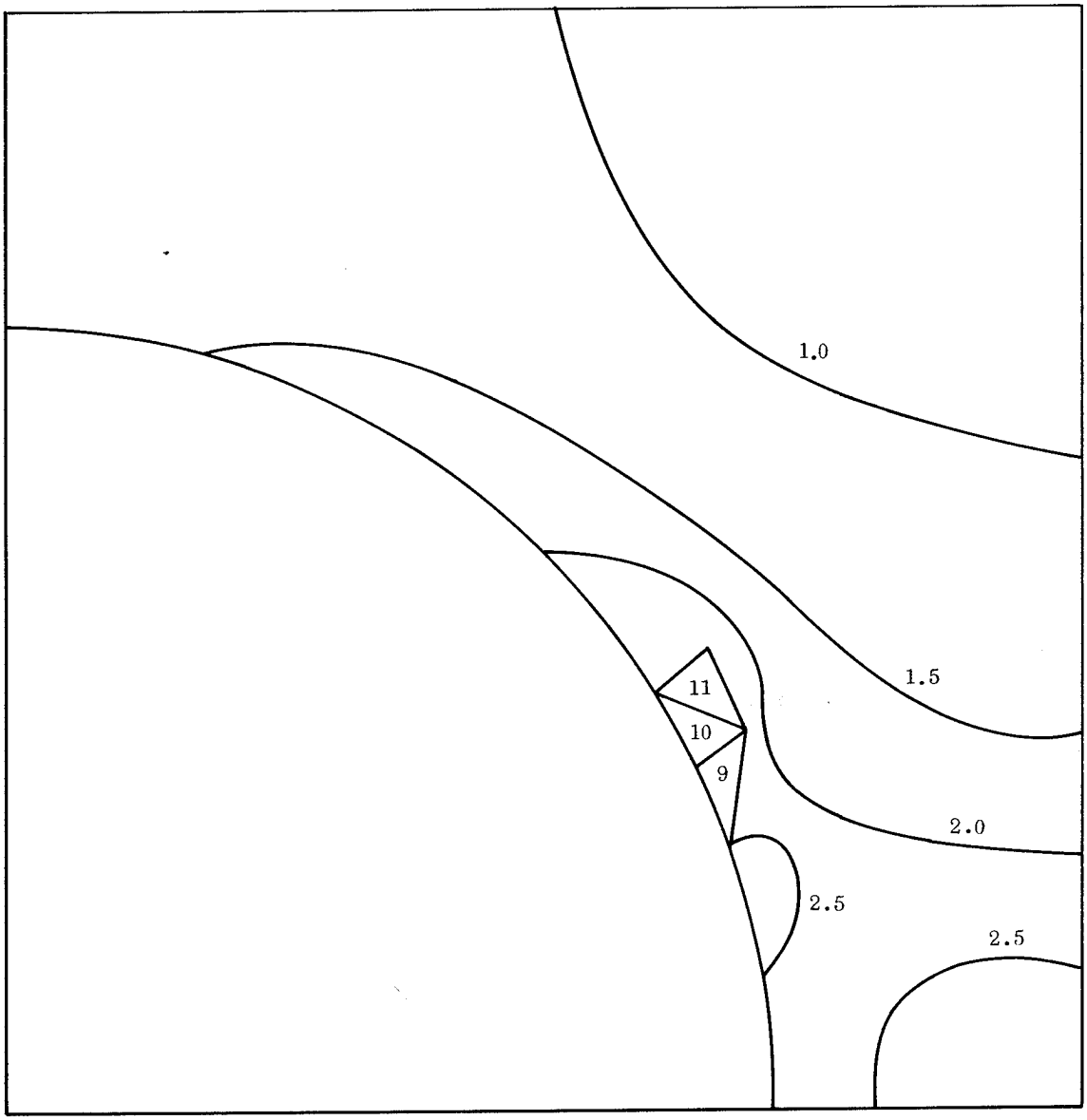

Fig. 14 — Failed elements and octahedral shear stress contours (normalized)
Computer run 8A-19-25, applied stress increment 11

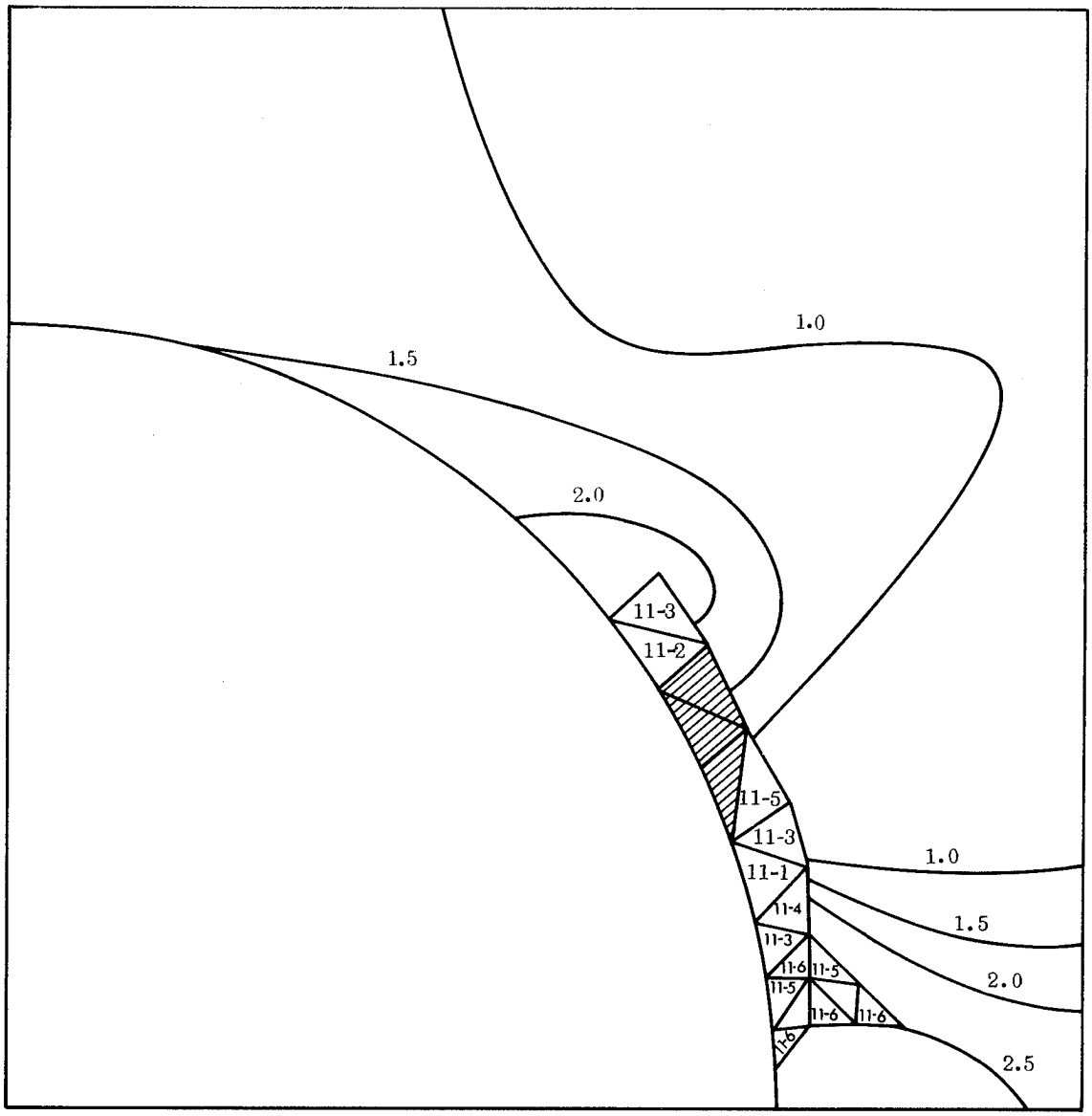

Fig. 15— Failed elements and octahedral shear stress contours (normalized)
Computer run 8A-19-25, applied stress increment 11-6

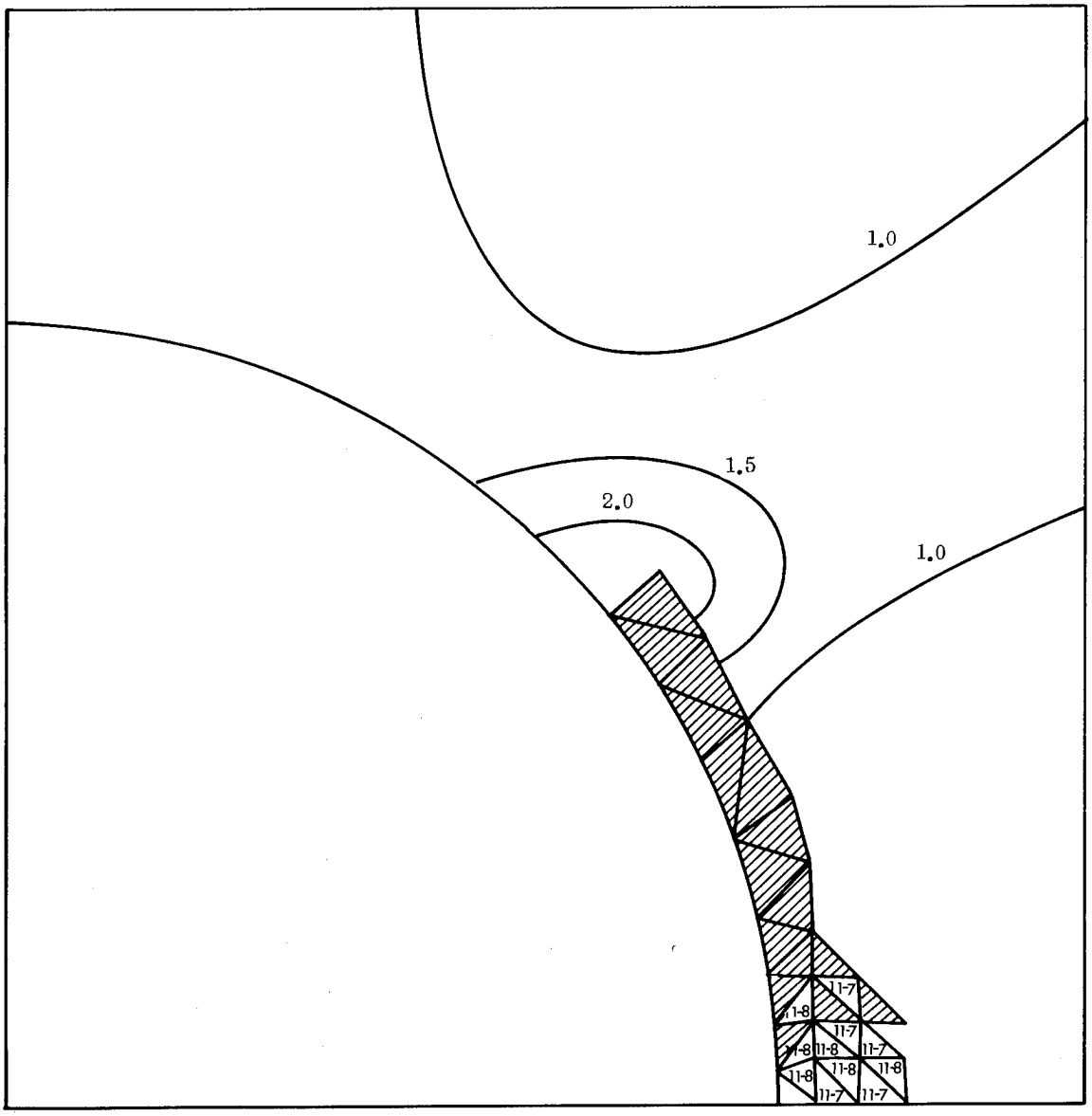

Fig. 16 — Failed elements and octahedral shear stress contours (normalized)
Computer run 8A-19-25, applied stress increment 11-9

the crack began to propagate again, moving away from the interface, as shown in Fig. 17, causing another drop in the applied stress. During the next three increments the applied stress again increased, with no elements failing. But the stiffness of the composite was considerably reduced, as shown in Fig. 13 by the slope of the curve segment between 3043 lb/in.^{2} and 3883 lb/in.^{2} applied stress. This was due to the drastic reduction of the load-carrying cross-sectional area caused by the extensive crack in the composite. As may be seen in Fig. 17, only a narrow strip of material between the crack tip and the upper boundary remained to carry the applied stress.

During the final three applied stress increments, nos. 24 through 26, the crack propagated to the upper boundary, as shown in Fig. 18. The applied stress dropped to zero, as illustrated in Fig. 13, defining total failure. As Fig. 18 shows, a very well-defined crack was obtained.

A comparison of computer runs 8A-10-17 and 8A-19-25, which, as previously stated, were essentially identical except for the magnitude of the applied stress increments assumed, reveals several points. One is that a basic assumption of the incremental loading procedure is that the material behavior is linear within each applied stress increment. That is, the slope of the octahedral shear stress-plastic octahedral shear strain curve is assumed to remain constant during each increment. This effectively means that each material element follows a stress-strain curve made up of a series of straight-line segments rather than the actual input curve. A new straight-line segment of proper slope is established at the beginning of each successive applied stress increment. Thus, large increments may cause the element material response to oscillate excessively about the smooth input stress-strain curve. During a given increment, the material response of one element may be overshooting the input curve while an adjacent element is undershooting. This results in a nonuniform local stress distribution, particularly in regions where the stresses are on a portion of the stress-strain curve where the slope is rapidly changing. This in fact did occur in computer run 8A-19-25 as first failure was being approached. When element 139 failed (at a lower applied stress level than in computer run 8A-10-17 because of the increased stress due to an overshoot) and the required

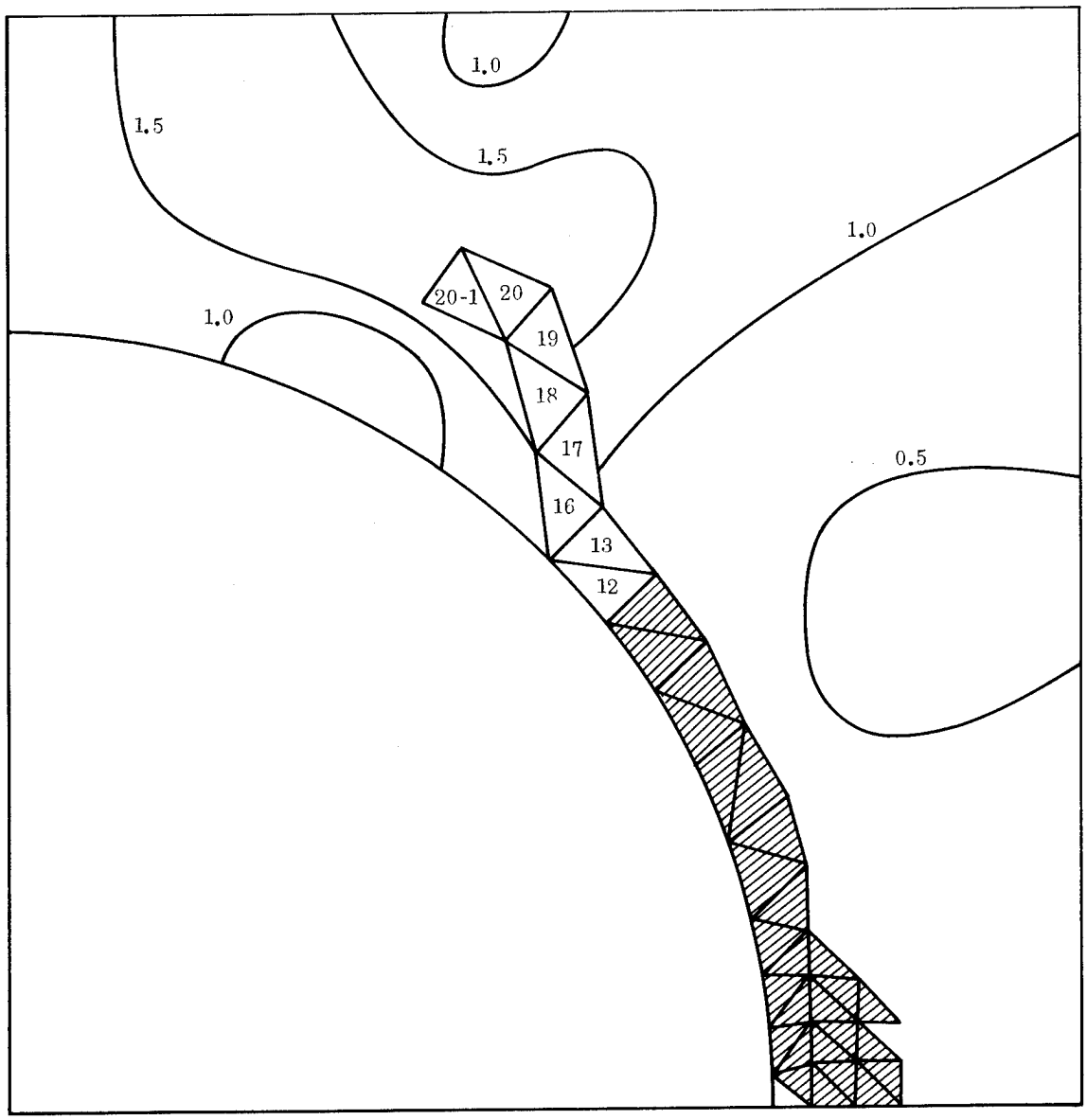

Fig. 17— Failed elements and octahedral shear stress contours (normalized)
Computer run 8A-19-25, applied stress increment 20-2

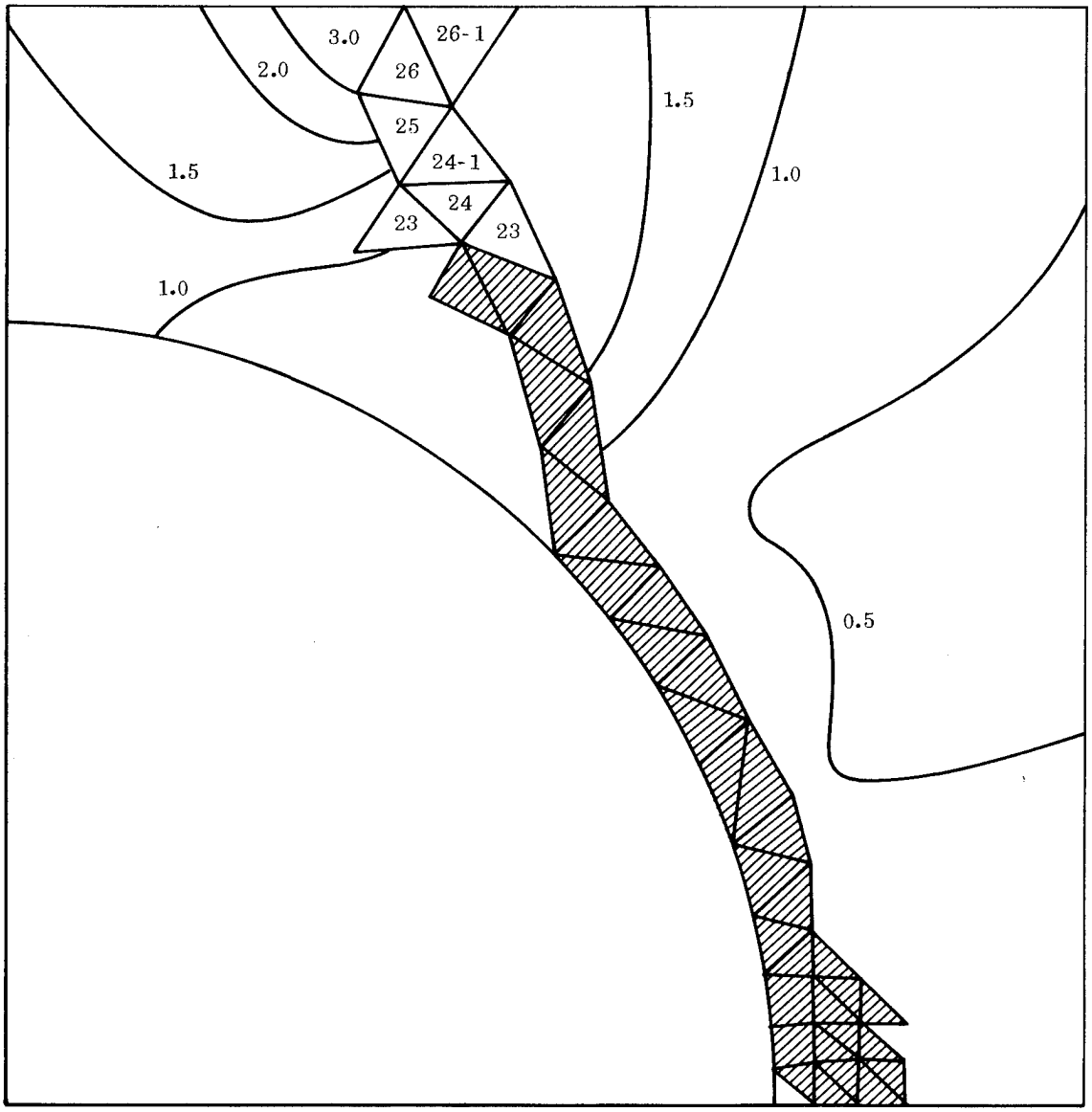

Fig. 18— Failed elements and octahedral shear stress contours (normalized)
Computer run 8A-19-25, applied stress increment 26-2 (total failure)

stress adjustment increment was performed, the stress in element 150 overshot the actual stress-strain curve excessively, exceeding the ultimate stress level. This element failure in turn caused adjacent elements to fail, setting up an almost self-propagating effect. This accounted for the very sudden drop from the maximum applied stress down to zero stress that is exhibited in Fig. 13.

It should be noted that a similar sharp drop occurred in Fig. 7 when the crack began to propagate along the interface. However, in that case, considerable strain at the high stress levels had already occurred while the crack was initially propagating in the matrix region away from the interface.

V. DISCUSSION

It became obvious during the investigation described here that much additional work remains to be done in problem areas that range from improving the accuracy of the basic finite element solution technique to developing a more representative model of the propagating crack. Many of these areas for additional research are well-defined and require only the time to develop them. The solutions to other problems are not so clear.

The author has briefly explored some of these research areas, often only enough to discover certain inherent problems. Others have been outlined in detail and only await accomplishment. The following paragraphs define the more important of these problems, indicate what has been done to date, and discuss what remains to be done.

FINITE ELEMENT METHODOLOGY

As discussed in detail in Sec. II, constant strain triangular elements were used in the investigation. Inaccuracies in the incremental solution results, particularly as manifested by the shear strains, apparently are associated with the finite element representation. Higher order elements have been developed that more closely model the actual strain variation across an element. The linear strain triangular element has, for example, received considerable attention. Each element involves six node points, one at the midpoint of each side of the triangle and one at each apex. The author has not attempted to use higher order elements as a means of improving accuracy, and this should be explored. It must be established whether using additional node points in a higher order approximation is a better technique than simply increasing the number of constant strain elements proportionally. A thorough discussion of the general use of higher order elements may be found in a report by Felippa.[14]

Another source of error is in the construction of the grid array itself. Since the triangular elements can be assembled in an arbitrary manner, any number of elements can have a common node point. Thus,

various patterns are created. Walz, et al.[15] have investigated this source of discretization error for specific grid patterns. A brief study was also performed as part of the author's investigation. Since inaccuracies were noted in even the first (elastic) applied stress increment, only elastic behavior was analyzed.

The finite element equations that express force equilibrium at a given node point in terms of node point displacements are expanded in Taylor series about that node point to obtain differential equations. These differential equations are then compared with the classical continuum equations of equilibrium. Any differences represent the error terms.

For the present two-dimensional plane strain analysis and an arbitrary grid pattern, the following results were obtained:

- For interior node points surrounded by elements all having the same material properties, no error terms involving first-order derivatives exist.
- For interior node points surrounded by elements not all having the same material properties, e.g., at a filament-matrix interface, there are error terms involving $\frac{\partial u}{\partial x}$, $\frac{\partial v}{\partial y}$, $\frac{\partial u}{\partial y}$, and $\frac{\partial v}{\partial x}$, which contribute to errors in ε_x, ε_y, and γ_{xy}.
- For node points on the boundaries $x = 0$ and $x = a$ (see Fig. 2), error terms involving $\frac{\partial u}{\partial x}$ and $\frac{\partial v}{\partial y}$ exist in the equation representing equilibrium in the x-direction; error terms involving $\frac{\partial u}{\partial y}$ and $\frac{\partial v}{\partial x}$ exist in the equation representing equilibrium in the y-direction.
- For node points on the boundaries $y = 0$ and $y = b$, there are error terms involving $\frac{\partial u}{\partial y}$ and $\frac{\partial v}{\partial x}$ in the equation representing equilibrium in the x-direction; error terms involving $\frac{\partial u}{\partial x}$ and $\frac{\partial v}{\partial y}$ exist in the equation representing equilibrium in the y-direction.

Note that, except for certain special grid patterns, there will also be error terms involving second-order derivatives. All of these error terms are independent of the element size--they do not reduce to zero as the element size vanishes. There are other discretization errors that do vanish as the element size vanishes, but they are not of principal concern here.

The general conclusion is that additional errors are introduced by the presence of material interfaces and boundaries (neither of which was considered in Ref. 15) and cannot be avoided. Their severity is dependent upon the specific local grid pattern, but they are difficult to evaluate analytically. A more detailed and thorough investigation of this aspect of the accuracy of finite element approximations and the various sources of error is needed.

The entire problem of inherent local errors leading to numerical instabilities that has been observed in this study is by no means unique. The same problem has been reported and discussed by others, including Zienkiewicz[16] and Argyris,[17] two recognized authorities on the use of finite element methods. These authors were concerned primarily with elastic analyses, for which only one matrix inversion is needed. The error problem is compounded when an incremental solution technique involving a large number of matrix inversions is required, as in the application of the tangent modulus method of elastoplastic analysis described in this report (or when a large number of iteration processes are required, as in the method of initial strains).

Both Zienkiewicz[16] and Argyris[17] have suggested the use of some type of averaging procedure to smooth out local irregularities, and have indicated successful methods for doing so. Based upon the general suggestions of Argyris, the problem might be approached as follows. It was noted in this report that the dominant irregularities occurred in the shear strains, particularly in regions of high shear strain gradients. This suggests that as a first attempt, only the shear strains for each individual boundary-value problem solution be averaged, before these solutions are combined during each increment. A possible procedure is to:

1. Assign the average of the shear strain values in pairs of adjacent elements to the midpoint of their common side. At the boundaries of the material region being analyzed, this midpoint value will equal the element value, because of the assumed symmetry across the boundary. At the filament-matrix interface, assign the element value to the midpoint of the side along the interface, i.e., do not average across the interface since the materials are dissimilar and the stresses discontinuous.
2. Average the values on the three sides of each element together and assign this average value to the element.

This averaging procedure is straightforward and can be readily incorporated into the existing computer program. Although not as satisfying analytically as using a higher order element representation, it may provide numerical results of satisfactory accuracy for most engineering applications and be much more economical of computer time required. In addition, it may be that similar irregularities and instabilities will occur if higher order elements are introduced.

CRACK REPRESENTATIONS AND FAILURE CRITERIA

The method of creation of a crack by "failing" an element and allowing the surrounding material to adjust to the failure was described in Sec. II. A possible alternative method of modeling a crack is discussed in Appendix A. In some actual materials, very high stress and strain gradients exist at the tip of a sharp crack. The adequacy of using finite elements to model these gradients should be explored further. Obviously the "failed element" approach used in the study reported here does not represent the actual crack tip geometry very closely. However, in most real materials there is a plastic zone around the crack tip that tends to reduce the magnitude of the local stress gradients, and may make it an adequate model. Certainly, many practical difficulties can arise when developing a crack model, as pointed out in Appendix A.

The definition of what constitutes material failure should also be explored further. Here, exceeding specified ultimate values of octahedral shear stress and octahedral plastic shear strain defines failure. Other theories of failure have been proposed and they should be evaluated for the application discussed in this report. It is hoped that the sharp increase in interest in fracture mechanics concepts also will prompt applications relevant to this problem.

GENERALIZED PLANE STRAIN

This analysis assumes a condition of plane strain, i.e., that the normal strain ε_z in the z-direction (the direction of the filament reinforcement) is zero throughout the composite body. Correspondingly, the z-component of displacement, w, is zero everywhere. When transverse normal loadings $\bar{\sigma}_x$ and $\bar{\sigma}_y$ are applied, however, σ_z components of stress are induced. Thus, an average stress in the z-direction, $\bar{\sigma}_z$, exists.

In actual applications it may be desirable to keep this average stress $\bar{\sigma}_z$ equal to zero to simulate a real loading condition. This can be done by assuming a uniform nonzero axial displacement w rather than a zero value. Such a condition is referred to as generalized plane strain. The magnitude of w required to achieve $\bar{\sigma}_z = 0$ is initially unknown and must be solved for. For the problem considered here, this will require the solution of an additional boundary-value problem for each increment, with Δw an arbitrarily specified constant and the normal displacement increments Δu and Δv along the boundaries $x = a$ and $y = b$, respectively, set equal to zero. The constitutive relations must also be modified slightly to accommodate the nonzero value of ε_z. A more detailed discussion is contained in Ref. 11.

The additional boundary-value problem is then combined with the appropriate two problems defined in Sec. II (Problems 1 and 2 for an applied stress increment, or Problems 2 and 3 for an adjustment increment) to obtain the desired values of $\Delta\bar{\sigma}_x$ and $\Delta\bar{\sigma}_y$, and the generalized plane strain condition, $\Delta\bar{\sigma}_z = 0$.

Generalized plane strain was not used in the present analysis because the required solution of three rather than two boundary-value problems per applied stress or adjustment increment would have increased

the computation time by approximately fifty percent. Interest here has been concentrated on developing the concept of crack propagation rather than on producing an all-encompassing solution technique. Generalized plane strain will be a logical extension, however, particularly because of the interest in combined loadings, as discussed below.

COMBINED LOADINGS

In a laminated composite system, the individual laminae are usually subjected to a combination of axial, transverse, and shear loadings due to interactions between the laminae, even when the composite body is subjected to a simple loading state.

The same basic methodology developed here for crack propagation in a composite subjected to transverse normal loading can be applied to combined loading. The generalized plane strain condition discussed in the previous subsection is, in fact, one special case of axial loading, i.e., when $\bar{\sigma}_z = 0$. Thus, by specifying $\bar{\sigma}_x = \bar{\sigma}_y = 0$ and $\bar{\sigma}_z \neq 0$, axial loading of a unidirectional composite is obtained. By specifying arbitrary values of $\bar{\sigma}_x$, $\bar{\sigma}_y$, and $\bar{\sigma}_z$, combined axial and transverse normal loading is obtained. The longitudinal shear loadings $\bar{\tau}_{zx}$ and $\bar{\tau}_{zy}$ remain to be added.

A finite element analysis of the elastoplastic behavior of a unidirectional composite subjected to longitudinal shear loading was described in Ref. 11 using the method of initial strains, and in unpublished work by Adams and Wilson* using the tangent modulus method. Combined axial, transverse, and shear loadings of an elastoplastic material were also considered in Ref. 11.

These same methodologies can be applied to the problem of crack initiation and propagation. The addition of specified increments of applied longitudinal shear stress components to the combined loading will require the solution of one additional boundary-value problem per solution increment if only one of the two components $\Delta\bar{\tau}_{zx}$ or $\Delta\bar{\tau}_{zy}$ is to be included, and two additional solutions if both are to be included. Thus,

*D. F. Adams and H. B. Wilson, Jr., "Inelastic Analysis of a Unidirectional Composite-Longitudinal Shear Loading," unpublished work, Aeronutronic Division, Philco-Ford Corporation, August 1966.

a complete combined loading problem involving the applied stress increments $\Delta\bar{\sigma}_x$, $\Delta\bar{\sigma}_y$, $\Delta\bar{\sigma}_z$, $\Delta\bar{\tau}_{zx}$, and $\Delta\bar{\tau}_{zy}$ will require the solution and combination of five separate boundary-value problems per solution increment. However, longitudinal shear loading involves only one unknown displacement component per node point (a displacement in the z-direction) rather than two as in the case of axial or transverse normal loading (displacements in both the x- and y-directions). Thus, only an $N \times N$ matrix rather than a $2N \times 2N$ matrix needs to be inverted to obtain a solution (N represents the total number of node points in the finite element array). This suggests that the computation time required to solve a longitudinal shear boundary-value problem will be only about one-fourth as long.

The general expressions for octahedral shear stress and octahedral plastic shear strain given by Eqs. (7) and (6), respectively, are used to define material yield and failure. The consideration of crack initiation and propagation under combined loading should be a straightforward extension of the investigation given here and that found in Ref. 11.

THERMAL EFFECTS

Thermal effects are of special interest in studies of composite material micromechanical behavior because the differences in coefficients of thermal expansion among the constituents almost always result in local stresses being introduced during a temperature change, even a uniform temperature change. Most composite materials, both metal and polymer matrix composites, are produced at elevated temperatures and subsequently are used in room temperature applications. Thus, even the as-received composite material contains (thermal) residual stresses. If the composite is also subjected to thermal environments during service, additional thermal stresses are developed.

Since the thermal stresses introduced in fabrication are developed while the composite is not being subjected to significant mechanical loads, i.e., during cool-down from fabrication temperatures, the constituent materials will, at least initially, exhibit linear elastic behavior. In most instances, these thermal stresses will not be high

enough to cause yielding. This is particularly true because the elastic stiffness (Young's modulus) of the constituents, especially the matrix material that must flow during the compositing process, will be lower at the fabrication temperature. Thus, a linearly elastic thermostress analysis is often applicable. The variation of material properties with temperature, particularly the Young's modulus, should be taken into account, however, which complicates the analysis.

A linearly elastic micromechanical analysis of thermal residual stresses was included in Ref. 2. The variation of the Young's modulus with termperature was taken into account in an approximate way by using room temperature material properties but an assumed temperature change less than the actual value. The actual temperature change associated with cool-down can be applied in increments using the analysis described here, with the material properties modified at the beginning of each increment. This procedure will provide a more accurate representation of the actual physical behavior.

Similarly, thermal loading need not be limited to elastic response. By suitably modifying the elastoplastic analysis, arbitrary (including nonuniform) temperature variations can be combined with the mechanical loading increments. This will require the specification of appropriate material properties, including a complete stress-strain curve, for each temperature increment used. Since, in the tangent modulus method, the stiffness matrix is reconstructed and inverted in each increment anyway, this modification will not involve excessive additional computational time. However, the inclusion of a thermal loading (temperature change) during a solution increment, just as any of the other loadings previously discussed, will require the solution of an additional boundary-value problem, to be combined with the others. The conditions for the problem will be: zero shear stress τ_{xy} and zero normal displacement along all four rectangular boundaries, and specification of the desired incremental temperature change in each element.

The governing field equations must also be modified for this boundary-value problem to include the thermal strain effect. For example, the strain-displacement relation given by Eq. (35) must be amended to include a thermal strain term $[\bar{\alpha}]\Delta T$, i.e.,

$$[\dot{\epsilon}] = [\theta]\ [\dot{\delta}] + [\bar{\alpha}]\Delta T$$

where

$$[\bar{\alpha}] = \begin{bmatrix} \alpha \\ \alpha \\ o \end{bmatrix}$$

represents the coefficient of thermal expansion and ΔT is the incremental temperature change. The constitutive relation, Eq. (30), remains unchanged. Following through the analysis of Sec. II, Eq. (42) becomes

$$[\dot{F}] = [K]\ [\dot{\delta}] + A_n[\theta]^T\ [H]\ [\alpha]\ \Delta T$$

The additional term is a known constant for each element during the increment. Thus, no special complications will occur in formulating a solution procedure.

DIAMOND PACKING ARRAYS

Filament packing geometries and the desirability of maintaining a regular periodic array was discussed in Sec. II. Although this investigation has been limited to rectangular arrays, diamond arrays, of which a hexagonal array is a special case, are of equal interest. As noted on the left side of Fig. 1c and in the text of Sec. II, this analysis also can be used to treat diamond arrays. It is possible to reduce the area in the first quadrant that must be analyzed to one-half by redefining the boundary-value problem to include only that region indicated by the solid lines on the right side of Fig. 1c. This region of the first quadrant is redrawn in Fig. 19.

The greater difficulty in analyzing a diamond array as compared with a rectangular array is associated with the fact that the boundary represented by the line COD in Fig. 19 does not remain a straight line under loading. However, it does deform antisymmetrically about the midpoint 0, i.e., the displacements of two points on line COD at equal distances on opposite sides of point 0 will be equal in magnitude but opposite in direction. Also, because of the assumed geometric symmetry,

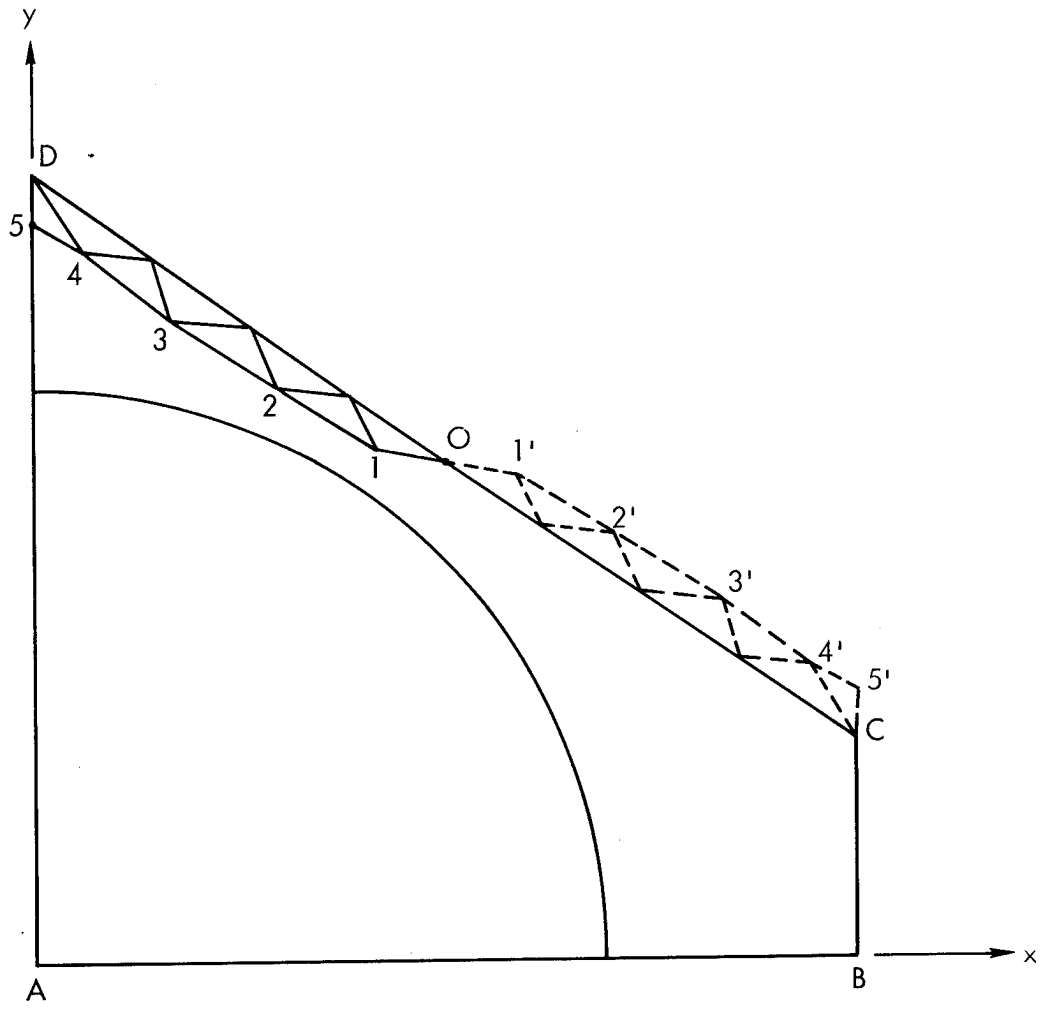

Fig. 19— First quadrant of a typical repeating unit for a diamond array of filaments

forces acting on these points will be of equal magnitude and direction. Thus, by constructing node points on boundary COD symmetric about the midpoint 0, both displacement and force relations between pairs of node points can be established.

This is adequate information to solve the boundary-value problem. However, there are also certain practical difficulties. These relationships are of a different form than those making up the remainder of the stiffness matrix, and thus the solution procedure must be modified. Node points as widely separated as C and D are now related, a fact to be considered when numbering the node points so as to minimize the matrix bandwidth.

An alternative scheme, which eliminates the need for including displacement and force equivalence relations in the stiffness matrix directly, is to add additional node points and elements on the outside of boundary COD. The node points on COD are still placed symmetrically about midpoint 0. Additional fictitious node points, symmetric about point 0 to node points inside the material region, are added outside so that elements can be constructed that completely surround the node points on one-half of boundary COD, say between C and 0, as shown in Fig. 19. The displacements of the boundary node points between 0 and D are related to those of their symmetric counterparts between C and 0 as before--they are of equal magnitude but opposite direction relative to point 0. Equilibrium equations can then be written for the node points on the boundary between C and 0 just as if they were interior nodes, and the displacements of the fictitious nodes are eliminated by using the known relationships to their symmetric counterparts in the interior.

This scheme eliminates the need for satisfying force equivalences across the midpoint of the boundary COD; the resulting stiffness matrix retains a form similar to that for a rectangular array. Numbering the node points to keep the matrix bandwidth small remains an important consideration, just as it is for the first scheme.

OTHER TOPICS

There are a number of other topics requiring additional investigation, only a representative sample of which will be mentioned here. For

example, this investigation has only considered regular arrays of filaments, whereas in actual composite materials the filaments are often not regularly spaced. The influence of random filament packing on elastic stiffness properties was investigated in Ref. 3. The influence of randomness on crack propagation and composite ultimate strength should also be studied.

Anisotropy of the constituents is also a consideration. Graphite filaments, for example, are known to be anisotropic due to their crystalline structure.

Certain filament reinforcements, e.g., graphite produced from a rayon precurser, have noncircular and often very irregular cross-sectional shapes. The analysis described in this report can readily handle an irregular geometry. A study should be performed to determine the influence of an irregular shape on crack propagation and ultimate strength.

Voids in the matrix material and local unbonded regions at the filament-matrix interface are examples of defects often present in an actual composite. A systematic study of their influence on crack propagation and ultimate strength should be conducted.

Appendix A

INVERSE OF THE CONSTITUTIVE EQUATION

The inverse of Eq. (25) can be obtained by first expanding it into the three equations it represents, $\dot{\varepsilon}_{11}$, $\dot{\varepsilon}_{22}$, and $\dot{\varepsilon}_{12}$, and then solving these equations for $\dot{\sigma}_{11}$, $\dot{\sigma}_{22}$, and $\dot{\sigma}_{12}$ by successive elimination. Because such a process is lengthy, it is much simpler to invert exclusively in index notation, as follows. Repeating Eq. (25),

$$\dot{\varepsilon}_{\alpha\beta} = \frac{1+\nu}{E} (\dot{\sigma}_{\alpha\beta} - \nu\dot{\sigma}_{\gamma\gamma}\delta_{\alpha\beta}) + \frac{1}{D} t_{\alpha\beta}t_{\gamma\delta}\dot{\sigma}_{\gamma\delta}$$

from which the following two equations are obtained:

$$\dot{\varepsilon}_{\alpha\alpha} = (\frac{1 + \nu}{E})(1 - 2\nu)\dot{\sigma}_{\alpha\alpha} + \frac{1}{D} t_{\alpha\alpha}t_{\gamma\delta} \qquad \text{(A-1)}$$

and

$$t_{\alpha\beta}\dot{\varepsilon}_{\alpha\beta} = \frac{1+\nu}{E} (t_{\alpha\beta}\dot{\sigma}_{\alpha\beta} - \nu t_{\alpha\alpha}\dot{\sigma}_{\gamma\gamma}) + \frac{1}{D} t_{\alpha\beta}t_{\alpha\beta}t_{\gamma\delta}\dot{\sigma}_{\gamma\delta} \qquad \text{(A-2)}$$

Letting $x = \dot{\sigma}_{\alpha\alpha}$ and $y = t_{\alpha\beta}\dot{\sigma}_{\alpha\beta}$, Eqs. (25), (A-1), and (A-2) can be written as

$$\dot{\varepsilon}_{\alpha\beta} = \frac{1+\nu}{E} (\dot{\sigma}_{\alpha\beta} - \nu\delta_{\alpha\beta}x) + \frac{1}{D} t_{\alpha\beta}y \qquad \text{(A-3)}$$

$$\dot{\varepsilon}_{\alpha\alpha} = \frac{(1 + \nu)(1 - 2\nu)}{E} x + \frac{1}{D} t_{\alpha\alpha}y \qquad \text{(A-4)}$$

$$t_{\alpha\beta}\dot{\varepsilon}_{\alpha\beta} = \frac{1+\nu}{E} (y - \nu t_{\alpha\alpha}x) + \frac{1}{D} t_{\alpha\beta}t_{\alpha\beta}y \qquad \text{(A-5)}$$

Eliminating x and y, solving for $\dot{\sigma}_{\alpha\beta}$, and simplifying give the desired inverse, Eq. (26).

Alternatively, the inverse of Eq. (25) can be obtained as follows. First, determine $s_{\alpha\beta}\dot{\varepsilon}_{\alpha\beta}$ from Eq. (25),

$$s_{\alpha\beta}\dot{\varepsilon}_{\alpha\beta} = \frac{1+\nu}{E}\left[s_{\alpha\beta}\dot{\sigma}_{\alpha\beta} - \nu s_{\alpha\beta}\dot{\sigma}_{\gamma\gamma}\delta_{\alpha\beta}\right] + \frac{1}{D}\, t_{\alpha\beta}t_{\gamma\delta}s_{\alpha\beta}\dot{\sigma}_{\gamma\delta}$$

noting that, as usual, the repeated indices indicate summation. Thus, the second term in the brackets can be expressed as $\nu(s_{11} + s_{22})\dot{\sigma}_{\gamma\gamma}$, or as $-\nu s_{33}\dot{\sigma}_{\alpha\beta}\delta_{\alpha\beta}$, since $(s_{11} + s_{22}) = -s_{33}$ and $\dot{\sigma}_{\gamma\gamma} = \dot{\sigma}_{\alpha\beta}\delta_{\alpha\beta}$. The expression within the brackets becomes $[(s_{\alpha\beta} + \nu s_{33}\delta_{\alpha\beta})\dot{\sigma}_{\alpha\beta}]$. But the quantity within the parentheses here is equal to $t_{\alpha\beta}$, as previously defined. Therefore, the full equation can be rewritten as

$$s_{\alpha\beta}\dot{\varepsilon}_{\alpha\beta} = \left(\frac{1+\nu}{E} + \frac{t_{\alpha\beta}s_{\alpha\beta}}{D}\right) t_{\alpha\beta}\dot{\sigma}_{\alpha\beta}$$

Setting the terms in parentheses over the common denominator $\frac{E}{1+\nu}\, D$ and expanding $t_{\alpha\beta}s_{\alpha\beta}$ gives

$$s_{\alpha\beta}\dot{\varepsilon}_{\alpha\beta} = \left\{\left(A + Es_{33}^2\right) + \frac{E}{1+\nu}\left[s_{11}^2 + s_{22}^2 + s_{33}^2 + 2s_{12}^2 + \nu s_{33}\left(s_{11} + s_{22}\right) - s_{33}^2\right]\right\} \frac{t_{\alpha\beta}\dot{\sigma}_{\alpha\beta}}{\frac{E}{1+\nu}\, D}$$

where the term s_{33}^2 has been added and subtracted within the brackets. The first four terms within the brackets are now equal to $3\tau_0^2$. Also, since $(s_{11} + s_{22}) = -s_{33}$, the remaining terms within the brackets reduce to $-(1 + \nu)s_{33}^2$. This term, when multiplied by the $\frac{E}{1+\nu}$ appearing outside the brackets, becomes $-Es_{33}^2$, which cancels with the second term within the braces. Thus, the complete equation reduces to

$$s_{\alpha\beta}\dot{\varepsilon}_{\alpha\beta} = \left(A + \frac{E}{1 + \nu}\, 3\tau_0^2\right) \frac{t_{\alpha\beta}\dot{\sigma}_{\alpha\beta}}{\frac{E}{1+\nu}\, D}$$

which can be rewritten as

$$\frac{t_{\alpha\beta}\dot{\sigma}_{\alpha\beta}}{D} = \frac{s_{\alpha\beta}\dot{\varepsilon}_{\alpha\beta}}{3\tau_0^2 + (1+\nu)\frac{A}{E}} \tag{A-6}$$

This equation relates the stress $\dot{\sigma}_{\gamma\delta}$ in Eq. (25) to the strain $\dot{\varepsilon}_{\gamma\delta}$.

The next step is to relate $\dot{\sigma}_{\gamma\gamma}$ in Eq. (25) to $\dot{\varepsilon}_{\gamma\gamma}$. Writing Eq. (25) for $\dot{\varepsilon}_{\alpha\alpha}$,

$$\dot{\varepsilon}_{\alpha\alpha} = \frac{1+\nu}{E}(\dot{\sigma}_{\alpha\alpha} - \nu\dot{\sigma}_{\gamma\gamma}\delta_{\alpha\alpha}) + \frac{t_{\gamma\delta}\dot{\sigma}_{\gamma\delta}}{D} t_{\alpha\alpha}$$

Simplifying the first term and substituting Eq. (A-6) into the second gives

$$\dot{\varepsilon}_{\alpha\alpha} = \frac{1+\nu}{E}(1 - 2\nu)\dot{\sigma}_{\alpha\alpha} + \frac{s_{\gamma\delta}\dot{\varepsilon}_{\gamma\delta}}{3\tau_0^2 + (1+\nu)\frac{A}{E}} t_{\alpha\alpha}$$

Substituting the expansion of $t_{\alpha\alpha}$ below,

$$\begin{aligned} t_{\alpha\alpha} &= (s_{11} + \nu s_{33}) + (s_{22} + \nu s_{33}) \\ &= (s_{11} + s_{22}) + 2\nu s_{33} \\ &= -s_{33} + 2\nu s_{33} \\ &= -(1 - 2\nu)s_{33} \end{aligned}$$

into the above equation and solving for $\dot{\sigma}_{\alpha\alpha}$ gives

$$\dot{\sigma}_{\alpha\alpha} = \frac{E}{(1+\nu)(1-2\nu)}\left[\dot{\varepsilon}_{\alpha\alpha} + \frac{(1 - 2\nu)s_{33}s_{\gamma\delta}\dot{\varepsilon}_{\gamma\delta}}{3\tau_0^2 + (1+\nu)\frac{A}{E}}\right] \tag{A-7}$$

Substituting Eqs. (A-6) and (A-7) into Eq. (25) gives

$$\dot{\varepsilon}_{\alpha\beta} = \frac{1+\nu}{E}\left\{\dot{\sigma}_{\alpha\beta} - \frac{\nu E}{(1+\nu)(1-2\nu)}\left[\dot{\varepsilon}_{\gamma\gamma} + \frac{(1-2\nu)s_{33}s_{\gamma\delta}\dot{\varepsilon}_{\gamma\delta}}{3\tau_0^2 + (1+\nu)\frac{A}{E}}\right]\delta_{\alpha\beta}\right\}$$

$$+ t_{\alpha\beta}\frac{s_{\gamma\delta}\dot{\varepsilon}_{\gamma\delta}}{3\tau_0^2 + (1+\nu)\frac{A}{E}}$$

Solving for $\dot{\sigma}_{\alpha\beta}$

$$\dot{\sigma}_{\alpha\beta} = \frac{E}{1+\nu}\left[\dot{\varepsilon}_{\alpha\beta} + \frac{\nu}{1-2\nu}\dot{\varepsilon}_{\gamma\gamma}\delta_{\alpha\beta} + \frac{(\nu s_{33}\delta_{\alpha\beta} - t_{\alpha\beta})s_{\gamma\delta}\dot{\varepsilon}_{\gamma\delta}}{3\tau_0^2 + (1+\nu)\frac{A}{E}}\right]$$

Since the quantity in parentheses in the numerator of the last term is, by definition, $-s_{\alpha\beta}$, the equation can be written as

$$\dot{\sigma}_{\alpha\beta} = \frac{E}{1+\nu}\left[\dot{\varepsilon}_{\alpha\beta} + \frac{\nu}{1-2\nu}\dot{\varepsilon}_{\gamma\gamma}\delta_{\alpha\beta} - \frac{s_{\alpha\beta}s_{\gamma\delta}\dot{\varepsilon}_{\gamma\delta}}{3\tau_0^2 + (1+\nu)\frac{A}{E}}\right] \qquad \text{(A-8)}$$

which is the inverse of Eq. (25).

Appendix B

ALTERNATIVE METHODS OF MODELING A CRACK

In addition to the "failed element" concept of modeling a local failure, which was used in the investigation discussed here, other methods were considered, one of which will be briefly outlined below. This discussion is included to point out some of the practical difficulties involved in modeling a crack and to serve as a starting point for additional investigations by the interested reader. There is clearly a need for much more study in this problem area.

When the stresses in a given element exceed the ultimate strength of the material, rather than dropping out that element to create a crack, an additional node point can be added at each of two of the three corners of the triangular element. These node points are co-located with, but not attached to, the existing ones. At each of these two locations, one node point is then associated with certain of the surrounding elements, and the other node point with the remainder. This is illustrated in Fig. B-1, which represents a local region of the full grid shown in Fig. 3. Suppose that failure is indicated in element 163. Additional node points 177 and 178 are added at nodes 68 and 78, respectively. (See Fig. B-1(b); the nodes of the pairs 68, 177 and 78, 178 are shown separated from each other for clarity, and the shaded area represents the crack.) In this representation, a crack of zero initial width is created and no material is removed.

However, there are certain procedural difficulties created. For indicated failure in element 163, one of the other two sides could have been selected as the crack site instead, resulting, for example, in a crack through nodes 86, 77, 68, 59 or nodes 76, 77, 78, 79 rather than nodes 88, 78, 68, 58. These differences are significant, resulting in possible cracks almost perpendicular to the one indicated in Fig. B-1(b).

These are not the only three crack path choices possible, although they are perhaps among the more obvious for the particular local region selected as an example here. For instance, the crack between nodes 78

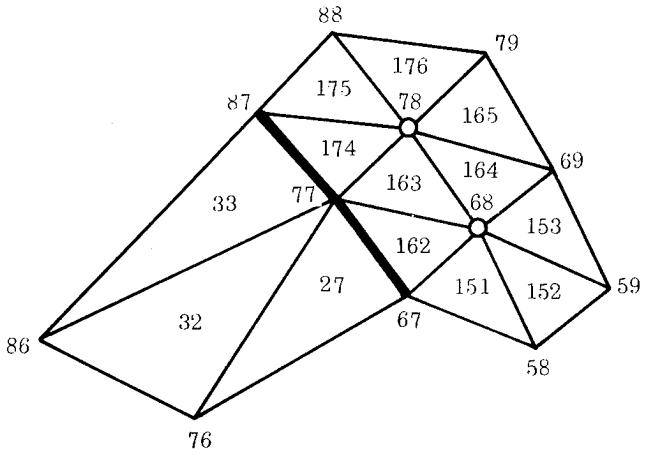

(a) Local grid region prior to failure

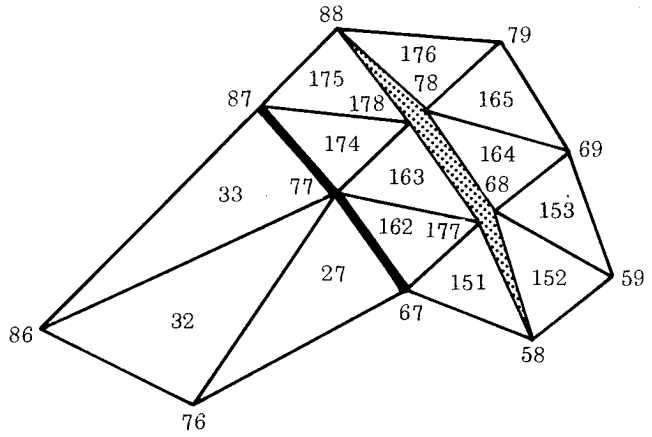

(b) Local material failure

Fig. B-1 — Crack representation by double-numbered nodes

and 68 could have been assumed to run from node 68 to node 67, 59, or 69 rather than to node 58. Similar choices were possible for the other end. Thus, a scheme would have to be developed for selecting the most logical path, perhaps based upon the stress gradients existing around the element in which failure is indicated.

Figure B-1 demonstrates another potential problem. An assumed crack along either of the other two sides of element 163 would necessarily extend either into the adjacent material region (from matrix into filament) or along the interface. In an actual material this may not be realistic, particularly if one material has significantly different properties than the adjacent one, as is usually the case. The problem stems from the fact that, although failure is indicated in only one element, the crack is modeled to extend along the sides of as many as three adjacent elements, as may be seen in Fig. B-1(b). To use this model, a method would also have to be devised to insure that the crack created by colocated node points can only open up; the material region on one side of the crack cannot be allowed to move into the material region on the other side, based upon physical considerations.

A serious computational difficulty also occurs if the "double node" crack representation is used. As was discussed in Sec. II, the bandwidth of the diagonalized stiffness matrix $[\underline{K}_{11}]$ in Eq. (51) must be kept to a minimum to achieve an efficient solution. This bandwidth is proportional to the maximum difference between the highest and lowest node point number associated with each of the various elements in the array. For the grid array shown in Fig. 3, this maximum difference is only 11. However, if node points 177 and 178 were added as indicated in Fig. B-1(b), this maximum difference would increase to 119 (for element 151). Thus, some scheme would have to be developed for automatically renumbering all of the node points each time additional node points were added. At present, not even the initial set of node points are numbered automatically; because of the computational problems involved, they are numbered by hand.

An alternative scheme would be to double-number (consecutively) all of the node points, and use, for example, only the odd numbers initially.

The even-numbered nodes could be introduced as needed to model the crack formation. This scheme would approximately double the matrix bandwidth, however, which would make it of questionable utility.

REFERENCES

1. Adams, D. F., *Inelastic Analysis of a Unidirectional Composite Subjected to Transverse Normal Loading*, The Rand Corporation, RM-6245-PR, May 1970; see also D. F. Adams, "Inelastic Analysis of a Unidirectional Composite Subjected to Transverse Normal Loading," *J. Composite Materials*, Vol. 4, July 1970, pp. 310-328.

2. Adams, D. F., and D. R. Doner, "Transverse Normal Loading of a Unidirectional Composite," *J. Composite Materials*, Vol. 1, No. 2, April 1967, pp. 152-163.

3. Adams, D. F., and S. W. Tsai, *The Influence of Random Filament Packing on the Elastic Properties of Composite Materials*, The Rand Corporation, RM-5608-PR, December 1968.

4. Adams, D. F., and S. W. Tsai, "The Influence of Random Filament Packing on the Transverse Stiffness of Unidirectional Composites," *J. Composite Materials*, Vol. 3, July 1969, pp. 368-381.

5. *PRD-49, DuPont's New High Modulus Organic Fiber*, E. I. duPont de Nemours & Company, Inc., April 1971.

6. Hill, R., *The Mathematical Theory of Plasticity*, Oxford University Press, London, 1950, p. 27.

7. Swedlow, J. L., "Elasto-Plastic Cracked Plates in Plane Strain," *Int. J. Fracture Mech.*, Vol. 5, No. 1, March 1969, pp. 33-44.

8. Zienkiewicz, O. C., *The Finite Element Method in Engineering Science*, McGraw-Hill Book Co., Inc., London, 1971.

9. Foye, R. L., *Advanced Design Concepts for Advanced Composite Airframes*, Air Force Materials Laboratory, Contractor Report AFML-TR-68-91, Vol. 1, July 1968.

10. Marcal, P. V., "A Comparative Study of Numerical Methods of Elastic-Plastic Analysis," *AIAA Journal*, Vol. 6, No. 1, January 1968, pp. 157-158.

11. Foye, R. L., and D. J. Baker, *Design/Analysis Methods for Advanced Composite Structures*, Air Force Materials Laboratory, Contractor Report AFML-TR-70-299, Vol. I *Analysis*, Vol. II *Computer Programs*, February 1971.

12. Tsai, S. W., D. F. Adams, and D. R. Doner, *Effect of Constituent Material Properties on the Strength of Fiber-Reinforced Composite Materials*, Air Force Materials Laboratory, Contractor Report AFML-TR-66-190, August 1966.

13. Menke, G. D., and I. J. Toth, *The Time-Dependent Mechanical Behavior of Composite Materials*, Air Force Materials Laboratory, Contractor Report AFML-TR-70-174, June 1970.

14. Felippa, C. A., *Refined Finite Element Analysis of Linear and Nonlinear Two-Dimensional Structures*, University of California at Berkeley, Department of Civil Engineering, Report 66-22, 1966.

15. Walz, J. E., R. E. Fulton, and N. J. Cyrus, "Accuracy and Convergence of Finite Element Approximations," *Proc. Second Conference on Matrix Methods in Structural Mechanics*, Air Force Flight Dynamics Laboratory, Report AFFDL-TR-68-150, December 1969, pp. 995-1027.

16. Zienkiewicz, O. C., *The Finite Element Method in Structural and Continuum Mechanics*, McGraw-Hill Book Co., Inc., London, 1967, pp. 35-37.

17. Argyris, J. H., "Continua and Discontinua," *Matrix Methods in Structural Mechanics--Proceedings of the Conference*, Air Force Flight Dynamics Laboratory, Report AFFDL-TR-66-80, November 1966, p. 43.